CATALYSIS OF COAL GASIFICATION AT ELEVATED PRESSURE

W. P. Haynes, S. J. Gasior, and A. J. Forney

Bureau of Mines, U.S. Department of the Interior, Pittsburgh, Pa.

INTRODUCTION

The gasification of coal with steam and oxygen under elevated pressure is an essential step in the Bureau of Mines Synthane process for converting coal to synthetic pipeline gas. Use of a suitable catalyst or additive in the gasification step could conceivably improve the gasification of coal. Earlier investigators have catalyzed the gasification of coke and carbon with various additives and have demonstrated that some benefits would result from the catalysis of gasification at atmospheric pressure. Vignon (1), for example, showed that the percentage of methane in water gas made from coke can be increased significantly by addition of lime to the coke. Neumann, Kroger, and Fingas (2) demonstrated the feasibility of improving the gasification of graphite at 450° to 1,000° C through addition of K_2O, CuO, and other salts. Continuation of the studies by Kroger and Melhorn (3) indicated that addition of either 8 pct Li_2O or (8 pct K_2O + 3 pct Co_3O_4) to low-temperature coke increased steam decomposition at temperatures of 500° to 700° C. More recently, Kislykh and Shishakov (4) studied the effect of $Fe(CO)_5$, (Fe_2O_3 + $CuCl_2$), K_2CO_3, and NaCl upon fluid-bed gasification of wood charcoal at 750° C and atmospheric pressure. They found that sodium chloride was the most effective additive, accelerating gasification by 62 pct and increasing steam decomposition 2.5-fold.

The work on catalysis reviewed thus far does not include gasification at elevated pressures nor the use of volatile coals. The bench-scale work now reported compares the catalytic activity of various additives in the gasification of volatile coals with steam under pressure and studies other process parameters of interest such as gasification temperature, type of contact with the catalyst, degree of gasification, and repeated use of a catalyst. Results of pilot plant gasification tests using additives are also reported.

Bench-Scale Studies

The gasification tests were conducted in two bench-scale reactor units, units A and B. The units were essentially the same; each unit contained an electrically heated reactor constructed of a 21-in-long section of 3/4-in, schedule 160 pipe of type 321 stainless steel. The coal-additive charge was contained in the middle 6 in of the reactor to minimize the spread of bed temperatures. Alumina cylinders filled the void space at each end of the reactor. Three thermocouples were located in the 6-in reactor zone, 1/2 in, 3 in, and 5-1/2 in from the top of the zone. The maximum temperature occurred at the middle thermocouple and was considered the nominal temperature of the reaction. The top and bottom bed temperatures were generally within 35° C of the maximum temperature.

During a gasification test, the coal charge was gasified by steam, which was introduced by saturation of the nitrogen carrier gas.

Figure 1 shows a schematic flowsheet of a reactor unit and its auxiliary equipment: high-pressure gas supply, silica gel and charcoal purifiers, calibrated capillary meter as feed gas flow indicator, gas saturator to humidify the feed gas, condenser and trap for liquid product collection, and gasometer for metering and collecting of total product gas. Reactor pressure was controlled by a back-pressure regulator. Temperature of the gas saturation was controlled within $\pm$ 0.6° C by a chromel-alumel thermocouple control system.

Analyses of dry product gases were done by mass spectrometer as well as gas chromatography. The liquid product about 95 pct water, was drained and weighed.

Coal Used

The coal charged in all the tests discussed in this report was a single batch of high-volatile bituminous coal (Bruceton, Pa.) that had been pretreated at 450° C with a steam-air mixture to destroy its caking quality. The pretreated coal was crushed and sieved to a particle size of 20 to 60 mesh. Proximate and ultimate analyses of the pretreated coal are shown in table 1 below, in weight percent:

TABLE 1. - Analyses of pretreated coal used for feedstock

Proximate		Ultimate	
Moisture	1.5	Hydrogen	3.9
Volatile	22.4	Carbon	74.3
Fixed carbon	65.5	Nitrogen	1.5
Ash	10.6	Oxygen	8.7
		Sulfur	1.0
		Ash	10.6

Standard Gasification Tests for Screening Additives

Standard gasification tests were conducted in units A and B to determine the effect of various additives upon rate of carbon gasification, rate of gas production, and other gasification parameters.

In unit A, the standard gasification tests using various catalysts were made at the selected operating conditions of 850° C, 300 psig, and 5.8 g/hr steam feed carried by 2,000 cm^3 N_2/hr. The coal charge was 10 g plus 0.5 g of catalyst. All catalysts were either powders or crystals that were admixed with the coal except in the case of experiment 203. In experiment 203, a metal tubular insert was flame-spray coated with about 10 g of unactivated Raney nickel, then inserted in the coal bed. In experiment 200, the Raney nickel catalyst powder was activated or approximately 65 pct reduced by treatment with 2 pct sodium hydroxide solution. In the reduced activated state, the catalyst was dried, mixed with coal, and charged into the unit under an inert atmosphere of nitrogen.

Reaction time, at the desired reaction temperature, was held constant at 4 hrs. An additional heat-up time of about 40 min was needed to reach the desired reaction temperature. Steam flow was not started until bed temperature exceeded 200° C. Conditions in unit B were the same as in unit A except that the steam rate was slightly lower at 5.0 g/hr.

Generally, tests were conducted in triplicate or higher replication. The average deviations in carbon gasification rate determinations generally ranged from 1 to 5 pct.

The experimental results of the screening tests conducted in unit A are presented in tables 2a and 2b; and for unit B, are presented in tables 3a and 3b. The specific gas production rates and gasification rates presented are based on the approximate 4-hr reaction time at 850° C. The results indicate that methane production rates as well as carbon gasification rates can be increased significantly by admixing certain compounds with the coal feed.

The rate of carbon gasification for the uncatalyzed coal was about 10 pct higher in unit A than in unit B (experiment 167 vs 300). The slightly higher steam rate in unit A is suspected as the cause of the higher reaction rate. Because of this difference in absolute rates, the percent increases achieved in gasification rates and gas production rates due to additives were related only to rates obtained in the gasification of the uncatalyzed coal in the same unit. Shown in table 4 are the relative effects of 40 additives upon the production of methane and hydrogen; and shown in table 5 are their relative effects upon the production of carbon monoxide and the gasification of carbon. The additives are listed in decreasing order of percent increased production. The corresponding reactor unit used (either A or B) is also listed.

Table 4 shows that at standard test conditions, all the additives listed except $ZnBr_2$ increased methane production and that all the tested additives increased hydrogen production significantly. The sprayed Raney nickel catalyst increased methane production by 24 pct and was the most effective material for promoting methane production. The next three materials ranking highest in promoting methane production were $LiCO_3$, Pb_3O_4, and Fe_3O_4 with respective methane increases of 21, 20, and 18 pct.

A comparison of the methanation activity of zinc oxide with that of zinc bromide indicates that the anion group of a catalyst can exert significant influence on the activity.

As shown in table 4, the alkali metal compounds proved to be among the best promoters of hydrogen production. The percent increase in hydrogen produced was 105, 83, 55, and 53 pct, respectively, with the addition of KCl, K_2CO_3, $LiCO_3$, and NaCl. The sprayed Raney nickel was the third most effective promoter of hydrogen production yielding a hydrogen increase of 63 pct.

Table 5 shows that the alkali metal compounds K_2CO_3, KCl, and $LiCO_3$ gave the greatest increase in carbon monoxide production as well as in carbon gasification; the increases ranged from 40 to 91 pct. The compound NaCl provided a significant increase of 31 pct in carbon gasification but was much less effective in increasing the production of carbon monoxide (7-pct increase).

As shown in tables 2b and 3b, the unit heating values of the total product gases generally decreased as a result of mixing additives with the coal but, since the total gas make was increased, the total amount of fuel value produced as product gas increased.

Two methods of applying catalyst--by admixing with the coal or by coating the surface of an insert or carrier--may be compared in the case of unactivated Raney nickel catalyst (experiments 203 and 197).

TABLE 2a. - Specific rate of gas production when using various catalysts (Series A)

Test conditions - Unit A: Charge, 10 g pretreated Bruceton coal, 0.5 g catalyst; feed, 5.8 g H_2O/hr + 2000 std cc N_2/hr; approximately 4-hr duration; 300 psig; 850° C

Catalyst	Expt. No.	No. of test	Total dry gas production rate, N_2-free bases, std cc/hr/g coal charged	Specific production rate of constituent gases, std cc/hr/g coal charged							
				H_2	CO	CO_2	CH_4	C_2H_4	C_2H_6	C_3H_8	C_3H_6
No catalyst	166	6	331	166	49.7	70.2	43.7	0.06	0.93	0.24	0.12
Raney nickel, unactivated:											
Sprayed	203	6	453	271	53.7	72.3	54.2	.12	.80	.22	.05
Mixed	197	3	414	216	52.1	95.5	49.1	--	1.19	.18	--
Raney nickel, activated											
Mixed	200	3	442	243	47.9	104.5	45.31	.10	0.84	.13	--
NaCl	209	3	471	254	53.0	115.5	47.6	.33	.55		
KCl	212	3	615	340	90.1	137.3	46.7	.07	.64	.33	.03
ZnO	215	3	440	232	52.2	104.4	50.0	.05	.92	.13	.13
$NiCl_2.6H_2O$	216	3	442	237	51.7	103.6	48.4	.14	.82	.18	.16
$NiSO_4.6H_2O$	217	3	420	220	48.0	102.9	48.0	.21	.78	.23	.05
K_2CO_3	218	3	578	309	95.0	126.4	46.2	.31	.72	.22	.06
$ZnBr_2$	219	3	418	224	53.9	96.2	42.6	.18	.79	.10	.08
SnO_2	224	3	395	213	37.7	98.1	44.0	.15	.65	.33	.28
Fe	225	3	367	193	39.1	88.3	45.4	.09	.95	.38	.24

TABLE 2b. - Specific rate of liquid production, carbon gasification, and gaseous heating value production when using various catalysts (Series A)

Test conditions - Unit A: Charge, 10 g pretreated Bruceton coal, 0.5 g catalyst; feed, 5.8 g H_2O/hr + 2000 std cc N_2/hr; approximately 4-hr duration; 300 psig; 850° C

Catalyst	Expt. No.	Product liquid, g/hr/g coal charged	Carbon gasification rates, g/hr/g coal charged	Unit heating value N_2-free product gas, Btu/SCF	Gaseous heating value produced, Btu/hr/cu ft coal charged
No catalyst	167	0.478	89×10^{-3}	353	57,700
Raney nickel, unactivated:					
Sprayed	203	.472	98×10^{-3}	359	80,254
Mixed	197	.501	106×10^{-3}	336	68,712
Raney nickel, activated:					
Mixed	200	.489	107×10^{-3}	322	70,258
NaCl	209	.506	117×10^{-3}	318	74,032
KCl	212	.480	148×10^{-3}	307	93,250
ZnO	215	.490	112×10^{-3}	330	71,718
$NiCl_2.6H_2O$	216	.493	110×10^{-3}	328	71,716
$NiSO_4.6H_2O$	217	.498	108×10^{-3}	328	68,163
K_2CO_3	218	.494	144×10^{-3}	312	89,011
$ZnBr_2$	219	.454	104×10^{-3}	324	66,783
SnO_2	224	.507	98×10^{-3}	326	63,700
Fe	225	.517	94×10^{-3}	339	61,500

TABLE 3a. - Specific rate of gas production when using various catalysts (Series B)

Test conditions - Unit B: Charge, 10 g pretreated Bruceton coal, 0.5 g catalyst; feed, 5.0 g H_2O/hr plus 2000 std cc N_2/hr; approximately 4-hr duration; 300 psig; 850° C

Catalyst	Expt. No.	No. of tests	Total dry gas production rate, N_2-free bases, std cc/hr/g coal charged	Specific production rate of constituent gases, std cc/hr/g coal charged							
				H_2	CO	CO_2	CH_4	C_2H_4	C_2H_6	C_3H_8	C_3H_6
No catalyst	300	3	297	147	37.7	69.9	40.8	0.18	0.72	0.20	0.24
$Ca(OH)_2$	301	3	345	180	32.0	86.2	45.4	.09	.63	.12	.19
Ni_2O_3	302	3	359	189	43.9	80.9	42.8	.07	.74	.73	.50
NiO	303	3	373	194	52.0	82.0	43.9	--	.94	.22	.29
Ni	304	3	366	189	53.6	76.6	46.2	.17	.46	.29	.27
Fe_3O_4	305	3	380	195	60.3	78.0	45.6	.15	.49	.27	.22
CuO	306	3	385	201	56.3	79.9	46.8	.12	.52	.17	.07
MnO_2	307	3	375	193	45.7	90.2	44.9	.10	.79	.10	.15
BaO	308	3	395	202	48.9	97.1	45.5	.13	.73	.15	.13
ZrO_2	309	3	377	192	57.8	80.0	46.2	.12	.88	.05	.12
SrO	310	3	392	203	48.2	91.3	47.6	.15	.76	.15	.15
Bi_2O_3	311	2	390	200	63.9	80.4	44.4	.19	.72	.15	.04
Sb_2O_5	312	2	391	201	63.6	79.7	45.9	.19	.45	.15	.15
MgO	313	3	384	199	48.4	87.7	47.7	.18	.72	.30	.23
PbO_2	314	3	400	210	52.7	89.1	47.7	.08	1.00	.18	.23
MoO_3	315	3	380	202	45.0	86.6	45.5	.03	1.09	.30	.13
TiO_2	316	3	380	197	48.9	85.7	47.2	.33	0.68	.13	.23
CrO_3	317	3	378	194	52.5	84.4	46.1	.07	.79	.07	.15
$LiCO_3$	318	3	439	228	64.9	95.9	49.2	.19	.57	.27	--
V_2O_5	319	3	367	188	47.7	83.5	45.9	.12	.71	.20	.12
Cr_2O_3	320	3	374	184	58.6	83.0	47.4	.57	.57	.10	.12
Pb_3O_4	321	3	400	205	57.2	87.3	49.1	.13	.72	.15	.13
B_2O_3	322	3	394	203	61.0	79.0	47.4	.05	1.59	1.32	.08
Al_2O_3	323	3	380	196	54.6	82.2	46.7	.15	0.61	0.13	.09
CoO	324	4	383	201	48.6	87.0	45.4	.25	.43	.17	.7
Cu_2O	325	6	385	203	53.1	84.4	44.1	.28	.42	.14	.13

TABLE 3b. - Specific rate of liquid production, carbon gasification, and gaseous heating value production when using various catalysts (Series B)

Test conditions - Unit B: Charge, 10 g pretreated Bruceton coal, 0.5 g catalyst; feed, 5.0 g H_2O/hr plus 2000 std cc N_2/hr; approximately 4-hr duration; 300 psig; 850° C

Catalyst	Expt. No.	Product liquid, g/hr/g coal charged	Carbon gasification rates, g/hr/g coal charged	Unit heating value N_2-free product gas, Btu/SCF	Gaseous heating value produced, Btu/hr/cu ft coal charged
No catalyst	300	0.464	81×10^{-3}	350	51,300
$Ca(OH)_2$	301	.447	88×10^{-3}	339	57,700
Ni_2O_3	302	.439	92×10^{-3}	344	60,960
NiO	303	.422	97×10^{-3}	340	62,700
Ni	304	.413	96×10^{-3}	349	63,100
Fe_3O_4	305	.396	100×10^{-3}	345	64,800
CuO	306	.418	99×10^{-3}	344	65,500
MnO_2	307	.406	98×10^{-3}	333	61,700
BaO	308	.417	104×10^{-3}	328	64,050
ZrO_2	309	.405	99×10^{-3}	344	64,200
SrO	310	.417	101×10^{-3}	337	65,200
Bi_2O_3	311	.415	102×10^{-3}	340	65,500
Sb_2O_5	312	.414	102×10^{-3}	343	66,200
MgO	313	.391	100×10^{-3}	342	64,900
PbO_2	314	.397	103×10^{-3}	339	67,000
MoO_3	315	.438	96×10^{-3}	339	63,800
TiO_2	316	.364	99×10^{-3}	342	64,200
CrO_3	317	.398	99×10^{-3}	340	63,400
$LiCO_3$	318	.364	113×10^{-3}	334	72,400
V_2O_5	319	.402	96×10^{-3}	341	61,900
Cr_2O_3	320	.394	102×10^{-3}	345	63,700
Pb_3O_4	321	.410	105×10^{-3}	342	67,600
B_2O_3	322	.399	104×10^{-3}	355	69,200
Al_2O_3	323	.424	99×10^{-3}	342	64,300
CoO	324	.355	98×10^{-3}	336	63,800
Cu_2O	325	.363	98×10^{-3}	336	63,900

TABLE 4. - Increase in the production of methane and hydrogen

Catalyst	Unit	Increase in CH_4, pct	Catalyst	Unit	Increase in H_2 produced, pct
Raney nickel, unactivated spray	A	24	KCl	A	105
$LiCO_3$	B	21	K_2CO_3	A	83
Pb_3O_4	B	20	Raney nickel unactivated spray	A	63
Fe_3O_4	B	18	$LiCO_3$	B	55
MgO	B	17	NaCl	A	53
PbO_2	B	17	Raney nickel activated mix	A	46
SrO	B	17	$NiCl_2 \cdot 6H_2O$	A	43
TiO_2	B	16	PbO_2	B	43
Cr_2O_3	B	16	ZnO	A	40
B_2O_3	B	16	Pb_3O_4	B	39
CuO	B	15	SrO	B	38
ZnO	A	14	B_2O_3	B	38
Al_2O_3	B	14	Cu_2O	B	38
Ni	B	13	CuO	B	37
ZrO_2	B	13	BaO	B	37
Sb_2O_5	B	13	Sb_2O_5	B	37
CrO_3	B	13	MoO_3	B	37
V_2O_5	B	13	CoO	B	37
Raney nickel unactivated mix	A	12	Bi_2O_3	B	36
BaO	B	12	$ZnBr_2$	A	35
MoO_3	B	12	MgO	B	35
$NiCl_2 \cdot 6H_2O$	A	11	TiO_2	B	34
$Ca(OH)_2$	B	11	$NiSO_4 \cdot 6H_2O$	A	33
CoO	B	11	Fe_3O_4	B	33
$NiSO_4 \cdot 6H_2O$	A	10	Al_2O_3	B	33
MnO_2	B	10	NiO	B	32
NaCl	A	9	CrO_3	B	32
Bi_2O_3	B	9	MnO_2	B	31
NiO	B	8	ZrO_2	B	31
Cu_2O	B	8	Raney nickel unactivated mix	A	30
KCl	A	7	Ni_2O_3	B	29
K_2CO_3	A	6	Ni	B	29
Ni_2O_3	B	5	SnO_2	A	28
Raney nickel activated mix	A	4	V_2O_5	B	28
Fe	A	4	Cr_2O_3	B	25
SnO_2	A	1	$Ca(OH)_2$	B	22
$ZnBr_2$	A	-3	Fe	A	16

TABLE 5. - Increase in production of carbon monoxide and gasification of carbon.

Catalyst	Unit	Increase in CO produced, pct	Catalyst	Unit	Increase in carbon gasified, pct
K_2CO_3	A	91	KCl	A	66
KCl	A	81	K_2CO_3	A	62
$LiCO_3$	B	72	$LiCO_3$	B	40
Bi_2O_3	B	69	NaCl	A	31
Sb_2O_5	B	69	Pb_3O_4	B	30
B_2O_3	B	62	BaO	B	28
Fe_3O_4	B	60	B_2O_3	B	28
Cr_2O_3	B	55	PbO_2	B	27
ZrO_2	B	53	Bi_2O_3	B	26
Pb_3O_4	B	52	Cr_2O_3	B	26
CuO	B	49	Sb_2O_5	B	26
Al_2O_3	B	45	ZnO	A	26
Ni	B	42	SrO	B	25
Cu_2O	B	41	$NiCl_2 \cdot 6H_2O$	A	24
PbO_2	B	40	MgO	B	23
CrO_3	B	39	Fe_3O_4	B	23
NiO	B	38	CuO	B	22
BaO	B	30	ZrO_2	B	22
TiO_2	B	30	TiO_2	B	22
CoO	B	29	CrO_3	B	22
MgO	B	28	Al_2O_3	B	22
V_2O_5	B	27	$NiSO_4 \cdot 6H_2O$	A	21
MnO_2	B	21	MnO_2	B	21
MoO_3	B	19	CoO	B	21
Ni_2O_3	B	16	Cu_2O	B	21
SrO	B	15	Raney nickel activated mix	A	20
Raney nickel, unactivated spray	A	8	NiO	B	20
$ZnBr_2$	A	8	Raney nickel unactivated mix	A	19
NaCl	A	7	Ni	B	19
Raney nickel, unactivated mix	A	5	MoO_3	B	19
ZnO	A	5	V_2O_5	B	19
$NiCl_2 \cdot 6H_2O$	A	4	$ZnBr_2$	A	17
$NiSO_4 \cdot 6H_2O$	A	-3	Ni_2O_3	B	14
Raney nickel activated mix	A	-4	Raney nickel, unactivated spray	A	10
$Ca(OH)_2$	B	-15	SnO_2	A	10
Fe	A	-21	$Ca(OH)_2$	B	9
SnO_2	A	-24	Fe	A	6

Admixing of the catalyst with the coal provides better contact between coal and catalyst than does the insertion of catalyzed surfaces into the bed of coal. The superior contact achieved by admixing the catalyst and coal is proven by the higher specific rate of carbon gasification obtained by the admixed Raney nickel (unactivated) in experiment 197 over that of sprayed Raney nickel (unactivated) in experiment 203 (tables 2a and 2b). This is further confirmed analytically by the larger amount of carbon left in the residue in the case of the sprayed Raney nickel catalyst.

Table 2a indicates that the Raney nickel (unactivated) catalyst was more effective in promoting methane production when sprayed on a surface than when it was admixed with the coal charge. Apparently, the process of methane synthesis from CO and H_2 was more effectively promoted by the sprayed Raney nickel (unactivated) catalyst. Another possible reason for the greater production of methane in the case of the sprayed Raney nickel (unactivated) catalyst is that the poorer contact between coal and catalyst resulted in less reforming of methane and other hydrocarbons. Hydrogen production was also greater when the sprayed Raney nickel (unactivated) catalyst was used than when Raney nickel (unactivated) was admixed with the coal.

Effect of Temperature and Steam Rate

Gasification experiments similar to the standard tests were conducted in unit A, except that the reaction temperatures were varied from 650° to 950° C and steam rates used were 1.16 and 5.8 g/hr. The catalyst used was flame-sprayed Raney nickel 65 pct activated. Also, tests were conducted at 750° C and 1.16 g/hr steam rate with sprayed Raney nickel activated and charged wet and at 850° C, and 5.8 g/hr steam rate with sprayed Raney nickel unactivated.

Results of these experiments are presented in figures 2, 3, 4, 5, and 6, where rates of production of methane, hydrogen, carbon monoxide, carbon gasification, and production of total dry gas, respectively, are shown. At the temperatures and steam rates shown in these figures, the presence of the sprayed Raney nickel insert has resulted in a higher production of nearly all the major gases and in a higher carbon gasification than that achieved without catalysts. One exception is in the case of methane production with the activated sprayed Raney nickel at 850° and 950° C for 5.8 g/hr steam rate (fig. 2), when methane production was greater for the uncatalyzed reaction than for the catalyzed reaction. However, a 6-pct increase in methane production was achieved at 850° C and 5.8 g/hr steam rate when the unactivated sprayed Raney nickel was used as compared to when no catalyst was used (fig. 2). The other exception is in the production of carbon monoxide at 950° C and 1.16 g/hr steam rate (fig. 4). In this case, carbon monoxide production was 5 pct lower for the catalyzed reaction than for the uncatalyzed reaction.

In general, effectiveness of the catalyst decreases as temperature is increased. For example, the increases achieved in carbon gasification and in total gas production due to the use of catalyst became smaller as the reaction temperature increased from 750° to 950° C (Figs. 5 and 6). In the 5.8 g/hr steam rate tests, the carbon gasification rate at 750° C was increased by 0.017 g/hr/g coal charged for a 33-pct increase, whereas at 950° C the increase in carbon gasification was negligible at an increment of 0.001 g/hr/g coal charged. Similarly, total gas production was increased 43 pct at 750° C and 10 pct at 950° C.

As shown by the gas production and carbon gasification rates presented in figures 2 through 6, for reaction temperatures of 750° C and higher, the higher steam feed rate of 5.8 g/hr resulted in significantly higher production rates over that achieved at the lower steam rate of 1.16 g/hr.

Repeated Use of Sprayed Raney Nickel Catalyst

To determine the stability of sprayed Raney nickel catalyst, a single insert flame-sprayed with Raney nickel catalyst was subjected to four gasification tests at 750° C, 300 psig, and a steam rate of 1.16 g/hr. The resulting gas production rates are shown in fig. 7; also shown is the base case, with no catalyst inserted in the bed.

Gas production rates presented in figure 7 indicate that the activity of the sprayed Raney nickel catalyst insert decreased rapidly with use. The gas production of the fourth test (17.8 hr service), was only about 10 pct greater than that obtained when no catalyst was used. An extrapolation of the total gas production rate as a function of accumulated service time on one catalyst insert indicates that the catalyst insert would be completely ineffective after about 20 hrs of operation. Considerable flaking-off of the catalyst is apparent; thus the need is indicated for an effective bonding agent or alloying substance that will increase the physical durability of the catalyst. Sulfur compounds gasified from the coal are also suspected of poisoning the nickel catalyst and resulting in the decline in activity with time.

Effect of Extent of Gasification Time

A series of tests were conducted to determine whether catalysts remain effective as the extent of gasification increases. Sprayed Raney nickel inserts and CaO powder were subjected to the standard test conditions of 850° C, 300 psig, 5.8 g/hr steam rate but with gasification times varying from 2 to 8 hrs. The abridged results presented in table 6 show that although the overall rate of gasification decreases with extent of gasification or with the length of time of gasification, the catalysts tested still generally increased the rate of carbon gasification, and the rate of gas production, as indicated by CH_4 production, over that achieved with no catalyst.

TABLE 6. - Effect of extent of gasification time upon overall effectiveness of catalyst

Unit A. - Temperature, 850° C, N_2 flow, 2000 std cc/hr; steam rate, 5.8 g/hr

	CH_4 production		Carbon gasification	
Gasification time, hr	2	6	2	6
Rates with no catalyst	53.3 cc/hr/g	28.6 cc/hr/g	0.087 g/hr/g	0.062 g/hr/g
Rates with CaO	56.9 cc/hr/g	30.7 cc/hr/g	.090 g/hr/g	.062 g/hr/g
Increase due to CaO	7 pct	7 pct	3 pct	0 pct
Rates with sprayed Raney nickel catalyst	70.9 cc/hr/g	38.3 cc/hr/g	.093 g/hr/g	.063 g/hr/g
Increase due to Raney nickel	33 pct	34 pct	7 pct	2 pct

Effect of Residues from Catalytic Gasification

The catalytic effectiveness of ash residues (some contain either residual KCl or K_2CO_3) from total gasification operations were tested and compared with the effectiveness of the fresh additive, K_2CO_3 and KCl.

The gasification residues were prepared by nominally complete steam-gasification of coal in a 1-in diameter electrically heated, vertically mounted stainless-steel reactor. The coal charge consisted of 70 g of pretreated Bruceton coal plus 3.5 g of admixed catalyst; the charge was gasified at 950° to 970° C and atmospheric pressure using a steam feed rate of 45 g/hr. The preparatory gasification step was stopped whenever the flow of dry product gas appeared to cease. Carbon and ash content of the pretreated coal and of residues after total gasification and residue analyses are presented in table 7. The ash analyses show that ash from the catalyzed coals contained significantly larger amounts of potassium than did the ash of uncatalyzed coal.

In the standard screening tests conducted in unit A, the amount of residue admixed with the 10-g coal charge was one-seventh of the residue from the total gasification. Thus, a theoretical equivalent of 0.5 g of the original 3.5 g of catalyst was charged with the coal in the standard screening test. Production rates obtained in the standard screening tests are presented in table 8 for the case of plain pretreated coal, for the cases of addition of catalyst-free residue, pure K_2CO_3 and KCl, and for the addition of residues from the total gasification of the coals admixed with K_2CO_3 and KCl.

The results of the tests on residues from total gasification of coal indicate that potassium compounds, K_2CO_3 and KCL, in the residues retained most of their activity in increasing the production of methane, lost part of their capability of increasing hydrogen production, and inhibited carbon monoxide production. The addition of 1.14 g of catalyst-free residue had very little effect on either methane or total gas production (experiment 220 vs 167).

Pilot-Plant Tests

Tests using additives mixed in the coal feed were conducted in the Bureau's 4-in diameter Synthane gasifier system. In this system, coal is first decaked in a fluidized-bed pretreater and then dropped into the fluidized-bed gasifier for steam-oxygen gasification. The general operation has been described by Forney and others (5).

Ranges of pretreater and gasifier conditions used in this series of tests were as follows:

		Pretreater	Gasifier
Coal rate,	lb/hr	17.8 - 21.2	----- ----
O_2 feed,	scf/lb coal	.31 - .37	2.12 - 3.4
N_2 feed,	scf/lb coal	5.4 - 6.2	----- ----
Steam feed,	scf/lb coal	----- -----	19.6 - 25.4
Av. temp.,	° C	388 515	907 - 945

Pretreater and gasifier pressure was 40 atm.

TABLE 7. - Carbon, ash content, and ash analysis of pretreated Bruceton coal and of residues from total gasification

Gasification conditions: Charge, 70 g pretreated Bruceton coal, 3.5 g of catalyst; water rate, 45 cc/hr 950-970° C, atmospheric pressure

	Expt. No.	Carbon and ash content, pct		Mineral analysis of ash, pct									
		Carbon	Ash	Al_2O_3	CaO	Fe_2O_3	Mgo	P_2O_5	K_2O	SiO_2	Na_2O	SO_3	TiO_2
Charge coal	C-1	74.3	10.6	25.9	1.7	10.8	0.9	<0.01	1.7	54.8	1.6	1.6	1.0
Residues:													
No catalyst	D-1	1.67	98.9	25.1	1.6	14.4	.8	----	1.9	54.7	1.5	---	---
K_2CO_3	D-2	0.47	99.9	19.7	1.1	10.8	.8	----	24.3	41.7	1.6	---	---
KCl	D-3	4.7	95.1	22.2	1.3	12.4	.7	----	13.1	48.5	1.4	0.4	---

TABLE 8. - Specific production and gasification rates resulting from addition of potassium compounds and various gasification residues

Standard test conditions: Unit A: 10 g pretreated Bruceton coal, 0.5 g catalyst (residue charge as indicated); feed 5.8 g H_2O/hr + 2000 std cc N_2/hr; approximately 4-hr duration; 300 psig; 850° C

	Expt. No.	No. of tests	Residue charged		Total dry gas production rate, N_2-free basis, std cc/hr/g coal charged	Specific production rate of constituent gases, std cc/hr/g coal charged							
			No.	Amt., g		H_2	CO	CO_2	CH_4	C_2H_4	C_2H_6	C_3H_8	C_3H_6
No catalyst	167	6			331	166	49.7	70.2	43.7	0.06	0.93	0.24	0.12
Catalyst-free residue	220	3	D-1	1.12	344	180	39.2	79.3	43.9	.07	.81	.33	.21
K_2CO_3	218	3			578	309	95.0	126.4	46.2	.31	.72	.22	.06
K_2CO_3 residue	221	3	D-2	1.41	398	205	45.8	98.1	47.6	.27	.72	.12	.30
KCl	212	3			615	340	90.1	137.3	46.7	.07	.64	.33	.03
KCl residue	222	3	D-3	1.26	370	175	47.8	94.7	48.6	.22	.72	.19	.24

	Expt. No.	Product liquid, g/hr/g coal charged	Carbon gasification rates, g/hr/g coal charged	Unit heating value N_2-free product gas, Btu/SCF	Gaseous heating value produced, Btu/hr/cu ft coal charged
No catalyst	167	0.478	89×10^{-3}	353	57,700
Catalyst-free residue	220	.449	88×10^{-3}	344	58,500
K_2CO_3	218	.494	144×10^{-3}	312	89,000
K_2CO_3 residue	221	.487	104×10^{-3}	332	65,300
KCl	212	.480	148×10^{-3}	307	93,300
KCl residue	222	.469	104×10^{-3}	336	61,300

To alleviate operating difficulties in the pretreater due to unwanted steam condensation, a nitrogen gas feed was substituted for the steam feed of the pretreater.

The coal feed was Illinois No. 6, River King Mine, 20 x 0 mesh size. Additives used were hydrated lime and dolomite, and additive concentrations used in the coal feed mixtures were 5 and 2 pct by weight, respectively. The analyses and sizes of the additives were as follows:

Hydrated lime: minimum CaO, 72 wt pct
minimum MgO, .05 wt pct
95 pct less than 325 mesh, and

Dolomite : $CaCO_3$, 55 wt pct
$MgCO_3$, 44 wt pct
85 pct less than 100 mesh

Results

The effect of the additives upon the percent carbon gasified and percent steam decomposed can be seen in figure 8 for gasification temperature in the 900° to 950° C range. Addition of 5 pct of either hydrated lime or dolomite to the coal resulted in significant increases in carbon gasified. The 5-pct hydrated lime addition resulted in an increase in carbon gasified of about 29 pct at an average gasification temperature of 914° C. Addition of 5 pct dolomite gave a 20-pct increase in carbon gasified at 945° C. These increases compare favorably with the 9-pct increase obtained in the 850° C bench-scale test list using 5-pct addition of hydrated lime.

The 2-pct addition of dolomite did not significantly increase the percent carbon gasification.

Steam decomposition was not significantly increased by either dolomite or hydrated lime at the 2- and 5-pct levels, respectively.

The effect of the additive upon yield of hydrogen and methane in the pilot-plant unit is shown in figure 9. At an average gasification temperature of 914° C, addition of 5 pct hydrated lime in the coal feed increased the hydrogen yield approximately 30 pct from 6.25 to 8.1 scf/lb of moisture-and-ash-free coal feed. A similar increase of 17 pct was obtained by the use of 5 pct dolomite in the coal feed at 945° C average gasification temperature. Such significant increases in hydrogen production were also observed in the bench-scale tests.

The yield of methane was increased significantly by 25 pct at 914° C average gasification temperature through the addition of 5 pct hydrated lime. The use of 5 pct dolomite at 945° C gasification temperature brought no significant increase in methane yield. Failure of catalytic action to increase the yield of methane at the higher gasification temperature (945° C) agrees with the general trend observed on bench-scale tests--that the increase in gas yield due to catalyses decreases with increase in temperature.

The effect of additives upon the yield of carbon monoxide is shown in figure 10. Addition of hydrated lime and dolomite at the 5-pct concentration levels brought respective increases of 23 and 26 pct in yield of carbon monoxide. Figure 11 shows similar increases in product gas yield ($CO + H_2 + CH_4$), for the same additions.

Addition of dolomite at the 2-pct level failed to bring any significant increase in yields of methane, hydrogen, or carbon monoxide.

Other results in pilot-plant operation due to the use of dolomite and hydrated lime at the 2- and 5-pct concentration levels, respectively, are that higher peak temperatures could be tolerated in the gasifier without incurring excessive sintering. With no additive in the coal, if a local temperature in the gasifier exceeded 1000° C, the operation generally would terminate because of excessive sintering or slagging of the char ash. With the additives in the coal, local temperatures as high as 1045° C were encountered with no adverse effect on operations. A similar elevation in sintering temperature induced by the addition of limestone to the feed coal is reported to be a key feature of the high-temperature Winkler process (6).

SUMMARY AND CONCLUSIONS

The overall results of the bench-scale investigation suggest that the use of suitable additives would improve the coal gasification reaction at elevated pressures. In connection with possible benefits to the Synthane process for making high-Btu gas, it appears that appropriate additives could significantly increase production of methane and hydrogen in the gasification step.

The bench-scale study thus far has shown the following:

1. Alkali metal compounds and many other materials such as oxides of iron, calcium, magnesium, and zinc significantly increase the rate of carbon gasification and the production of desirable gases such as methane, hydrogen, and generally carbon monoxide during steam-coal gasification at 850° C and 300 psig.

2. The greatest yield of methane occurred with the use of an insert flame-sprayed Raney nickel catalyst (unactivated), which has a limited life of activity. Significant methane increase resulted from the addition of 5 pct by weight of $LiCO_3$, Pb_3O_4, Fe_3O_4, MgO, and many other materials.

3. The increased gasification resulted whether the extent of coal gasification was small or great.

4. At temperatures above 750° C, catalytic effectiveness decreased with further increase in temperature.

5. Residue from total gasification of coal mixed with potassium compounds still contained a significant concentration of potassium (over 10 pct) and was effective as an additive in increasing production of hydrogen and methane.

Operation of the 4-in diameter Synthane pilot-plant gasifier at 40 atm pressure and average temperature of up to 945° C with dolomite and hydrated lime additives at 5-pct concentration has increased product gas ($CO + H_2 + CH_4$) yield significantly and has increased allowable operating temperatures.

REFERENCES

1. Vignon, L., "Water Gas," Ann. Chim. v. 15, 1921, pp. 42-60.

2. Neumann, B., C. Kroger, and E. Fingas., "Die Wasserdampfzerzetzung an Kohlenstoff mit Aktivierenden Zusatzen," (Steam Decomposition on Carbon with Activating Additives.) Zeitschrift fur anorg. und allgen. Chemie, Band 197, 1931, pp. 321-338.

3. Kroger, C., and Gunter Melhorn, "The Behavior of Activated Bituminous Coal and Low-Temperature Carbonization and Gasification in a Current of Steam," Brennstoff-Chem., v. 19, 1938, pp. 257-262.

4. Kislykh, V.I., and N. V. Shishakov, "Catalytic Effect on Gasification in a Fluidized Bed," Gaz. Prom. v. 5, No. 8, 1960, pp. 15-19.

5. Forney, A. J., W. P. Haynes, and R. C. Corey, "The Present Status of the Synthane Coal-to-Gas Process." 46th Annual Fall Meeting Society of Petrol. Engrs. of AIME, Preprint - SPE 3586, Oct. 3-6, 1971.

6. Meraikib, M. and F. H. Franke, "Carbon Gasification by the High-Temperature Winkler Process." Chem. Eng. Tech. v. 42, 1970, pp. 834-36.

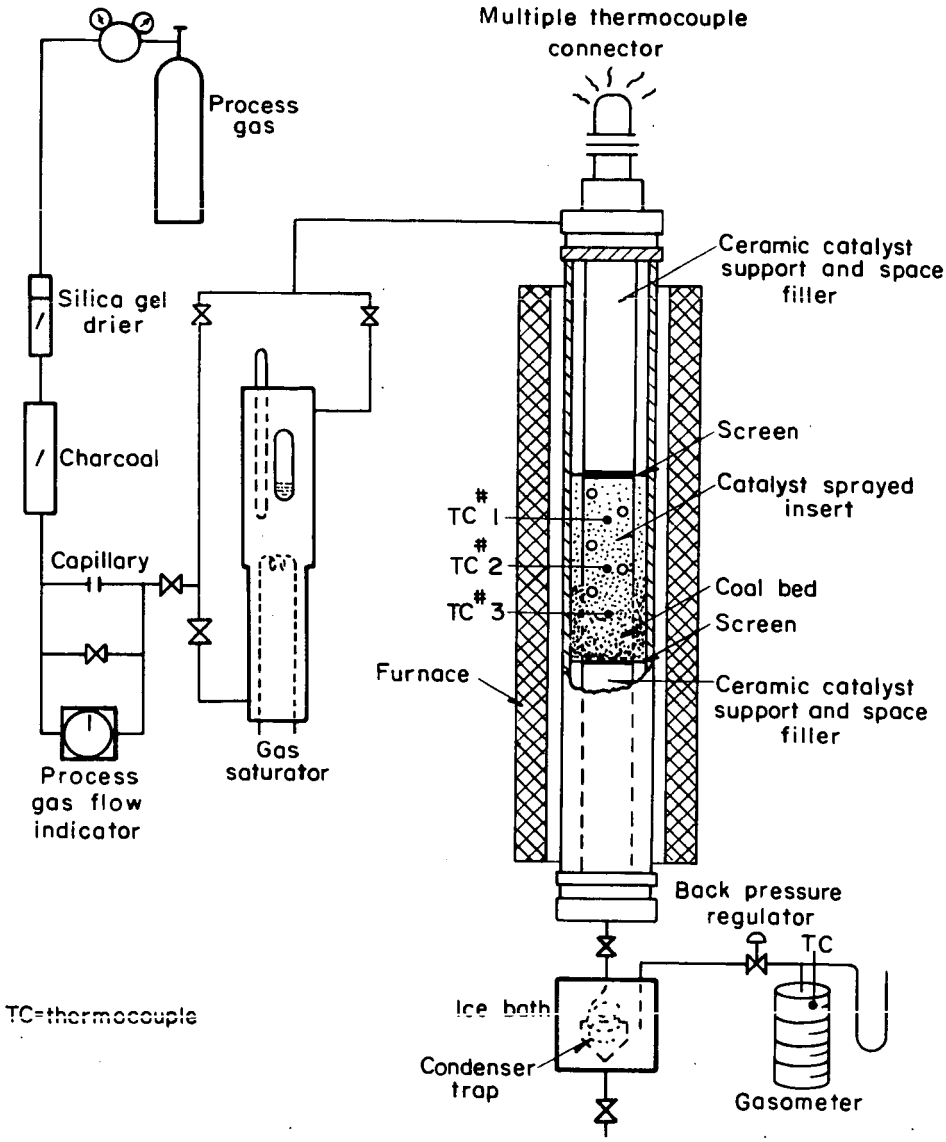

Figure 1.—Apparatus for the catalytic gasification of coal.

L-10298

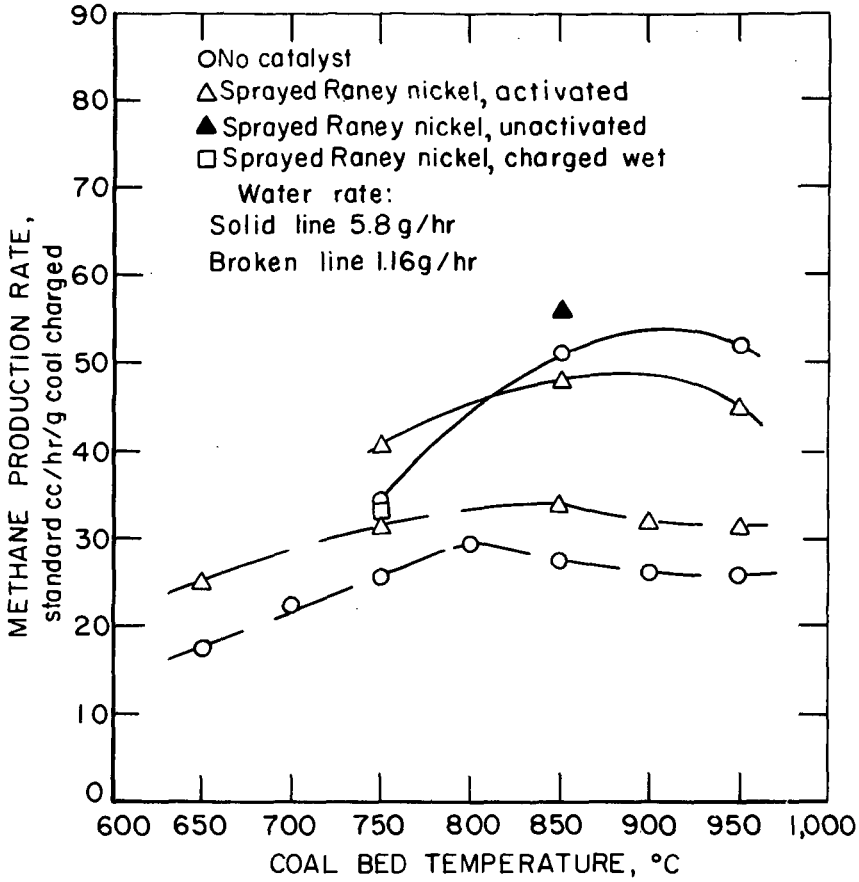

Figure 2-Effect of temperature upon methane production rate using sprayed Raney nickel. Test conditions: pressure, 300 psig; flow, 2,000 standard cc/hour N_2; water, 5.8 and 1.16 g/hour.

4-29-68 L-10556

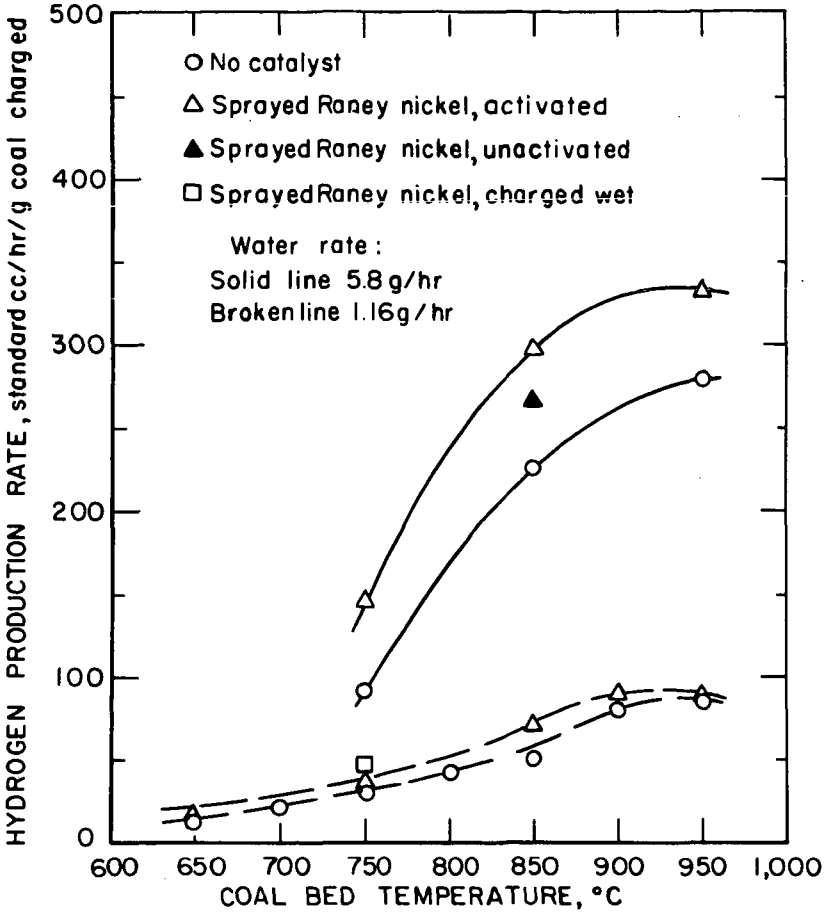

Figure 3. – Effect of temperature upon specific production of hydrogen, using sprayed Raney nickel. Test conditions: pressure, 300 psig, flow, 2,000 standard cc/hour N_2; water, 5.8 and 1.16 g/hour.

4-26-68 L-10551

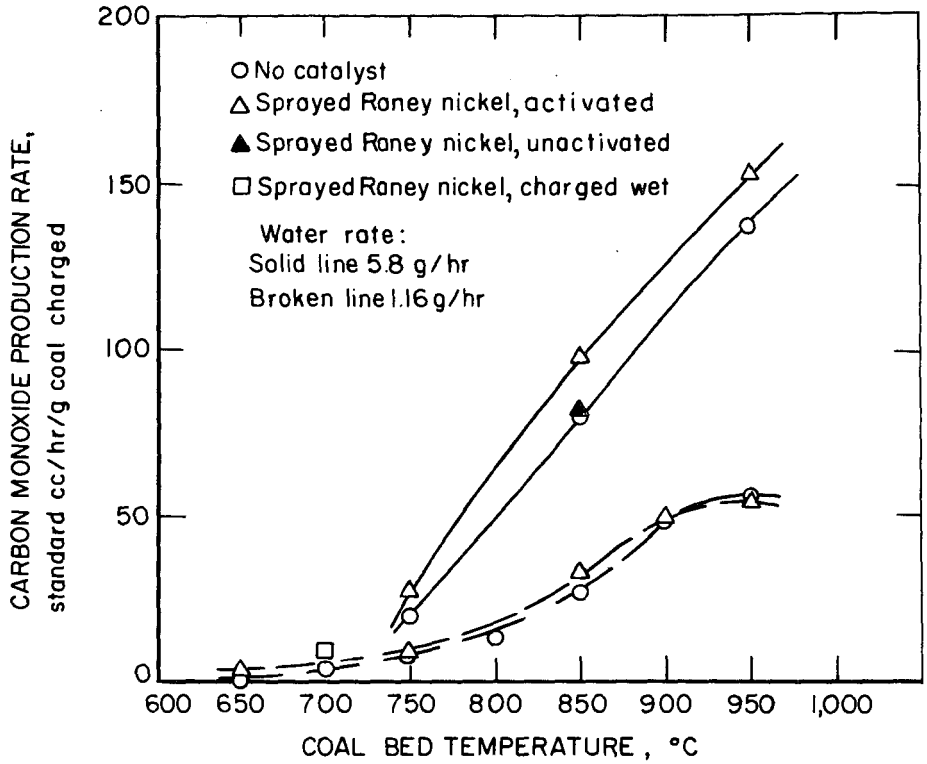

Figure 4.-Effect of temperature upon carbon monoxide production rate using sprayed Raney nickel. Test conditions: pressure, 300 psig; flow 2,000 standard cc/hour N_2; water, 5.8 and 1.16 g/hr.

4-29-68 L-10552

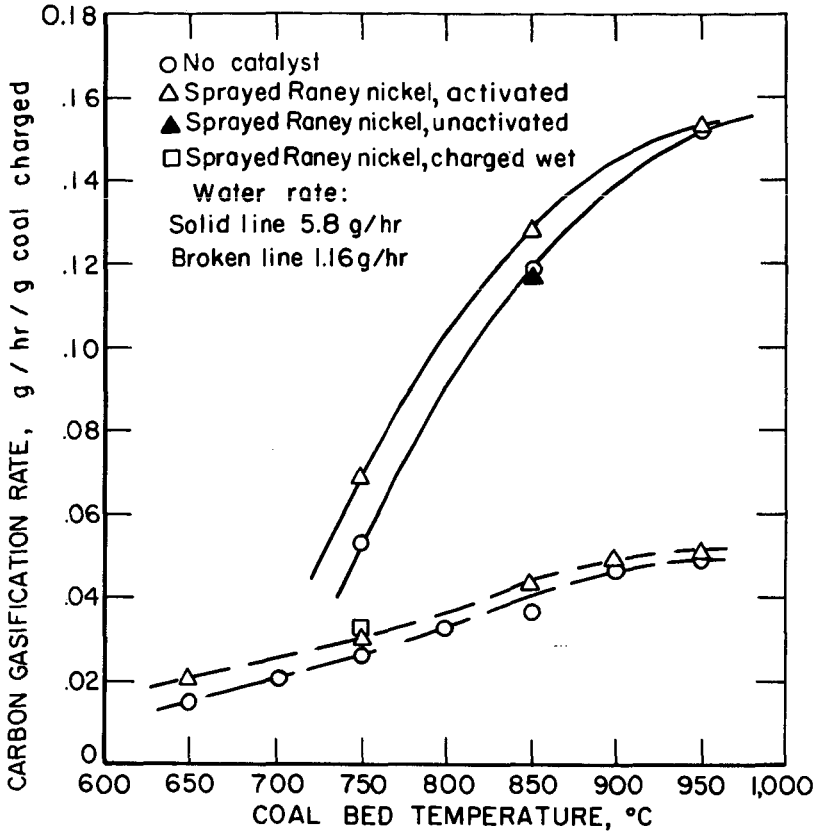

Figure 5.-Effect of temperature upon carbon gasification rate using sprayed Raney nickel. Test conditions: pressure, 300 psig; flow, 2,000 standard cc/hr N_2; water, 5.8 and 1.16 g/hr.

4-30-68 L-10555

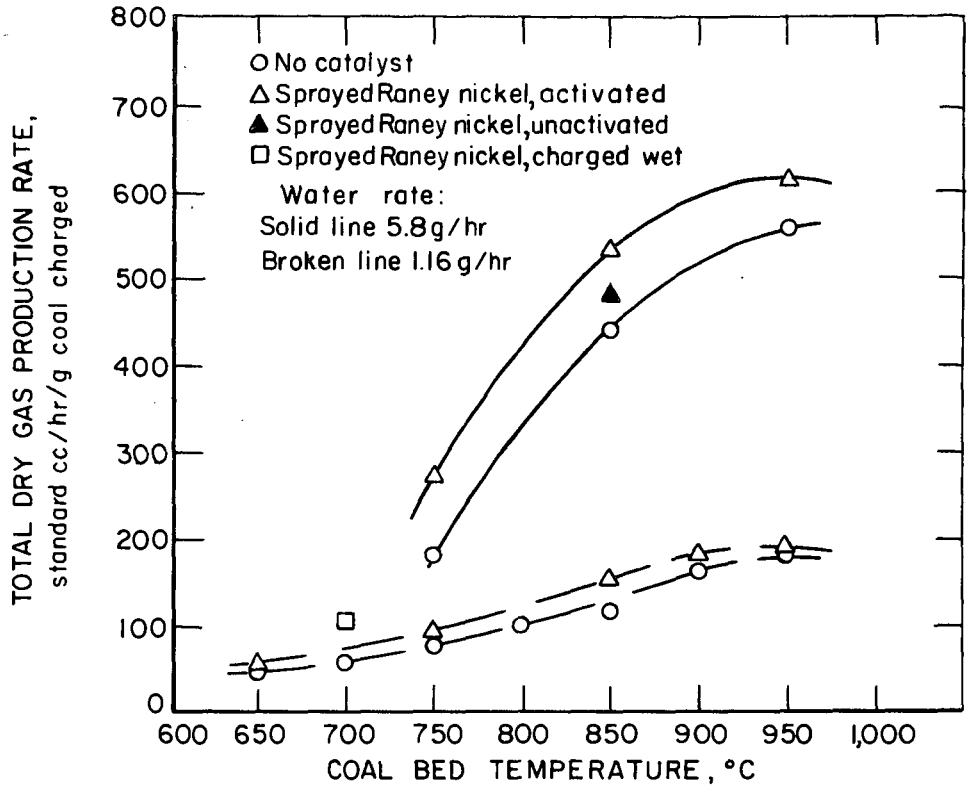

Figure 6.–Effect of temperature upon total dry gas production rate using sprayed Raney nickel. Test conditions: pressure, 300 psig; flow 2,000 standard cc/hour N_2; water, 5.8 and 1.16 g/hour.

4-29-68 L-10553

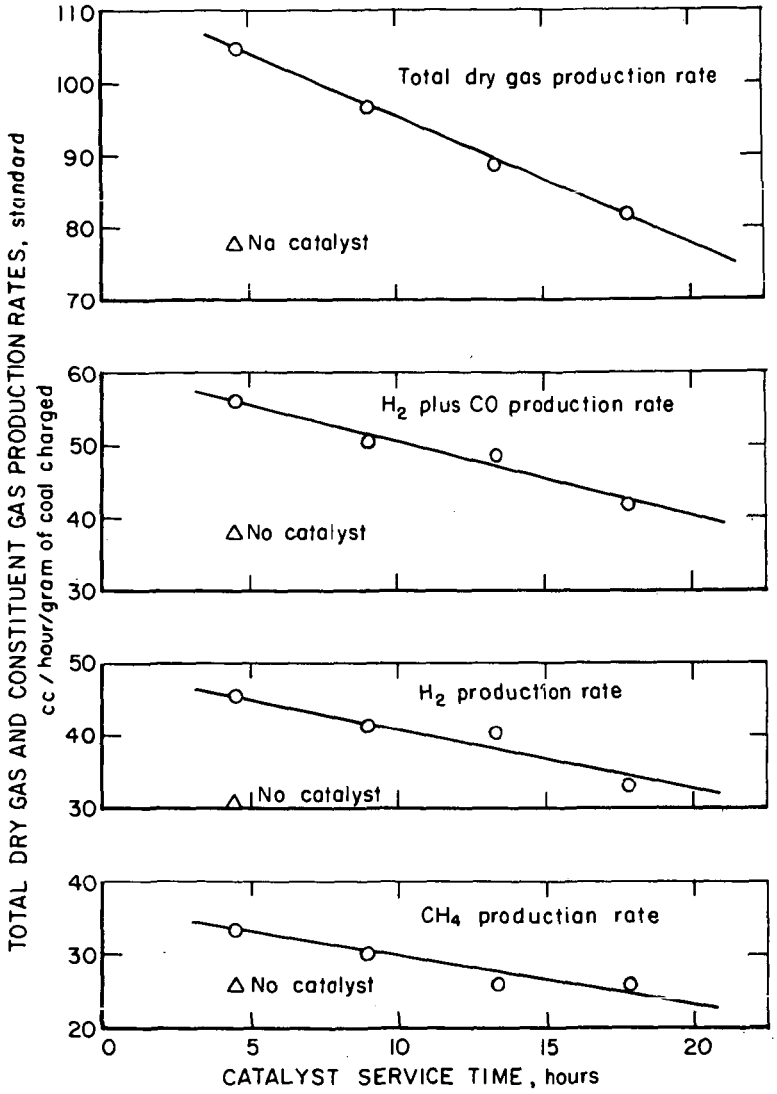

Figure 7.—Effect of catalyst service time upon gas production rates. Test conditions: temperature, 750°C; flow, 2,000 standard cc/hour N_2 and 1.16 g/hour water.

2-17-71 4-25-68 L-10545

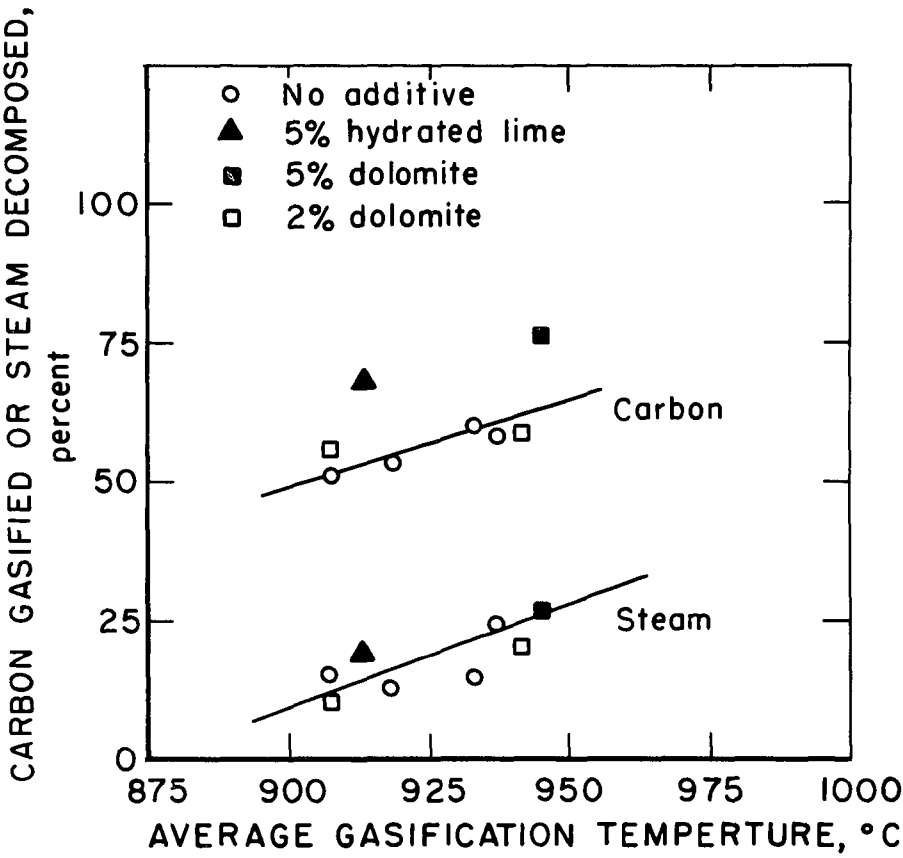

Figure 8– Effect of additives on percent carbon gasified and percent steam decomposition in 4" synthane gasifier operating at 40 atm.

L-13094

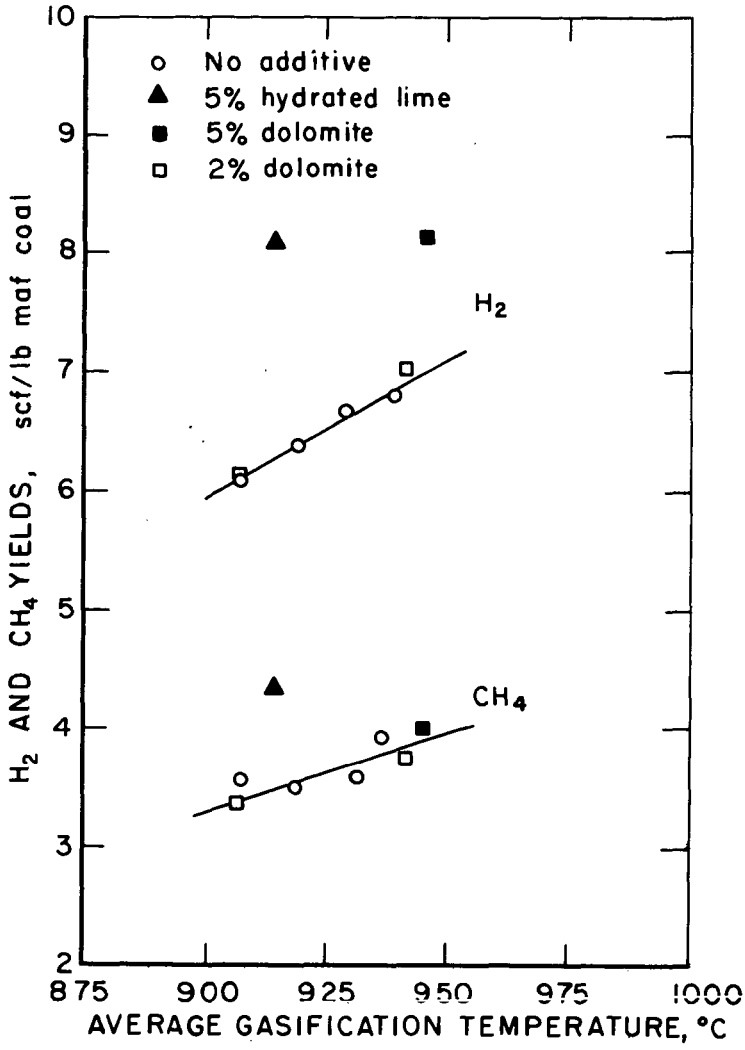

Figure 9 – Effect of additives on yield of hydrogen and methane in 4" synthane gasifier operating at 40 atm.

L-13095

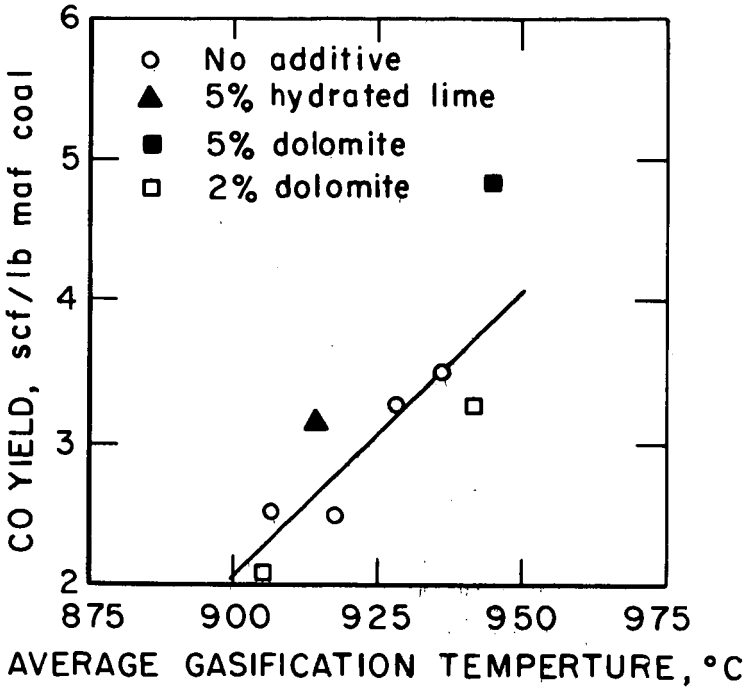

Figure 10- Effect of additives on yield of carbon monoxide in 4" synthane gasifier operating at 40 atm.

L-13096

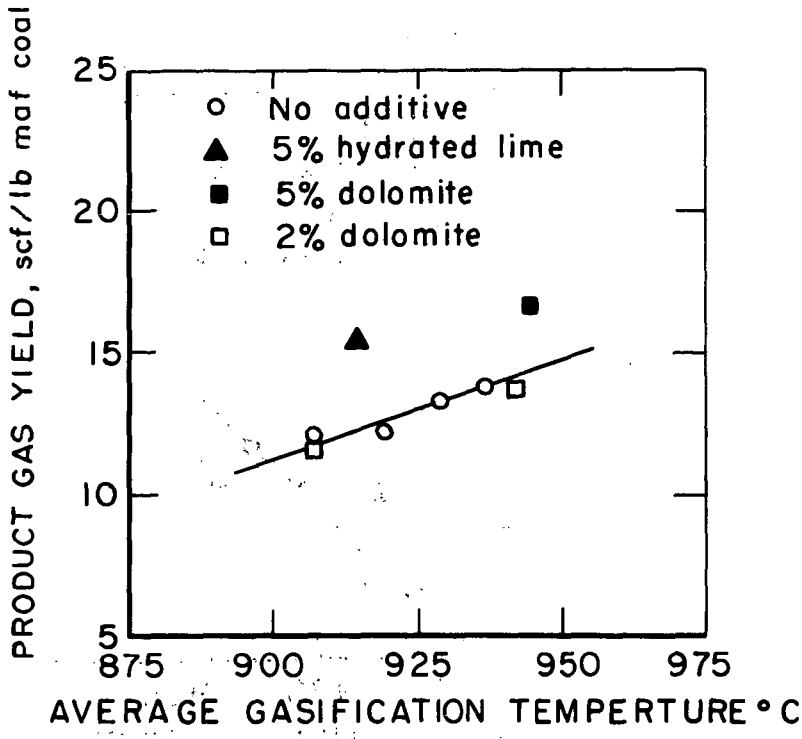

Figure 11 — Effect of additives on yield of product gas ($CO + H_2 + CH_4$) in 4" synthane gasifier operating at 40 atm.

L-13097

Alkali Carbonate and Nickel Catalysis of Coal Steam Gasification

W.G. Willson, L.J. Sealock, Jr., F.C. Hoodmaker,
R.W. Hoffman, J.L. Cox, and D.L. Stinson

Introduction

Considerable work has been carried out on the catalytic effects of various chemicals on the reactions of carbon with with steam. This work is of classic importance in the water gas reactions. In addition, many studies have been made to determine active catalysts for the synthesis of hydrocarbons from carbon monoxide and hydrogen. These two reaction systems are usually carried out at vastly different temperatures.

The carbon-steam reactions represented as $C + H_2O = CO + H_2$ and $C + 2H_2O = CO_2 + 2H_2$ are endothermic, and even in the presence of catalysts the operating temperature range of 800-1100°C is usually employed (1). One of the earliest investigations of catalysts for the carbon-steam reactions carried out by Taylor and Neville (2) was at temperatures from 490-570°C. Their most effective catalyst used with steam and coconut charcoal was potassium carbonate, although sodium carbonate also proved effective. Fox and White (2) demonstrated the catalytic effect of impregnating graphite with sodium carbonate over the temperature range of 750-1000°C.

Kröger (3) found that metallic oxides and alkali carbonates or mixtures catalyzed the carbon-steam reactions. Lewis and co-workers (4) stated that if reactive carbons are catalyzed with alkali carbonates reasonable gasification rates are attainable at temperatures as low as 1200°F. A process which uses molten sodium carbonate to catalyze as well as supply heat for the carbon-steam gasification, has been described (5).

In contrast to the carbon-steam reactions, the synthesis of hydrocarbons from carbon monoxide and hydrogen is usually carried out at temperatures below 450°C (6). The most active catalysts were found to be group VIII metals, mixed with various activating materials (7). A method for the direct production of hydrocarbons from coal-steam systems using multiple catalysts in a single-stage reactor has been described by Hoffman (8). Hoffman and co-workers (9) have described the effects of various commercial nickel methanation catalysts in a single-stage reactor. They stated that nickel was chosen for the methanation catalyst since the yield of hydrocarbons was limited essentially to methane.

It has been found in the single-stage reactor that most effective mixed catalysts which produce methane and carbon dioxide from coal-steam systems ($2C + 2H_2O = CH_4 + CO_2$) are potassium carbonate and nickel. In the single-stage reactor with the nickel methanation catalyst, potassium carbonate and coal mixed and charged, it is necessary in order to get effective contact time, to have the coal to nickel catalyst ratio about 1:1. With this in mind it was deemed significant to determine the optimum ratio of potassium carbonate to coal which would give the best methane production.

The principal objectives of this investigation were (1) to determine the optimum ratio of potassium carbonate to coal, holding the nickel catalyst concentration constant, (2) to determine by analytical methods and X-ray diffraction the form and recoverability of the potassium carbonate in the ash, and (3) to determine the amount of potassium that could be recovered economically.

Experimental Systems

Reactor Design: The gasification of coal was carried out in a one-inch (o.d.) diameter, semi-continuous flow reactor described in earlier papers (8,9). Due to the extremely active nature of the nickel catalyst towards oxygen, the re-reduced nickel catalyst had to be stored under nitrogen atmosphere. In addition, the reactor was charged under a nitrogen atmosphere in a glove box.

Feed Materials: The coal used in all runs was a sub-bituminous coal from Glenrock, Wyoming, ground to 60-100 mesh. An analysis of the coal is given in Table I. Certified A.C.S. anhydrous potassium carbonate was used for the alkali catalyst. This catalyst was approximately the same mesh size as the coal. X-ray studies indicate, however, that some of the potassium carbonate had become hydrated, for example $K_2CO_3 \cdot X(H_2O)$. In addition, a commercial nickel catalyst was employed. The nickel methanation catalyst (Ni-3210) containing approximately 35% by weight nickel on a proprietary support was purchased from the Harshaw Chemical Company. The nickel catalyst was reduced with H_2 at approximately 650°C for 12-18 hours and stored under a nitrogen atmosphere.

Table I. Analysis of Glenrock Coal

	Proximate Analysis	
	As Received	Moisture Free
Moisture (wt %)	12.2	----
Volatile Matter (wt %)	39.6	45.1
Fixed Carbon (wt %)	36.1	41.1
Ash (wt %)	12.1	13.8
Heating Value (Btu/lb)	9140	10410

	Ultimate Analysis	
	As Received	Moisture Free
Hydrogen (wt %)	5.1	4.3
Carbon (wt %)	52.7	60.0
Nitrogen (wt %)	0.6	0.7
Oxygen (wt %)	28.6	20.2
Sulfur (wt %)	0.8	1.0
Ash (wt %)	12.1	13.8

Gas Analysis: Product gas volumes were measured by a calibrated wet test meter. Gas compositions were determined with a Beckman Model GC-5 dual column, dual T.C.D. chromatograph. One detector used a helium carrier with

Pora-Pak Q column and other used an argon carrier with a molecular sieve column. Data reduction was aided by an Auto Lab System IV digital integrator equipped with a calculation module.

Analytical Analyses: The potassium remaining in the coal ash was determined with a Perkin-Elmer model 303 atomic absorption spectrophometer after performing a J. Lawrence Smith ignition on the sample. In order to obtain a total potassium balance it was necessary to recover the potassium that adhered to the nickel catalyst. This was accomplished by digesting the catalyst with acid and determining the potassium by atomic absorption.

The amount of carbonate retained in the ash was calculated from the quantity of carbon dioxide absorbed by ascarite after first scrubbing the gas evolved from the treatment of the ash with a 1:1 hydrochloric acid solution.

In order to determine the amount of potassium that was recoverable by an ambient temperature wash, 1g of ash was washed in 100ml of water for one hour. The amount of potassium in the filtrate was determined by atomic absorption.

X-ray Diffraction: The ground ash was mounted vertically in a General Electric XRD-5 diffractometer. Copper radiation at 50 KVP and 35 MA was used for the analyses. Each scan was started at an angle 2θ of 4° and continued through 70°. The "d" values in angstroms for the recorded X-ray peaks were determined from a copper $K\alpha$ (λ = 1.5418Å) table and compounds were identified from the A.S.T.M. X-ray Powder Data File.

Methodology: Experiments were carried out by charging the reactor with the coal, potassium carbonate and nickel catalyst mixture in a glove box under a nitrogen atmosphere. In those cases where no nickel catalyst was involved the reactor was not charged in the glove box. In all other runs 100g of coal and about 110g nickel catalyst with varying amounts of potassium carbonate were charged. The temperatures on the reactor and super heater were then brought to operating temperatures of approximately 650°C in less than two hours and maintained at the value for the duration of the run. In all cases the length of the run was 7 $^1/_2$ hours and approximately 28 ml of water were added. The product gas was monitored for composition every half hour. The reactor pressure was approximately 30 PSIA which in the pressure required to give an adequate sample to the chromatograph.

All runs were repeated until near duplication of two runs was obtained. The criteria for accepting the duplicate runs were based on the total mass balance and the quality of the gas produced. It was decided that a total mass balance of ±4% was sufficient to insure that there were no major leaks to prejudice the results. To insure that the nickel catalyst was properly reduced and had not oxidized during loading in the mixed catalyst runs, only the runs in which the average gas had a heating value of over 800 Btu/SCF (CO_2 free) were used. There were only two cases out of a total of twelve separate runs with the mixed catalyst where the quality of the gas produced was below 800 Btu/SCF. In both cases the runs were repeated a third time and the criteria for acceptance was met. The amounts of methane and gas produced per gram of coal reported in Table II are volume rated average compositions.

Results and Discussion

Table II contains a summary of the runs selected to determine the optimum amount of potassium carbonate to be mixed with the coal and nickel catalyst. Observations obtained with the single-stage reactor indicate that the initial reaction involved is devolatilization of the coal, followed by cracking and hydrogenation of unsaturated compounds in the presence of the nickel catalyst. This is followed by the carbon-steam reaction.

The first run in Table II was made using only coal and steam, and in this run the gas contained about 0.5% ethylene, 0.7% ethane as well as 4 ml of heavy liquids. In all the remaining runs the nickel catalyst was present, and in no case was any hydrocarbon heavier than methane detected. Methane and carbon dioxide were the major components, with hydrogen averaging between 10-14% and the carbon monoxide usually below 2.0% in the product gas. In run No. 2 only the nickel catalyst was employed. It more than tripled the methane production,while it only increased the total gas product by about 20%. This tends to indicate that a substantial quanity of the methane produced is derived from cracking and hydrogenating unsaturated compounds.

Figure 1 shows a plot of total gas production, as well as the methane production versus mass of potassium carbonate charged per 100g of coal. In both cases the dashed line indicates the runs were neither alkali or nickel

Table II Experimental Data for the Gasification Runs *

Run Number	1	2	3	4	5	6	7
K_2CO_3(g)	0.	0.	15.	20.	30.	45.	60.
Ni-3210(g)	0.	115.	111.	111.	111.	113.	114.
cm^3CH_4/g Coal	51.	185.	225.	281.	266.	232.	234.
cm^3Gas/g Coal	382.	453.	481.	612.	603.	493.	524.
Total Mass Recovery (wt %)	103.1	97.9	98.9	103.0	98.9	96.0	97.9
Total K Recovery (wt %)	____	____	94.2	105.7	105.9	95.0	98.7
K Recovery by Wash (wt %)	____	____	66.2	79.9	85.8	89.0	90.0
K Insoluble in Wash (g)	____	____	2.9	2.3	2.4	2.8	3.4
CO_3 Recovery (%)	____	____	97.7	101.2	104.1	101.8	104.8

*All runs were made at ~30 PSIA and an average temperature of ~650°C.

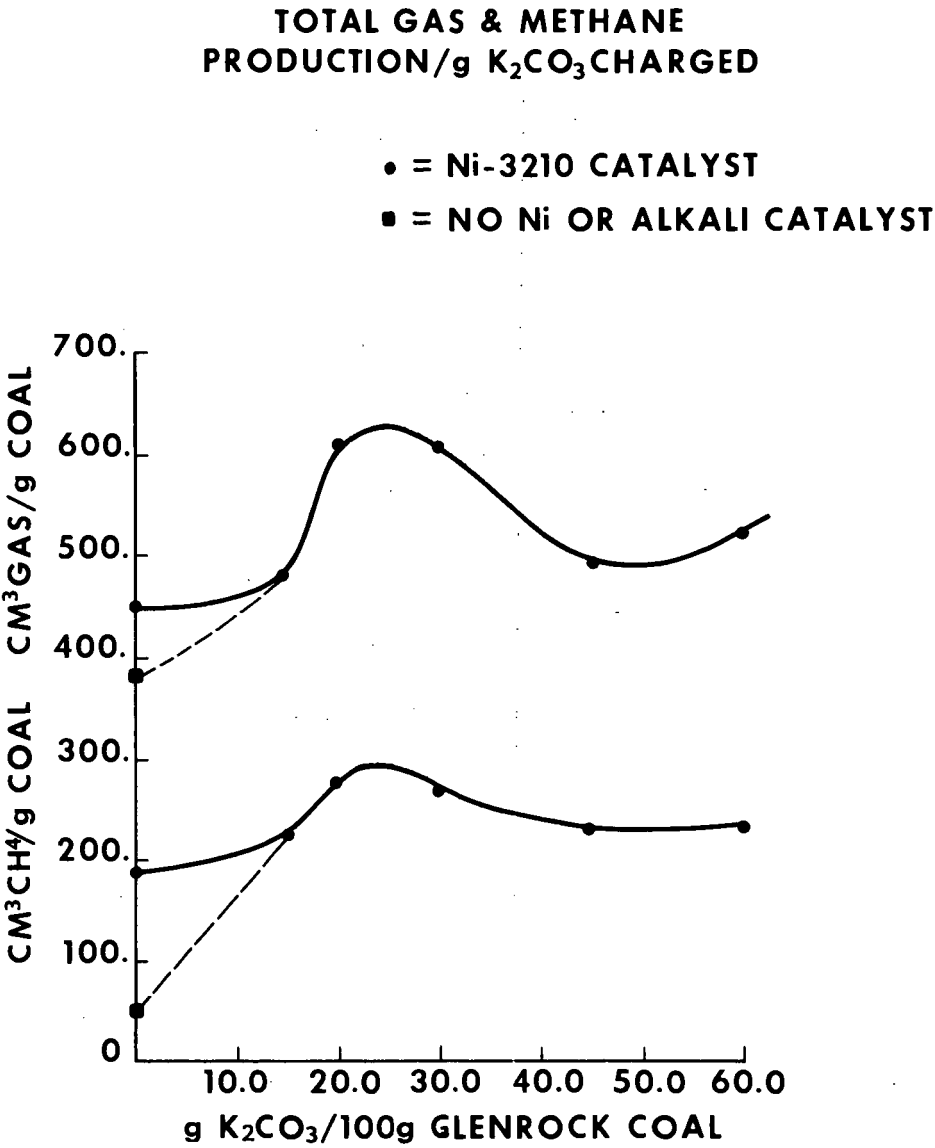
TOTAL GAS & METHANE
PRODUCTION/g K_2CO_3 CHARGED
• = Ni-3210 CATALYST
▪ = NO Ni OR ALKALI CATALYST
700.
600.
500.
400.
300.
200.
100.
0
CM^3CH^4/g COAL
CM^3GAS/g COAL
10.0
20.0
30.0
40.0
50.0
60.0
g K_2CO_3/100g GLENROCK COAL

Fig. 1

catalyst were present. These figures show that for the single-stage reactor, using a sub-bituminous coal at about 650°C, the optimum methane as well as gas production is obtained using between 20-25g of potassium carbonate per 100g of coal. Addition of more than 30g of potassium carbonate is detrimental to the methane production as well as total gas production. This decrease in production is readily apparant when the potassium carbonate has been increased to 45g.

Table II also contains the analytical results for potassium recovery and carbonate recovery. The total potassium recovery by the ignition method was satisfactory, giving deviations of ±6%. Potassium recovered in the wash solution varied from about 66 to 90%. This shows that between 2.3 - 3.4g of potassium are forming compounds that are insoluble in water at ambient temperatures. It is of interest to note that the least amount of insoluble potassium was obtained when the optimum amount of potassium carbonate was used. The carbonate recovered from the ash was good, giving a deviation of only ±5%.

Although the X-ray scan ran from an angle 2θ of 4-70°, the majority of the peaks of interest fell in the range of 20-44°. Table III compares "d" spacings and intensities of X-ray diffraction peaks from 20-44° 2θ for the published data on the hydrated potassium carbonate ($K_2CO_3.1\frac{1}{2}H_2O$) and silicon dioxide, with the potassium carbonate as received and the ashes from the runs containing 0, 20, 45, and 60g of potassium carbonate respectively. The "d" spacings and intensities of the potassium carbonate as received and of the ashes containing potassium carbonate do not correspond exactly to the published anhydrous or hydrated forms of potassium carbonate. For example, the published A.S.T.M. data shows the major peak for $K_2CO_3.1\frac{1}{2}H_2O$ (intensity 100) has a "d" spacing of 2.72Å, whereas the analyzed samples have major peak "d" spacings of 2.77Å for the ashes and 2.79Å for the potassium carbonate as received. It is believed that the analyzed form of the potassium carbonate as well as that in the ash is a partially hydrated compound.

Figure 2 shows the X-ray diffraction pattern for the potassium carbonate as received. Only the peaks with question marks are unidentified peaks. The peaks unlabelled correspond most nearly to those published for $K_2CO_3.1\frac{1}{2}H_2O$. The ash from the reactor run containing no potassium carbonate is shown in figure 3. It displays only silicon dioxide and some unidentified peaks. The ashes from runs using 20, 45, and 60g of potassium carbonate with 100g

Table III. Comparison of d Spacings and Relative Intensities for X-ray Diffraction Peaks from 20°-44° 2θ

$K_2CO_3 \cdot 1\frac{1}{2}(H_2O)$ ASTM 11-655		SiO_2 ASTM 5-0490		K_2CO_3 as received observed values			Ash with no K_2CO_3 observed values			Ash from 20g K_2CO_3 Run observed values			Ash from 45g K_2CO_3 Run observed values			Ash from 60g K_2CO_3 Run observed values		
				$K_2CO_3 \cdot x(H_2O)$		unidentified	SiO_2		unidentified	$K_2CO_3 \cdot x(H_2O)$		unidentified	$K_2CO_3 \cdot x(H_2O)$		unidentified	$K_2CO_3 \cdot x(H_2O)$		unidentified
d(1)	I/I_1(2)	d	I/I_1	d	I/I_1	d	d	I/I_1	d	d	I/I_1	d	d	I/I_1	d	d	I/I_1	d
-----	---	4.26	35	----	---	----	4.26	24	----	----	---	----	----	---	4.25	----	---	----
3.86	5	----	---	3.86	9	----	----	---	----	----	---	----	----	---	----	----	---	----
-----	---	----	----	----	---	----	----	---	----	----	---	3.71	----	---	----	----	---	----
-----	---	----	----	----	---	----	----	---	3.51	----	---	----	----	---	----	----	---	----
3.46	20	----	---	3.45	16	----	----	---	----	3.45	39	----	3.45	29	----	----	---	----
3.35	7	----	---	3.40	16	----	----	---	----	3.35	61	----	3.34	24	----	3.34	28	----
-----	---	3.343	100	----	---	----	3.35	100	----	----	---	----	----	---	----	----	---	----
3.31	20	----	---	3.30	11	----	----	---	----	3.30	48	----	----	---	----	----	---	----
-----	---	----	---	----	---	----	----	---	----	----	---	3.19	----	---	----	----	---	----
3.15	3	----	---	----	---	----	----	---	----	----	---	----	3.12	38	----	3.13	22	----
----	---	----	---	----	---	----	----	---	----	----	---	3.10	----	---	----	----	---	----
3.01	30	----	---	3.00	40	----	----	---	----	3.01	71	----	3.01	50	----	3.01	43	----
3.00	30	----	----	2.98	32	----	----	---	----	----	---	----	----	---	----	----	---	----
2.906	20	----	---	2.90	7	----	----	---	----	2.90	91	----	2.90	48	----	2.90	32	----
2.783	65	----	---	2.83	50	----	----	---	----	2.83	71	----	2.82	73	----	2.82	41	----
2.767	75	----	---	2.79	100	----	----	---	----	2.77	100	----	2.77	100	----	2.77	100	----
2.742	100	----	---	2.75	65	----	----	---	----	2.74	86	----	2.75	80	----	2.75	88	----
-----	---	----	---	----	---	2.62	----	---	----	----	---	2.63	----	---	2.629	----	---	2.63
-----	---	----	---	----	---	----	----	---	2.57	----	---	----	----	---	----	----	---	----
2.550	15	----	---	2.54	8	----	----	---	----	----	---	----	----	---	----	2.54	12	----
-----	---	----	---	----	---	----	----	---	----	----	---	2.49	----	---	----	----	---	----
-----	---	2.458	12	----	---	----	2.46	14	----	----	---	----	----	---	----	----	---	----
-----	---	----	---	----	---	2.38	----	---	----	----	---	----	----	---	----	----	---	----
-----	---	----	---	----	---	----	----	---	----	----	---	2.36	----	---	----	----	---	----
2.327	25	----	---	2.33	23	----	----	---	----	2.32	34	----	2.32 B	20	----	2.33	28	----
2.304	11	----	---	2.30	26	----	----	---	----	----	---	----	----	---	----	2.31	24	----
-----	---	2.282	12	----	---	----	----	---	----	----	---	----	----	---	----	----	---	----
2.267	15	----	---	----	---	----	----	---	----	----	---	----	2.26	18	----	2.26	18	----
2.259	15	----	---	2.26	17	----	----	---	----	----	---	----	----	---	----	----	---	----
-----	---	2.237	6	----	---	----	----	---	----	----	---	----	----	---	----	----	---	----
2.228	15	----	---	2.23	12	----	----	---	----	----	---	----	----	---	----	2.23	15	----
2.183	40	----	---	2.18	23	----	----	---	----	----	---	----	2.18	19	----	2.18	27	----
-----	---	----	---	----	---	----	----	---	----	----	---	2.16	----	---	----	----	---	----
-----	---	2.128	9	----	---	----	----	---	----	----	---	----	----	---	----	----	---	----
-----	---	----	---	----	---	2.11	----	---	----	----	---	----	----	---	----	----	---	2.11
-----	---	----	---	----	---	----	----	---	----	----	---	2.08	----	---	----	----	---	----

(1) Interplanar spacings

(2) Relative intensities

X-RAY DIFFRACTION PATTERN OF K_2CO_3 AS RECEIVED

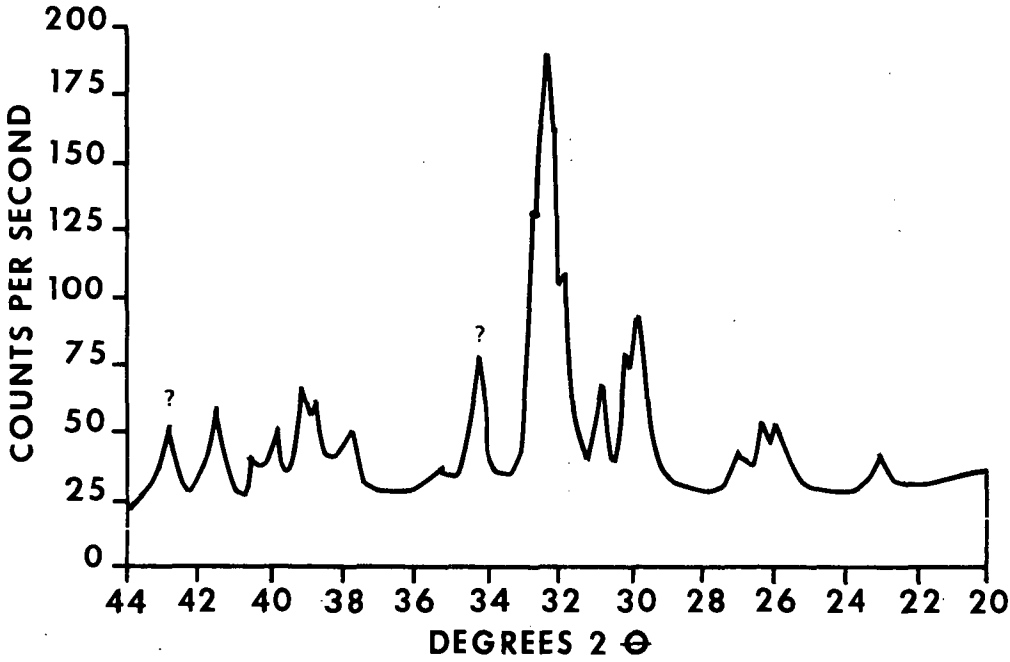

Fig. 2

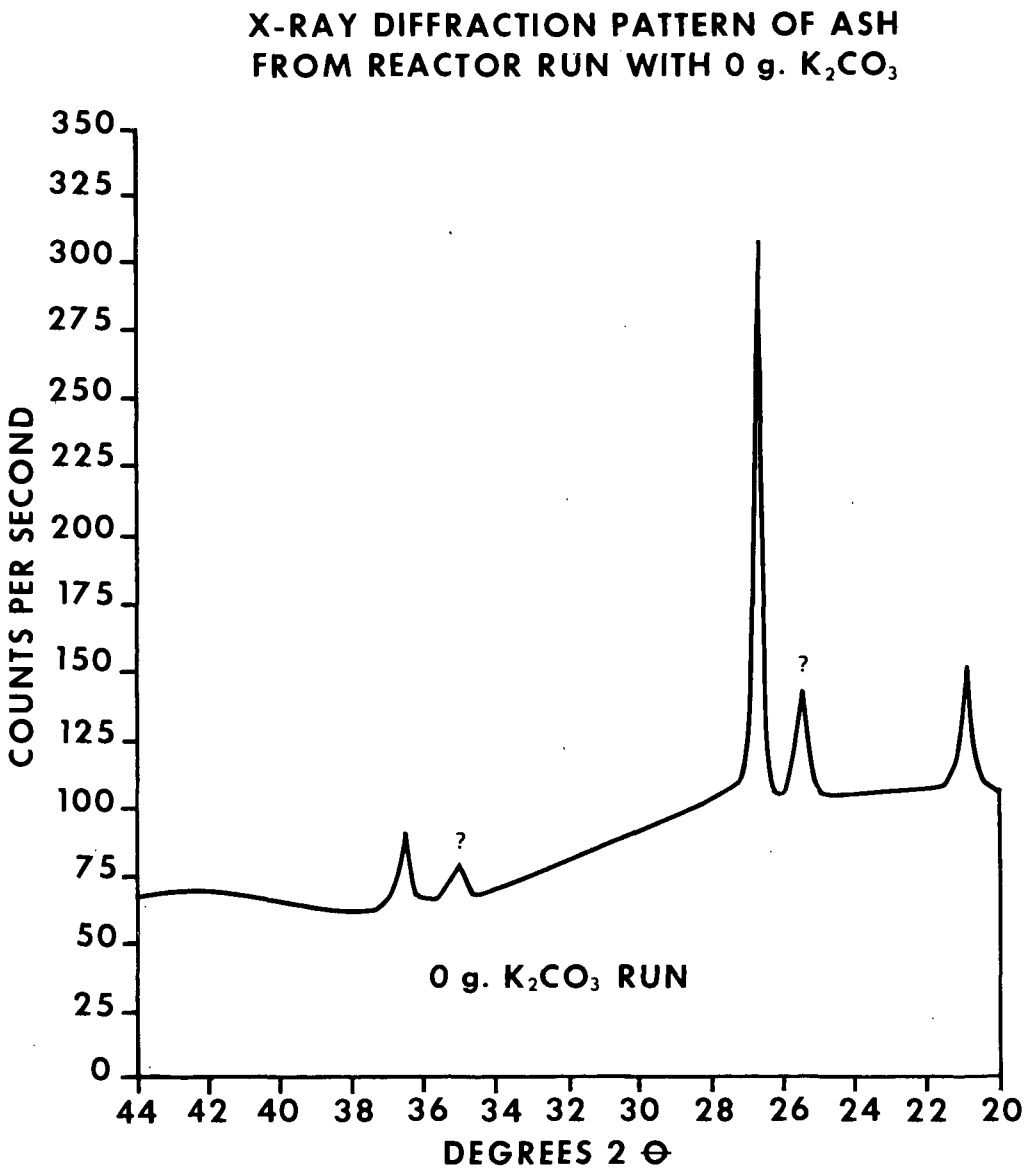
X-RAY DIFFRACTION PATTERN OF ASH
FROM REACTOR RUN WITH 0 g. K_2CO_3
COUNTS PER SECOND
350
325
300
275
250
225
200
175
150
125
100
75
50
25
0
?
?
0 g. K_2CO_3 RUN
44 42 40 38 36 34 32 30 28 26 24 22 20
DEGREES 2 Θ

Fig. 3

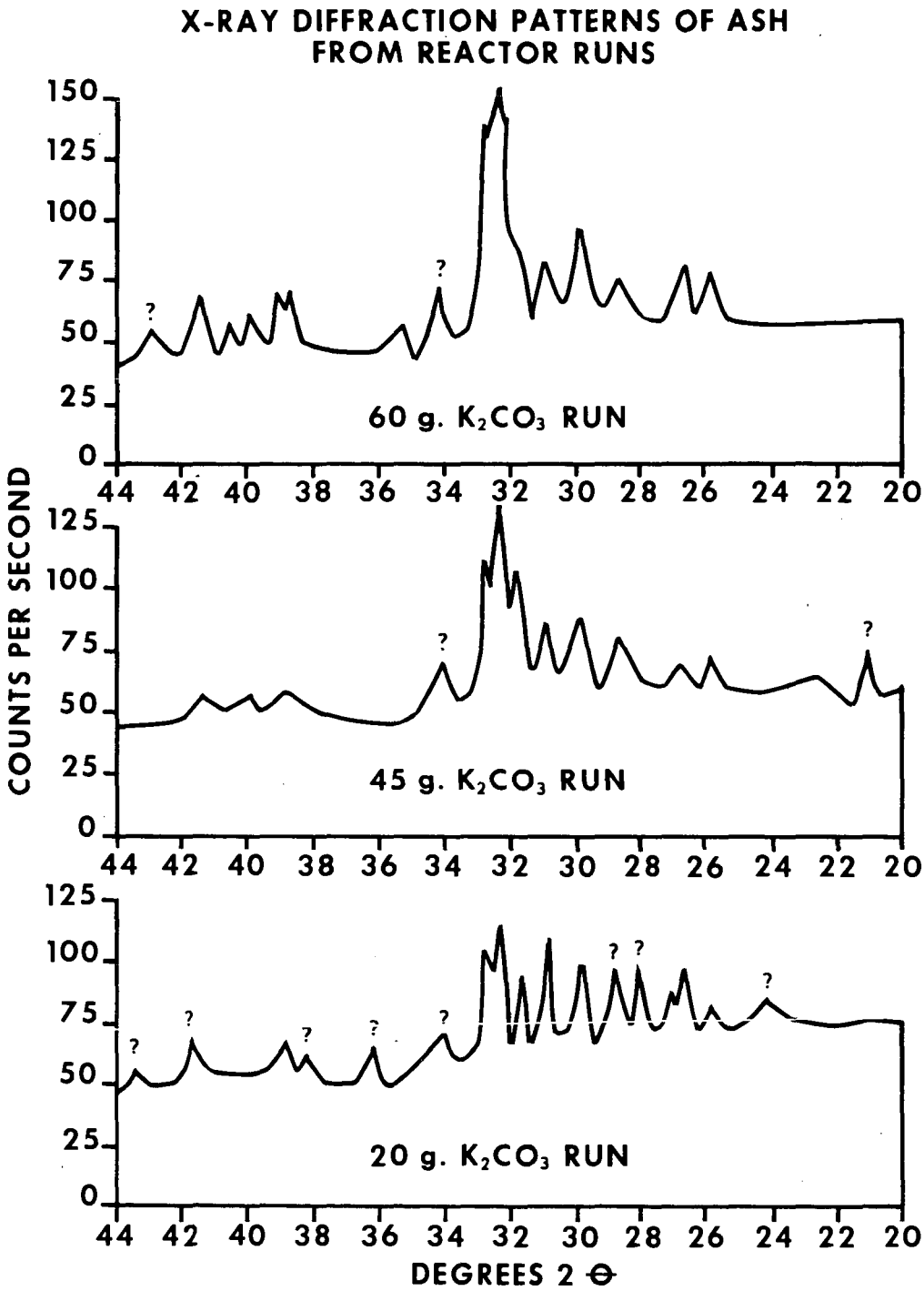
X-RAY DIFFRACTION PATTERNS OF ASH
FROM REACTOR RUNS
COUNTS PER SECOND
60 g. K_2CO_3 RUN
45 g. K_2CO_3 RUN
20 g. K_2CO_3 RUN
DEGREES 2 θ

 Fig. 4

of coal charged are shown in figure 4. It indicates that the amount of potassium carbonate remaining in the ash is proportional to the amount charged. This is best observed by noting the changes in the intensities of the major potassium carbonate peaks between 32-33° 2θ. Again the peaks that are unidentified are noted with question marks. Comparison of "d" values in table II indicate that the form of the potassium carbonate remains essentially unchanged after the reaction.

Conclusions

The investigations thus far indicate that it is possible in a single-stage reactor, by using a mixed catalyst of potassium carbonate and a nickel catalyst, to react coal and steam principally to methane and carbon dioxide at low pressure and temperatures of approximately 650°C. Under these conditions the optimum amount of potassium carbonate for maximum methane production is between 20-25% the mass of the coal. X-ray diffraction studies indicate that the form of the potassium carbonate remaining in the ash is essentially the same as that charged. At the observed optimum value of 20g of potassium carbonate to 100g of coal nearly 80% of the potassium is recoverable by a one hour wash with water at room temperature.

Selected References

1. Fox, D.A., and White, A.H., Ind. Eng. Chem., 23, 259-266,(1931).

2. Taylor, H.S., and Neville, H.A., J. Am. Chem. Soc., 43, 2055-2071, (1921).

3. Kroger, C., Angew. Chem., 52, 129-139,(1939).

4. Lewis, W.K., Gilliland, E.R., and Hipkin, H., Ind. Eng. Chem., 45, 1697-1703, (1953).

5. Lefrancois, P.A., Barclay, K.M., and Skaperdas, G.T., "Fuel Gasification," 69, 64-80, (1967).

6. Storch, H.H., "Chemistry of Coal Utilization," Volume II, H.H. Lowry, ed., 1797-1800, Wiley, New York (1945).

7. Storch, H.H., ibid, 1818-1824.

8. Hoffman, E.J., Preprints, Div. of Petrol. Chem., A.C.S., 16, No. 2, C 20 (1971).

9. Hoffman, E.J., Cox, J.L., Hoffman, R.W., Roberts, J.A. and Willson, W.G., Preprints, Div. of Fuel Chem., A.C.S., 16, No. 2, 64-67,(1972).

CATALYZED HYDROGASIFICATION OF COAL CHARS

N. Gardner, E. Samuels, K. Wilks

INTRODUCTION

The reaction of hydrogen with coal and coal chars to produce gaseous hydrocarbons (hydrogasification) has received considerable attention for at least thirty-five years, since Dent in 1937 first reported on the hydrogasification synthesis[1]. The reaction proceeds in two steps. In the initial stage, reaction rates are extremely rapid as the volatile matter and more reactive components of the coal are hydrogenated. Subsequent rapid hydrogenolysis of the higher homologs formed yields methane. In the second stage of the reaction, the structure of the remaining carbon char is more graphitic in character, resulting in a much slower hydrogasification reaction. It is the catalysis of the slow, second stage of the hydrogasification reaction that we have initiated a study of at Case Western Reserve University.

There have been numerous reports and patents on the catalysis of a similar reaction--the liquid phase hydrogenation of coal to liquid and gaseous products. Hydrogenation reactions are generally carried out at high pressures (several hundred atmospheres) and low temperatures (400 to 500°C) where the hydrocarbon products formed are substantially liquid. The ability of tin-halogen compounds, alkali metals[2], and many other materials to catalyze the coal hydrogenation reactions is well known. Although the reaction is carried out in conditions where coal has undergone agglomeration and liquifaction,

the method of contacting catalyst and coal particles has a strong influence on reaction rate. For example, the addition of powdered ferrous sulfate to coal particles has almost no effect on the hydrogenation rate[3]. Impregnation of the coal by immersing it in aqueous solutions of ferrous sulfate, followed by oven drying, resulted in a sharp increase in hydrogenation rate with high productions of asphalt and oil. Impregnated nickelous chloride, stannous chloride, and ammonium molybdate show similar increases in catalytic activity as compared to powders of the same materials[4].

In contrast to hydrogenation reactions, for the hydrogasification of coal chars, much less is known about the catalytic activity of materials and the dependency of catalyst contacting techniques. Alkali carbonates, one to ten percent by weight, have been shown to catalyze the hydrogasification of coals and cokes at temperatures of 800-900°C[5]. The suggested mechanism was that adsorption of the alkalies by carbon prevented graphitization of the surface. Zinc and tin halides have been shown to be effective hydrogasification catalysts. There is, however, little kinetic information on any of the catalyzed hydrogasification reactions.

There have been extensive studies on the ability of particulate metals and metal salts to catalyze the reactions of graphitic carbon with oxygen and carbon dioxide. For example, colloidal iron on Ticonderoga graphite reduces the activation energy for the carbon-oxygen reaction from 46 kcal/mole to 10 kcal/mole. A seven percent iron deposit impregnated from solution on sugar char reduced the

activation energy from 61.2 kcal/mole to 22.8 kcal/mole for the carbon-carbon dioxide reaction. In addition, dispersions of metals in carbon have been prepared by carbonization of polymers containing metal salts. The dispersions are catalytically active in the gasification reactions of carbon dioxide and oxygen. The mechanism of the substantial reduction in activation energy is not clear although a large amount of superfluous, quantitative information has been obtained. Two types of mechanisms have been proposed, oxygen-transfer and electron-transfer. In the oxygen-transfer mechanism the catalyst is presumed to assist the dissociation of molecular oxygen to chemisorbed atomic oxygen which then reacts with the carbon surface. Electron-transfer mechanisms involve the π electrons of graphitic carbon and the vacant orbitals of the metal catalysts. The catalytic effect presumably results from the altered electronic structure of the surface carbon atoms.

In contrast to the wealth of information on catalyzed hydrogenation of coal, and the catalyzed oxidation reactions of carbon by oxygen and carbon dioxide, little is known about catalyzed hydrogasification reactions as to the ability of materials to serve as catalysts. Also little is known about the kinetics and mechanisms of these reactions. We have initiated a kinetic study of catalyzed hydrogasification reactions using a high temperature, high pressure, recording balance. A thermobalance is particularly useful in gas-solid reactions because the weight of relatively small solid samples can be continuously measured. Direct kinetic analysis of the weight loss curves are straightforward.

II. EQUIPMENT AND PROCEDURES

The high pressure thermobalance is very similar to the balance described by Feldkirchner and Johnson[6]. The thermobalance was designed to operate isothermally at temperatures up to 1000°C and at hydrogen pressures up to 2000 psi. Details of the balance are shown in Figure 1, and a schematic diagram of the system is shown in Figure 2.

The reactor tube was constructed of Haynes 25 superalloy. The mass transducer is a Statham, Model UC 3, attached to a balance arm (Micro-scale accessory UL 5) and has a full scale range of 6 grams.

The sample is lowered into the reaction zone by an electric motor driven windlass at a rate of about one inch per second. The position of the sample in the reactor is obtained by utilizing a potentiometric technique. A small ten turn potentiometer is coupled directly to the windlass. Temperatures in the reactor are measured by stainless steel encased chromel-alumel thermocouples, the closest one to the sample being located 1/4" below the sample. Hydrogen flow rates were controlled ± 5 percent over the range 10 to 40 SCF/hr. Gas analysis was obtained by splitting a portion of the gas product stream to an infrared detector, where methane content was continuously measured, and a gas chromatograph where total gas composition was determined.

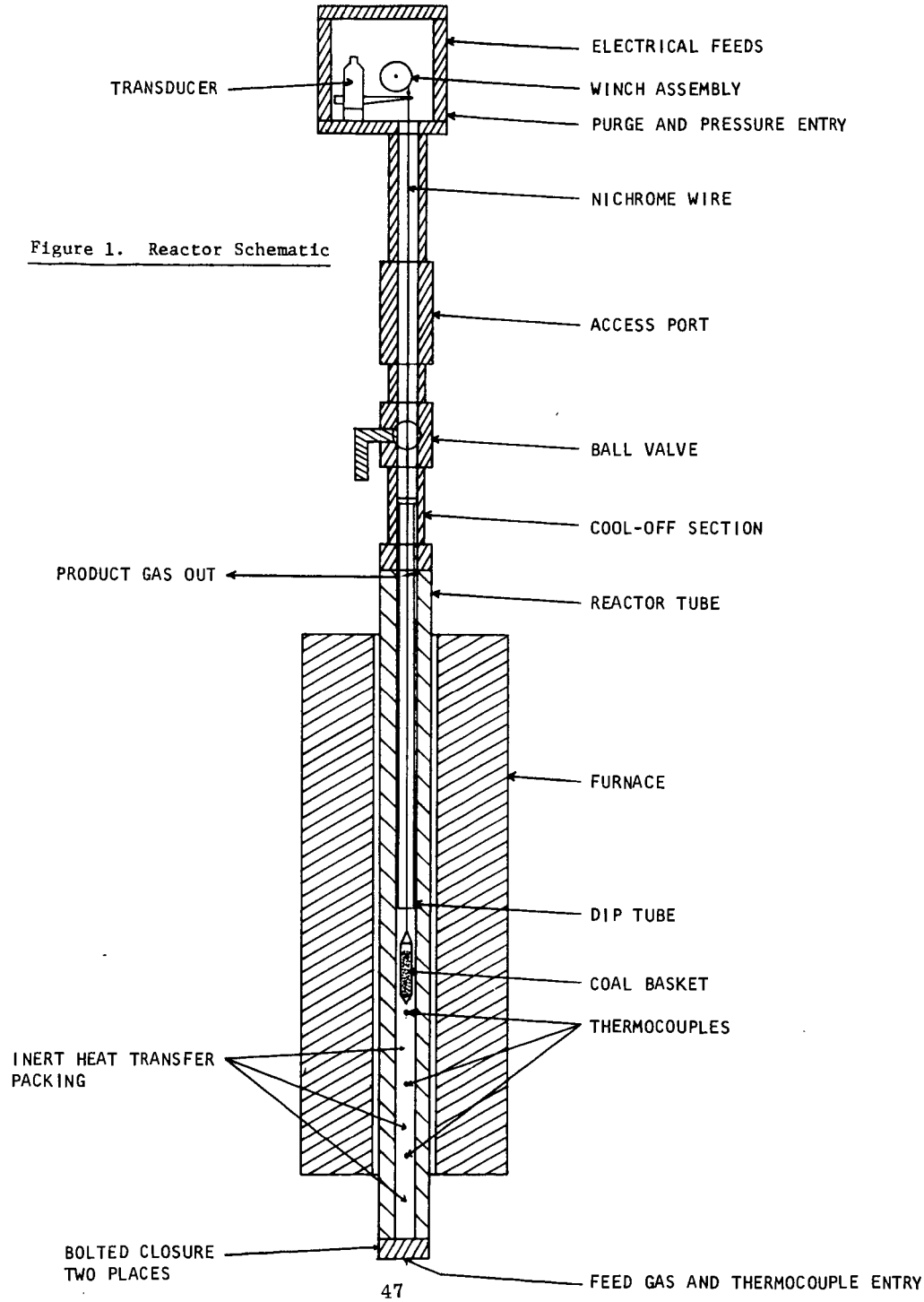

Figure 1. Reactor Schematic

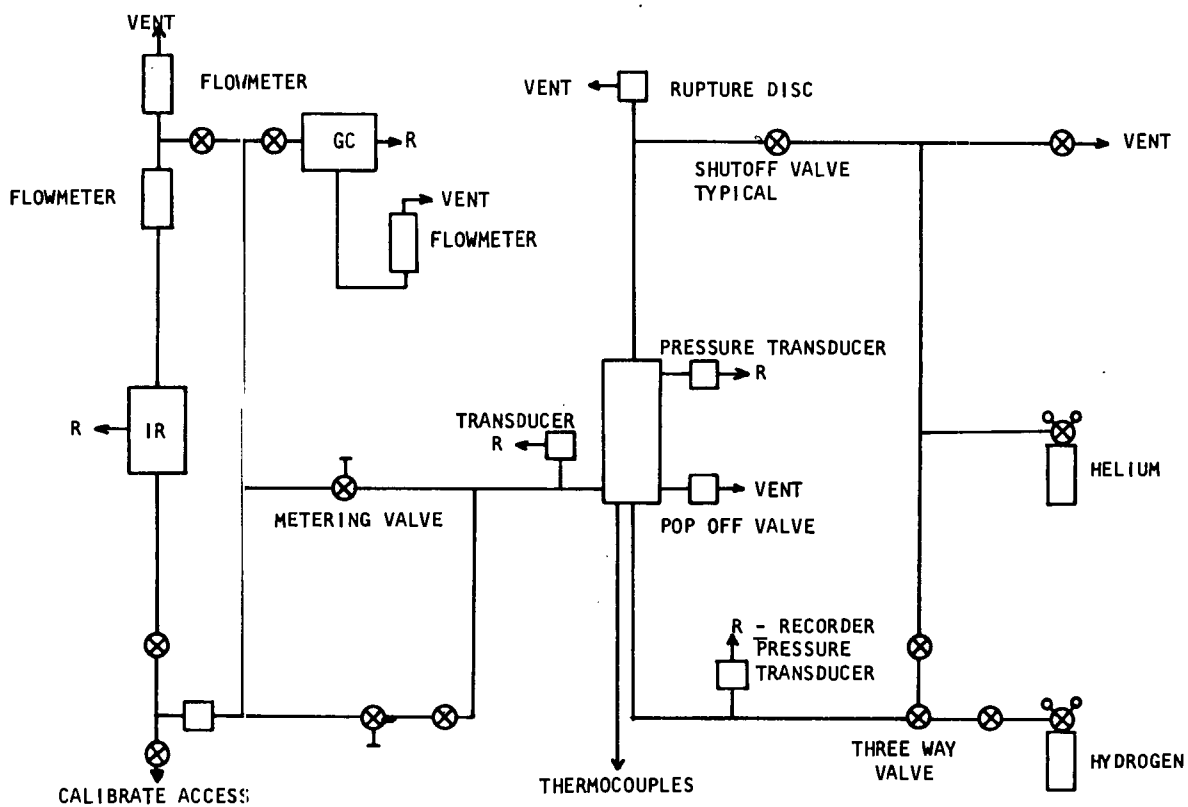

FIGURE 2: SCHEMATIC OF COAL GASIFICATION SYSTEM

All experiments used chars supplied by the Institute of Gas Technology. Char A was a hydrogasified Pittsburgh Seam, Ireland Mine Bituminous coal. Char B was from the same source, but was pre-oxidized (about 1 ft^3 of oxygen per pound of fresh coal at 400°C) in an air fluidized bed. An analysis of the two chars is shown in Table I. The char was sized 18 x 35 mesh sieve fraction, U. S. Standard. The sample weight in any given run was 1.5 - 2.5 grams. The sample bucket was constructed of 100 mesh stainless steel screen.

Catalysts were deposited on the char particles by evaporation from solution. Catalysts concentrations were five percent by weight metal. Catalyst distribution on the char was examined by electron microprobe and scanning electron microscopy.

TABLE I

CHEMICAL ANALYSIS

	Char A (hydrogasified)		Char B (pre-oxidized)	
		Uncatalyzed (mass percent)		
Carbon		81.45		67.86
Hydrogen		14.60		3.39
Oxygen		3.76		13.63
	Total	99.81	Total	84.88
Volatile		4.61		24.40
Ash		13.94		9.28
		$KHCO_3$ Catalyzed (mass percent)		
Carbon		61.45		55.21
Hydrogen		1.38		3.13
Oxygen		4.57		3.80
	Total	67.40	Total	62.14
Volatile		4.00		20.42
Ash		27.29		18.53

III. RESULTS AND DISCUSSION

Reaction of Non-Catalyzed Chars

Initial runs were performed on both chars to determine non-catalyzed reaction rates. Percent of carbon gasified versus time cruves are shown in Figures 3 and 4 for chars A and B, respectively, at 500 and 1000 psi, 950°C. Characteristically, the mass loss curves show high initial reaction rates as the more volatile matter in the char is gasified, followed by a much slower reaction regime where the rate slowly diminishes as the char is consumed. Such phenomena have been previously described by a number of investigators[7-11].

For kinetic analysis of the mass loss data, we propose a model different from those previously discussed. We assume that the reaction rate is given by the following kinetic expression:

$$\frac{dX}{dt} = v_n \, p_{H_2}^n \, (1 - X) \exp\left[- \Delta H^{\neq}/RT\right] \qquad (1)$$

where X = fractional conversion of carbon

v_n = frequency factor

n = order of reaction

$\Delta H^{\neq}$ = activation enthalpy for gasification.

In contrast to homogeneous reactions, where activation enthalpies are independent of extent of reaction, hydrogasification activation enthalpies are clearly a function of extent of reaction. One mechanism, postulated by a number of investigators, is based on the carbon structure becoming more graphitic with increasing extent

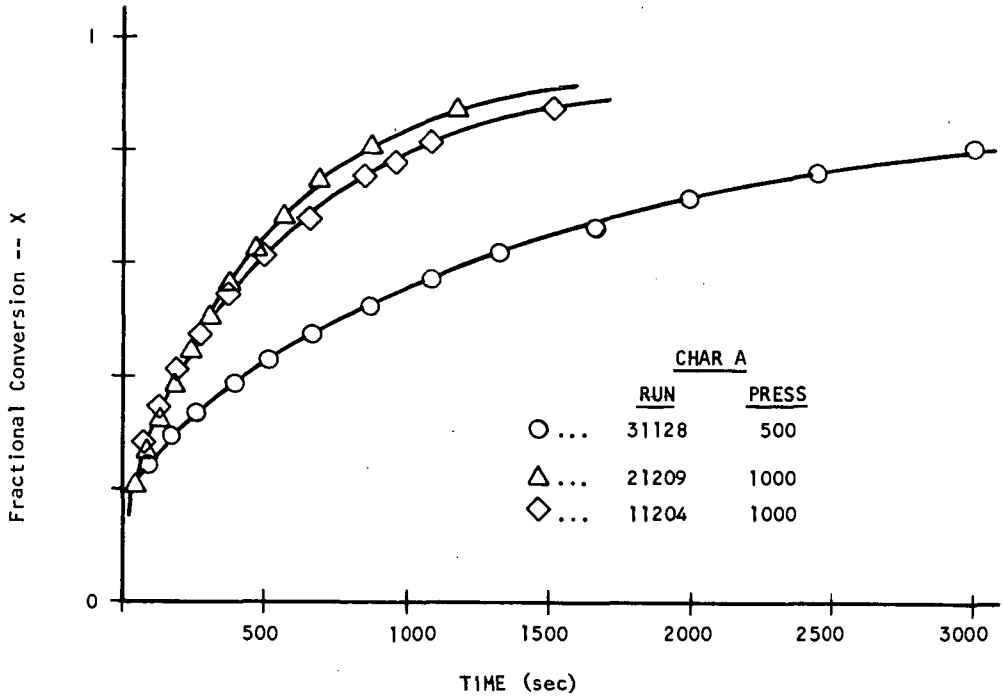

FIGURE 3. NON-CATALYZED HYDROGASIFICATION OF CHAR A AT 500 and 1000 psi, 950°C

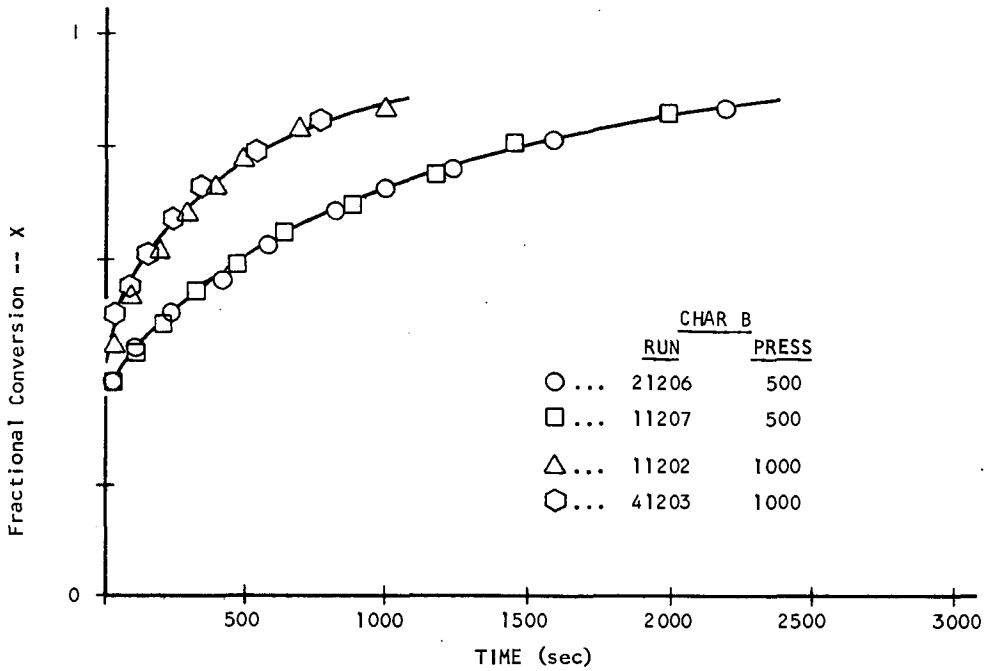

FIGURE 4. NON-CATALYZED HYDROGASIFICATION OF CHAR B AT 500 and 1000 psi, 950°C

of reaction. In the absence of any other information, the simplist function for $\Delta H^{\neq}$ (X) is a linear form

$$\Delta H^{\neq} (X) = \Delta H^0 + \alpha X \tag{2}$$

where

ΔH^0 = initial activation enthalpy

α = factor that determines sensitivity of $\Delta H^{\neq}$ to X.

Substituting this expression into equation (1), yields

$$\frac{dX}{dt} = kP^n_{H_2} (1 - X) \exp(- \Delta H^0/RT) \exp(- \alpha X/RT) . \tag{3}$$

By lumping the pressure and temperature terms into two constants, Equation (3) can be written in a simpler form in order to test its applicability as a rate expression. Thus,

$$\frac{dX}{dt} = kP^n_{H_2} \exp(- \Delta H^0/RT) \cdot \exp(\frac{-\alpha}{RT} \cdot X) \cdot (1 - X)$$

and then

$$\frac{dX}{dt} = K \exp(- bX) \cdot (1 - X) \tag{4}$$

where K and b are both constants and equal to

$$K = kP^n_{H_2} \exp (- \Delta H^0/RT)$$

$$b = \alpha/RT$$

Rearrangement and integration of equation (4) gives the final form of the rate expression used to test the kinetic data.

$$\int_o^X \frac{\exp(bX)}{(1 - X)} dX = \int_o^t Kdt = Kt \tag{5}$$

Figures 5 and 6 show plots of the integral on the left side of equation (5) versus time for chars A and B, respectively. The parameter b is chosen to minimize the sum of the squares of the

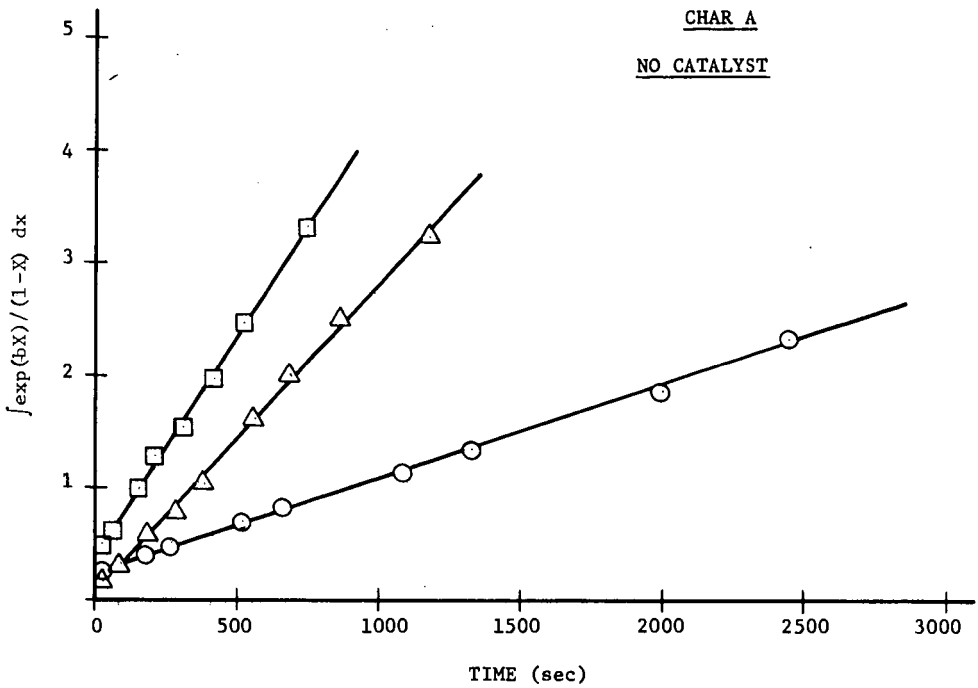

	RUN	PRESSURE	b	K(1/sec)
○...	31128	500	.9	.00081
□...	41121	1000	.8	.00386
△...	21209	1000	.8	.00274

Figure 5. Kinetic Test for the Non-Catalyzed Hydrogasification of Char A at 500 and 1000 psi, 950°C.

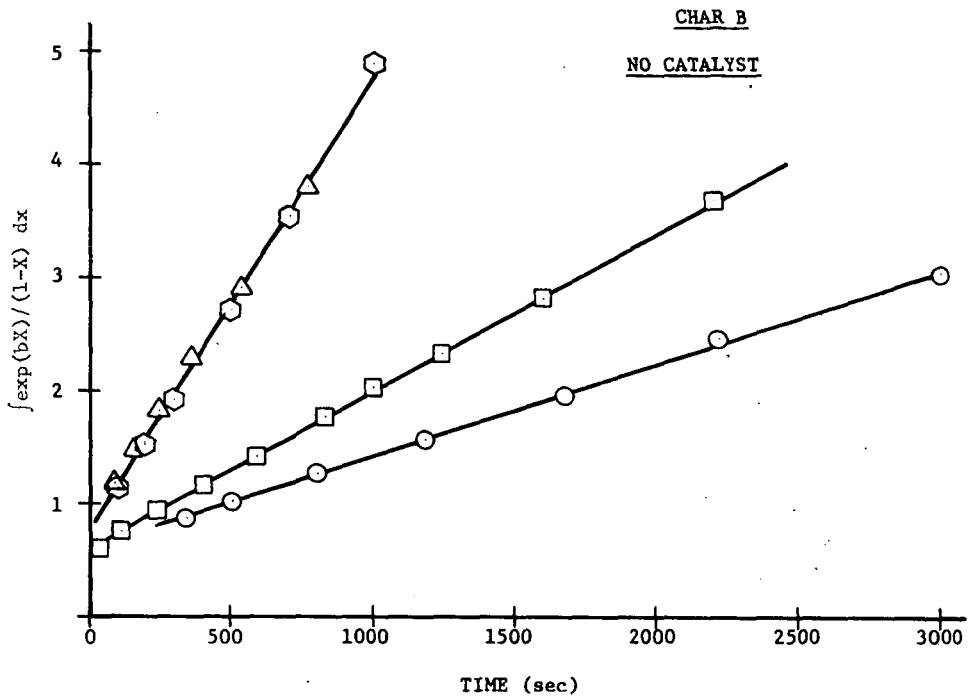

	RUN	PRESS	b	K(1/sec)
○ ...	11124	500	1	.000818
□ ...	21206	500	1	.00143
△ ...	41203	1000	1.2	.00386
⬡ ...	11127	1000	0.9	.00399

Figure 6. Kinetic Test for the Non-Catalyzed Hydrogasification of Char B at 500 and 1000 psi, 950°C.

errors of a least square fit to a straight line through the data points. The value of K is then evaluated from the slope of the straight line.

Table II shows the values of b and K determined from Figures 5 and 6.

The values of b are seen to be independent of the hydrogen pressure within experimental error. The ratio of the K values at 1000 and 500 psi, respectively, are for char A, $K_{1000}/K_{500} = 3.27$ and for char B, $K_{1000}/K_{500} = 2.89$. The hydrogen pressure appears in the K term raised to the power n, where n is the order of the reaction. Thus, the hydrogasification reaction order is approximately 1.6 in hydrogen pressure.

The y-axis intercept in Figures 5 and 6 should have been zero. The positive non-zero intercept results from the very rapid first stage of the hydrogasification reaction. For the pre-oxidized char B, the amount of carbon gasified in the rapid first stage of the reaction is greater than that for the hydrogasified char. This effect is due to the pretreatment of the char. In the second, slower part of the reaction, however, the chars behaved almost identically as indicated by similarity in the values of b and K.

Figure 7 shows the fraction of carbon gasified as a function of time for char B at 850 and 950°C, 1000 psi. The values of K and b at 850°C were found to be 2.3 and .00128 sec^{-1}, respectively. From the variation of K with temperature, the value of ΔH^0 can be estimated to be 29.3 kcal/mole. The activation enthalpy is then given by

TABLE II

TABULATION OF b AND K VALUES FOR
NON-CATALYZED CHAR A AND B

Char A (hydrogasified)					
	500 psi H_2			1000 psi H_2	
Run	b	K	Run	b	K
11122	0.25	0.000974	41121	0.8	0.00386
31128	0.9	0.000810	21209	0.8	0.00274
Average	0.57	0.000892	11204	0.8	0.00212
			Average	0.8	0.00291

Char B (pre-oxidized)					
	500 psi H_2			1000 psi H_2	
Run	b	K	Run	b	K
11124	1	0.000818	11127	0.9	0.00399
21206	1	0.00143	31209	0.8	0.00290
11207	1	0.00147	41203	1.2	0.00386
31207	0.5	0.00125	11202	1.2	0.00406
Average	0.88	0.00124	Average	1.025	0.00372

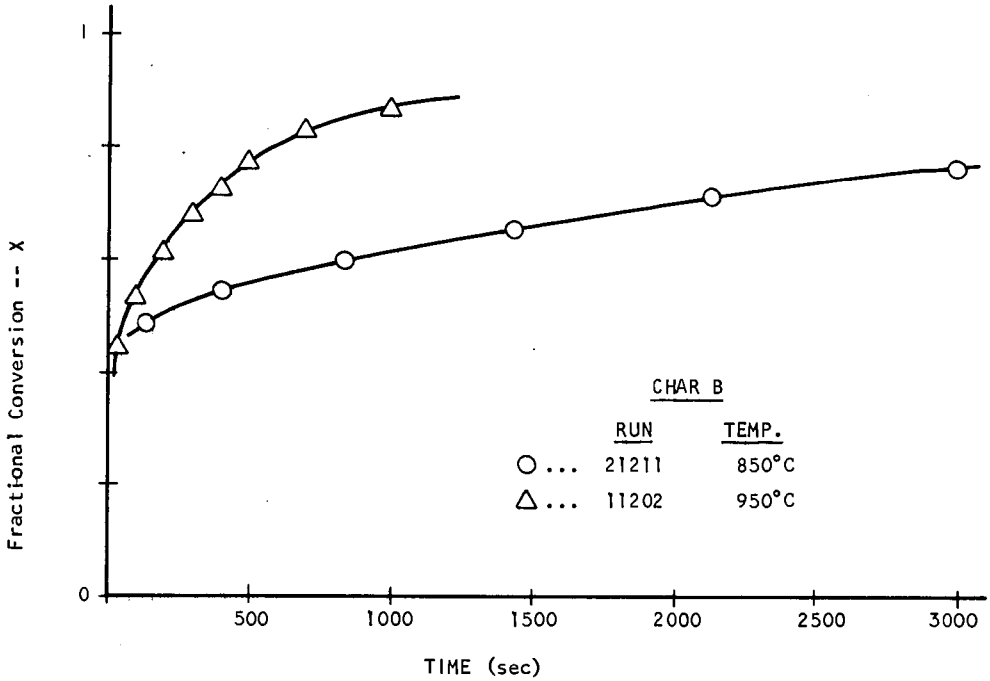

FIGURE 7. EFFECT OF TEMPERATURE ON THE NON-CATALYZED HYDRO-GASIFICATION OF CHAR B AT 850 and 950°C, 1000 psi

the expression,

$$\Delta H^{\neq} \frac{\text{kcal}}{\text{mole}} = 29.3 + 2.43\ X \qquad (6)$$

for an uncatalyzed char system.

Figure 8 shows a representative composite plot of the carbon fraction converted, the methane rate of production, and the temperature versus time for char B, Run 11128. The concentration of methane in the product stream is proportional to the rate of the hydrogasification reaction, as

$$r = \frac{dP_{CH_4}}{dt} = \frac{1}{12}\frac{1}{n_c}\left(\frac{dV}{dt}\right)\frac{P_{CH_4}}{RT} \qquad (7)$$

where r = rate (moles/minute/initial gms. of carbon)

n_c = initial moles carbon

P_{CH_4} = partial pressure CH_4 in atms

R = gas constant in L - atm/M - °K

T = temperature, °K

$\left(\frac{dV}{dt}\right)$ = product gas flow rate in liters/minute.

Equation (7) can be integrated numerically. The result is shown in Figure 9.

Although the infrared measurement of methane production leads to qualitative agreement with the direct mass determination, quantitative agreement is not good. This is most probably due to axial dispersion in the gas product stream, which results in a loss of kinetic information, and difficulties in precisely regulating the product stream flow rate, which would lead to cumulative errors.

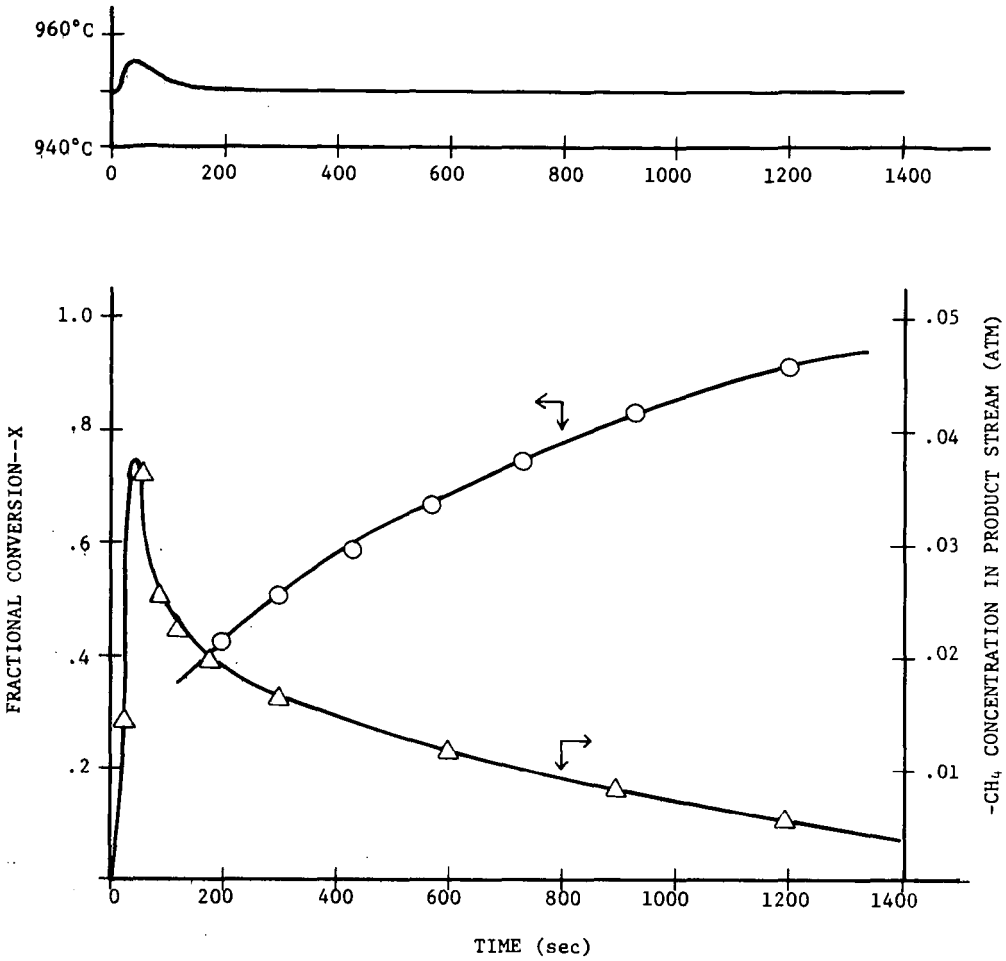

Figure 8. Composite Plot of Rate Data for $KHCO_3$ Catalyzed Char B, Run 11128, at 500 psi and 950°C.

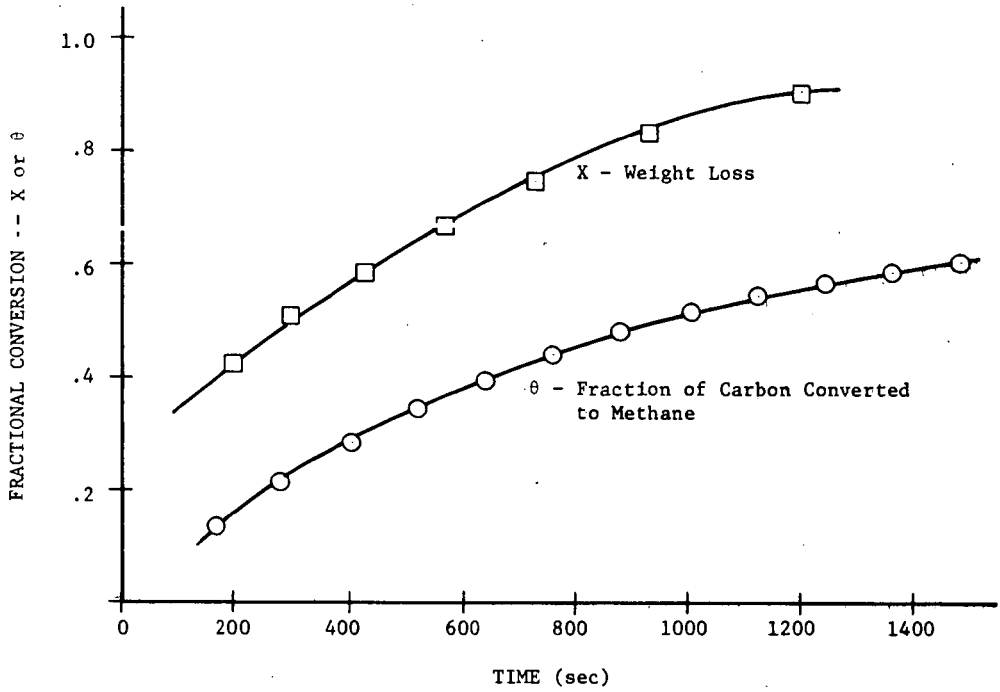

Figure 9. Fractional Conversion of Carbon to Methane for $KHCO_3$ Catalyzed Char A at 500 psi, 950°C.

The temperature versus time curve shown in Figure 8 indicates a small temperature increase resulting from the exothermic hydrogasification reaction, which diminishes with time. Unfortunately, the actual temperature of the char has not been measured directly.

Reaction of Catalyzed Chars

In this preliminary study we have concentrated on catalysts that have long been known to accelerate the hydrogasification reaction, the alkali metals and zinc salts[5]. Figures 10 and 11 show the percent carbon gasified versus time data for a $KHCO_3$ catalyst deposited on chars A and B, respectively, at 950°C, 500 and 1000 psi. Figures 12 and 13 show a representative comparison between the carbon converted in catalyzed and non-catalyzed runs on chars A and B, respectively, at 500 psi and 950°C. A substantial catalytic effect is observed. The time to achieve a gasification fraction X is roughly halved by the $KHCO_3$ catalyst. The kinetic analysis for the parameters b and K are shown in Figures 14 and 15. The kinetic equation (4) is seen to fit the data at high conversions. The evaluation of the b and K parameters for $KHCO_3$ catalyzed reactions is shown in Table III.

The rate enhancement due to the catalysts is shown by the evaluation of α from the parameter b. Taking -1 to be the average value of b for a catalyzed system, the corresponding value of α is -2.43. This term makes the linear expression for the activation enthalpy decrease with increasing carbon gasification

$$\Delta H^{\neq} \text{ (kcal/mole)} = 29.3 - 2.43\ X\ .$$

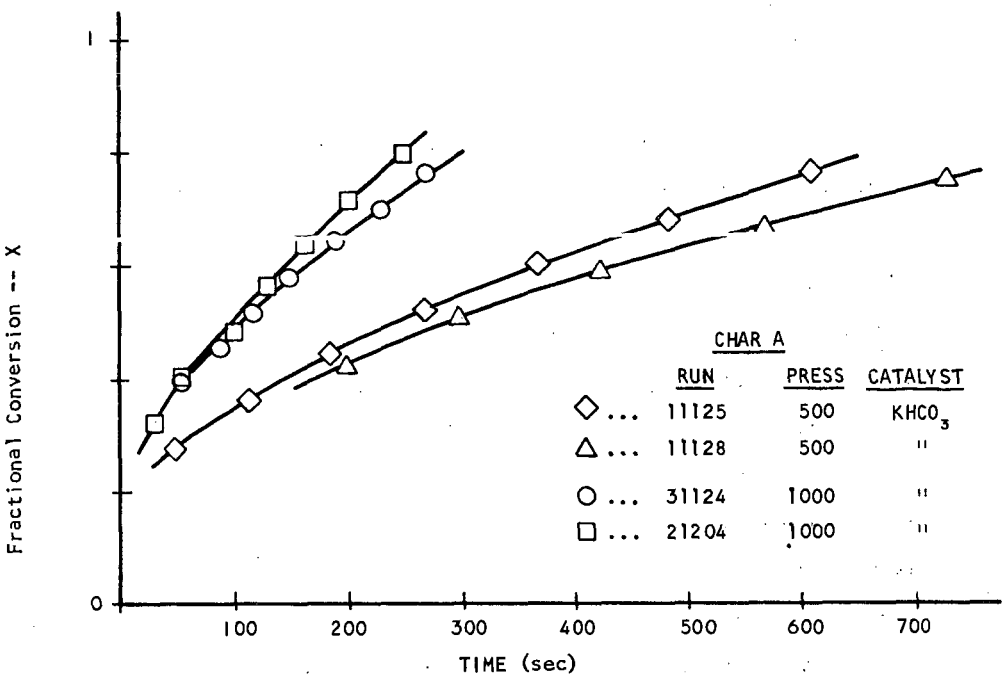

FIGURE 10. CATALYZED HYDROGASIFICATION OF CHAR A AT 500 and 1000 psi, 950°C

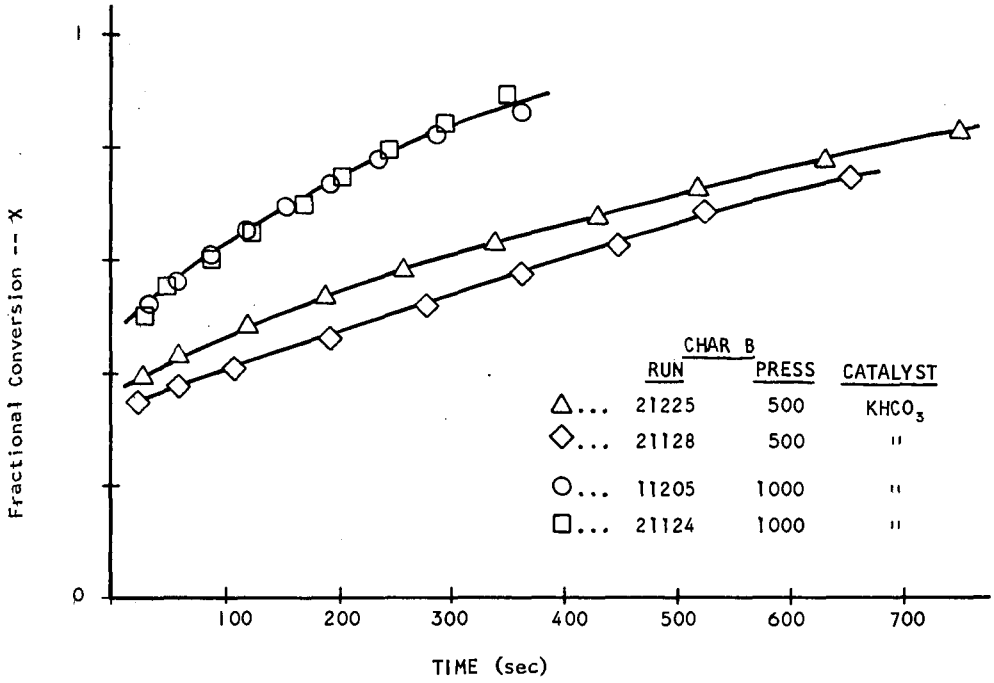

FIGURE 11. CATALYZED HYDROGASIFICATION OF CHAR B AT 500 and 1000 psi, 950°C

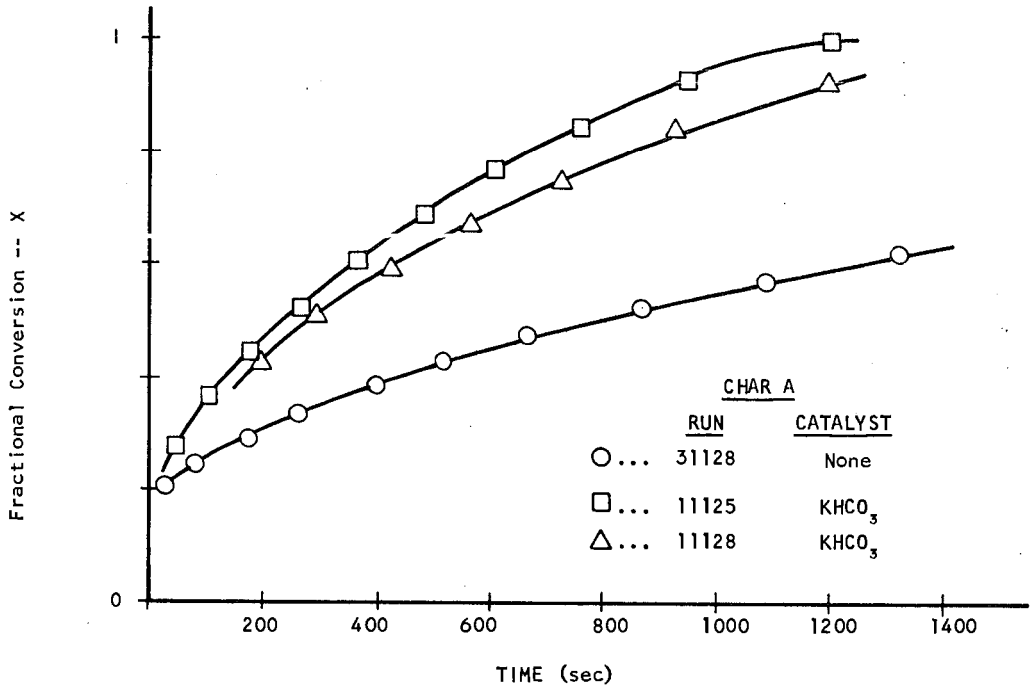

FIGURE 12. COMPARISON OF THE CATALYZED AND NON-CATALYZED HYDROGASIFICATION OF CHAR A AT 500 psi, 950°C

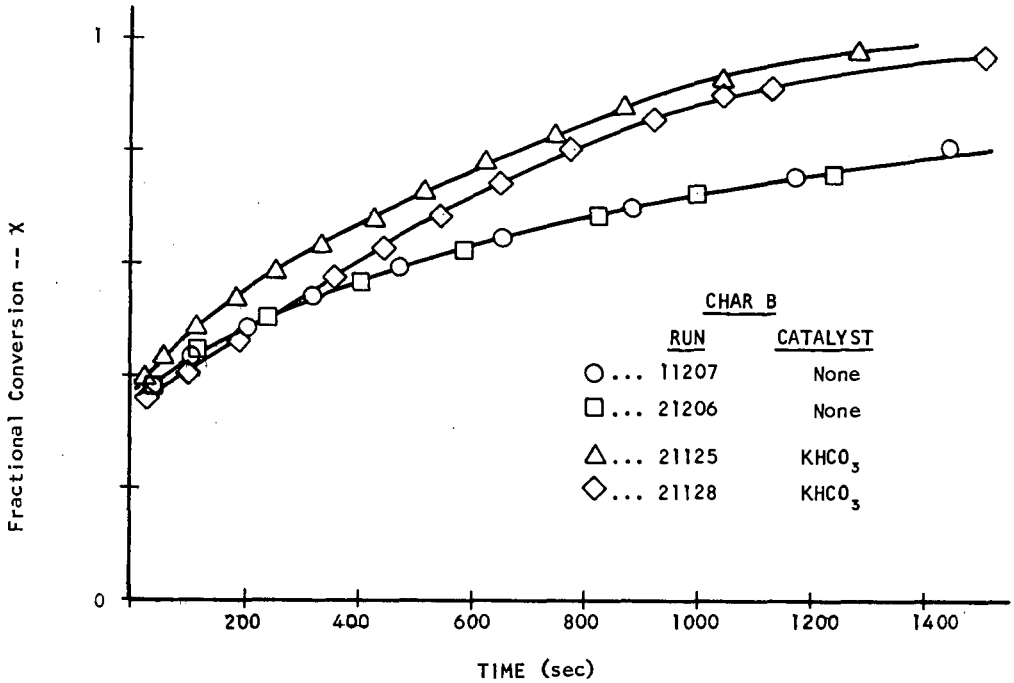

FIGURE 13. COMPARISON OF THE CATALYZED AND NON-CATALYZED HYDROGASIFICATION OF CHAR B AT 500 psi, 950°C

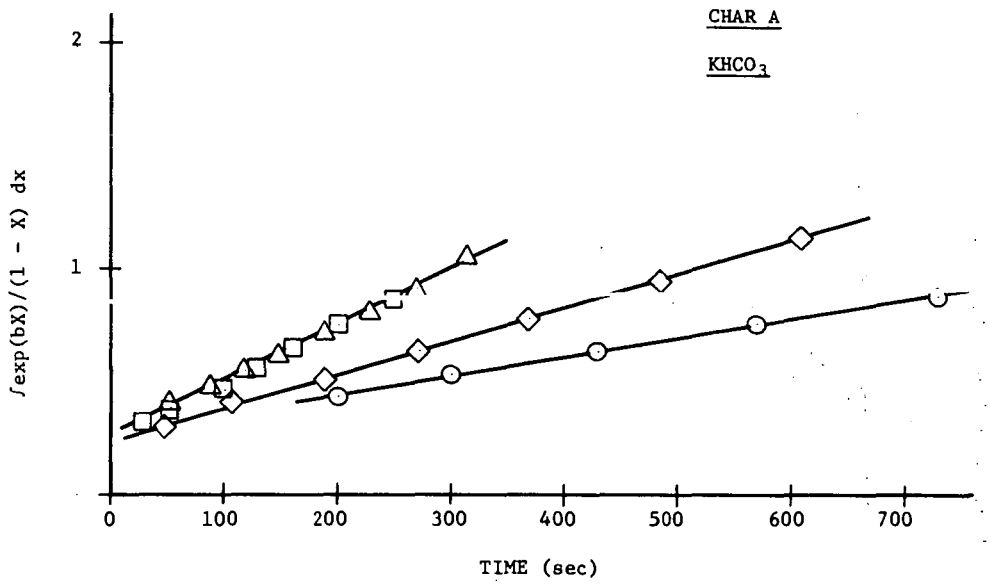

	RUN	PRESSURE	b	K(1/sec)
○...	11128	500	-1.0	.000877
◇...	11125	500	-0.5	.00150
△...	31124	1000	-1.0	.00236
□...	21204	1000	-1.3	.00252

Figure 14. Kinetic Test for the $KHCO_3$ Catalyzed Hydrogasification of Char A at 500 and 1000 psi, 950°C.

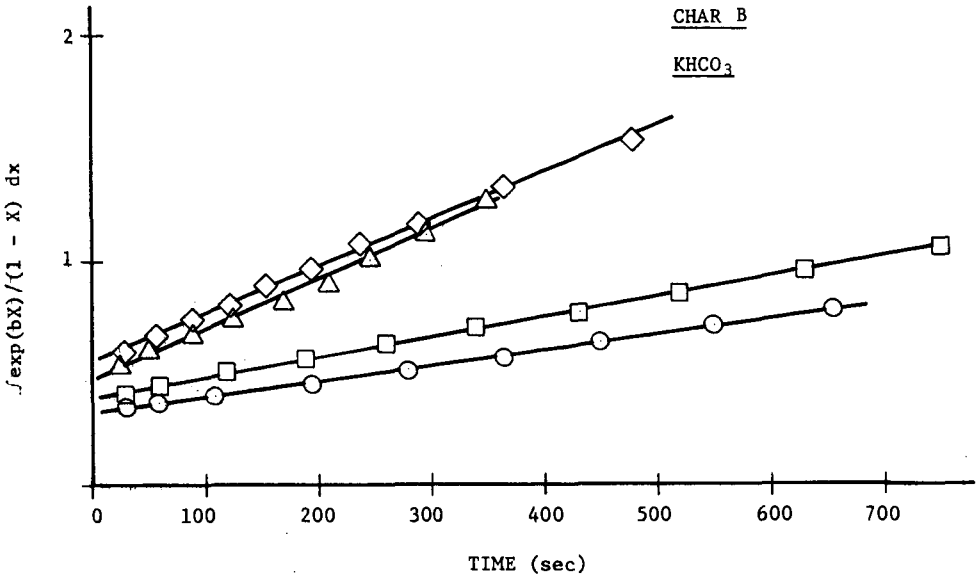

	RUN	PRESSURE	b	K(1/sec)
○...	21128	500	-1.3	.000712
□...	21125	500	-1.0	.000903
△...	21124	1000	-1.0	.00218
◇...	11205	1000	-0.75	.00221

Figure 15. Kinetic Test for the $KHCO_3$ Catalyzed Hydrogasification of Char B at 500 and 1000 psi, 950°C.

TABLE III

TABULATION OF b AND K VALUES FOR CHAR A AND B CATALYZED WITH $KHCO_3$

Char A (hydrogasified)					
500 psi H_2			1000 psi H_2		
Run	b	K	Run	b	K
11128	-1.0	0.000877	11208	-0.3	0.00224
11125	-0.5	0.0015	21204	-1.3	0.00252
Average	-0.75	0.00119	31124	-1.0	0.00236
			Average	-0.867	0.00237

Char B (pre-oxidized)					
500 psi H_2			1000 psi H_2		
Run	b	K	Run	b	K
21128	-1.3	0.000712	21124	-1.0	0.00218
21125	-1.0	0.000903	11205	-0.75	0.00221
Average	-1.15	0.000807	Average	-0.88	0.00219

Work has also begun on the catalysts potassium carbonate, K_2CO_3, and zinc chloride, $ZnCl_2$. These catalysts were also deposited by impregnation at a five percent by weight metal concentration. The K_2CO_3 catalyst behaved very similar to the $KHCO_3$. The weight loss curves for this catalyst at 500 and 1000 psi, 950°C are shown in Figure 16. Kinetic analysis of this catalyst produced values of b and K similar to those for $KHCO_3$ (see Table IV).

Microscopy of the Chars

Characterization of the chars is being carried out on the microprobe analyzer and the scanning electron microscope. Features such as particle structure, catalyst distribution, and structural change at the catalyst sites during reaction are of interest.

The scanning electron microscope can take high magnification, high resolution pictures of the char particles, while the microprobe analyzer can be calibrated to scan for any element on the char particle surface.

Presented here will be a cross section of representative photos for each char. Proper interpretation of these pictures is important. The scanning micrographs (scanning electron micrographs) are high quality pictures but are often slightly distorted at low magnification (75-100X). The back scattering electron micrographs (BSE) and x-ray micrographs are all taken on the microprobe analyzer. The BSE micrographs from this instrument are of low clarity because the microprobe was designed to do x-ray analysis. An x-ray micrograph is a scattering of white dots on the picture. If the element

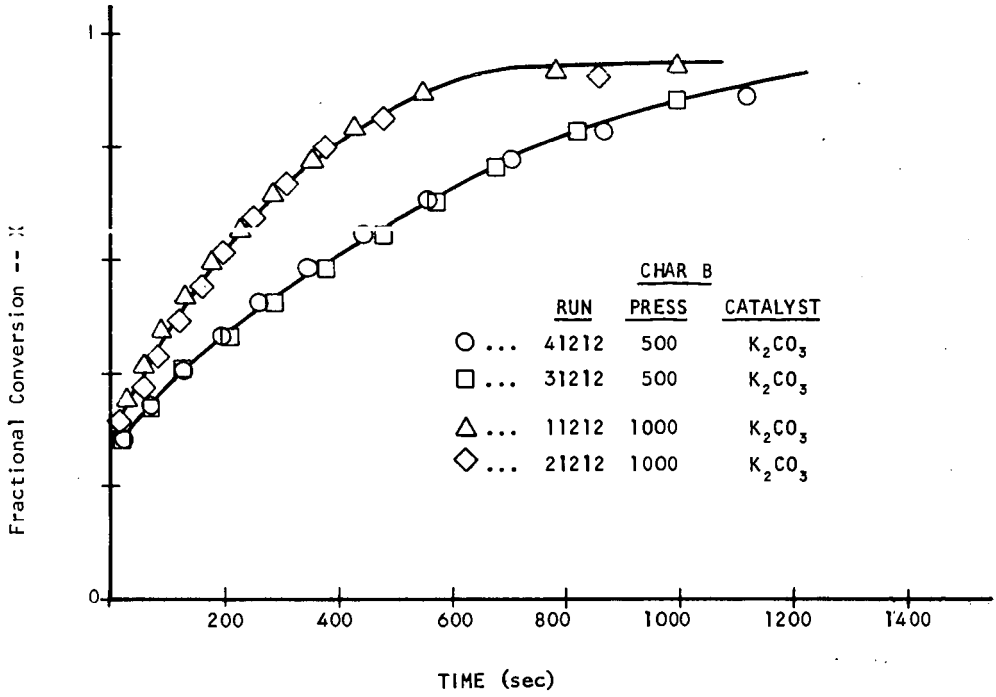

FIGURE 16. CATALYZED HYDROGASIFICATION OF CHAR B AT 500 and 1000 psi, 950°C

TABLE IV

TABULATION OF b AND K VALUES FOR CHAR A AND B CATALYZED WITH OTHER CATALYSTS

Char A (hydrogasified - $ZnCl_2$)					
	500 psi H_2			1000 psi H_2	
Run	b	K	Run	b	K
21214	0.5	0.00160	21208	0.5	0.00492
31214	0.25	0.00140	51208	0.2	0.00301
Average	0.37	0.00150	Average	0.35	0.00397

Char B (pre-oxidized - K_2CO_3)					
	500 psi H_2			1000 psi H_2	
Run	b	K	Run	b	K
41212	-0.15	0.00155	21212	-0.5	0.00245
31212	-1.2	0.000867	11212	-0.5	0.00248
Average	-0.67	0.00118	Average	-0.5	0.00247

being analyzed is not present, there is an even, but sparce distribution of white dots on the micrograph. (See upper right of Figure 20d where there is no iron present.) This artifact of the analyzer will be referred to as background. The locations where the element being analyzed is present, are then represented by a concentration of white dots. (See also Figure 20d.)

Figure 17a shows a low magnification scanning micrograph of the hydrogasified, $KHCO_3$ catalyzed char A. This is a representative picture of this type of a char, catalyzed or uncatalyzed. The particle surface is, in general, crumpled but smooth.

Higher magnification micrographs of the center of this particle are shown in Figures 17b and 17c. (See the area circled in Figure 17a.) These are both of the same area on the particle. Figure 17b is a scanning micrograph while 17c is a BSE micrograph. Figure 17d is the iron x-ray superimposed on the BSE of Figure 17c. This shows areas of the particle surface where iron deposits or ash concentrations are located. A close-up of the ash deposit circled in Figure 17b or 17c is shown in Figure 18a.

Figure 18b shows a potassium x-ray superimposed on the BSE of Figure 17c, which is $KHCO_3$ catalyzed char A. The heavy but even concentration of white dots indicates that the catalyst is present in a well-distributed manner. The catalyst must exist on the particle surface in a finely divided state since there are no distinguishable clumps, as noticed in earlier catalytic x-ray analysis.

a. Scanning - 75X

b. Scanning - 300X

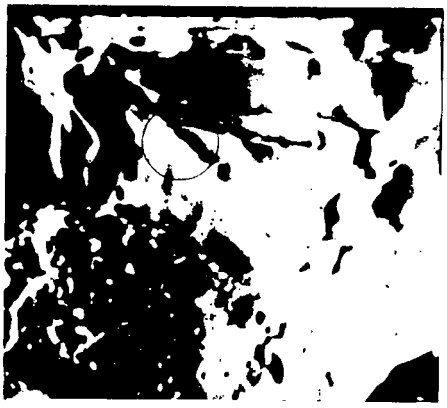

c. BSE - 200X

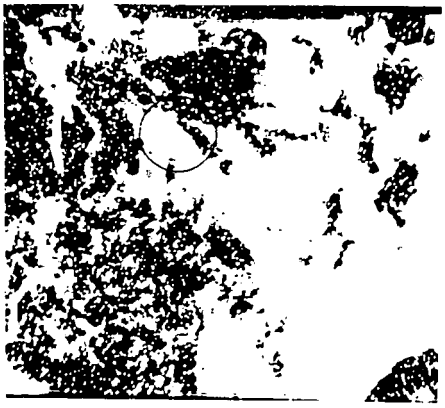

d. Iron X-ray on BSE - 200X

Figure 17. Micrographs of $KHCO_3$ Catalyzed Char A

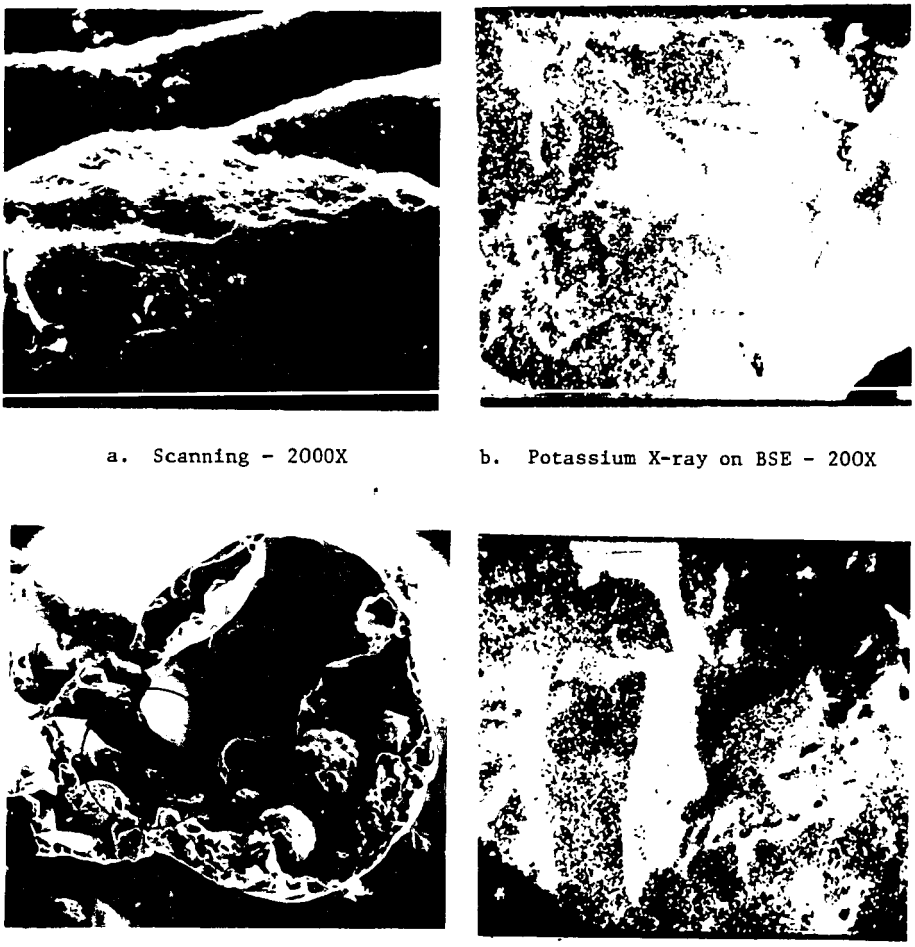

a. Scanning - 2000X

b. Potassium X-ray on BSE - 200X

c. Cut Particle - Scanning - 100X

d. Cut Particle, Potassium X-ray on BSE - 200X

Figure 18. Micrographs of $KHCO_3$ Catalyzed Char A

The scanning micrograph of a cut particle of char A similar to that in Figure 17a is shown in Figure 18c. The inside of the particle is filled with cavities or cells, somewhat like a sponge. This is very different from the outer surface of the particle. The pretreatment skin[12], or outer surface, and the resulting inner structure are a direct result of the pretreatment history of the char. A potassium x-ray on a BSE micrograph of the area circled in Figure 18c is shown in Figure 18d. This too shows a heavy catalyst concentration.

The pre-oxidized, uncatalyzed or catalyzed char B appears very similar to char A. Direct comparisons of the same type of outer and inner structure can be drawn from Figure 19a and 19b for char B and Figure 17a and 18c for char A. These are the same chars but have undergone different pretreatment histories.

Direct similarities of ash content can be shown with the scanning micrographs of a particle reacted in hydrogen for eight minutes. Figure 20a and 20b show a portion of an uncatalyzed particle with the close-up of an ash deposit in Figure 20b. This can be verified with the results of Figure 20c and 20d, which are the iron x-ray and BSE micrographs of the same area in Figure 20a. In these same areas lighter concentrations of potassium and silicon have also been found.

The analysis of the $KHCO_3$ catalyzed char B showed a good distribution, which was similar to that of char A. (See Figure 18b for char A.)

a. Cut Particle, Scanning - 75X

b. Whole Particle, Scanning - 200X

Figure 19. Micrographs of Uncatalyzed Char B

a. SEM - 500X

b. SEM - 2000X

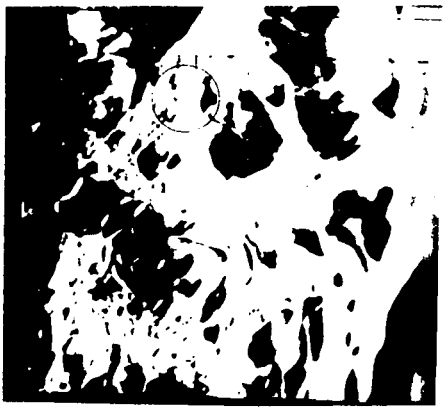

c. BSE - 200X

d. Iron X-ray - 200X

Figure 20. Micrographs of Uncatalyzed Char B

The high iron content is a common characteristic of the two chars and is seen in the x-ray analysis. These chars also have a high sulfur content, which is distributed fairly evenly in the particles. Analysis for zinc and nickel were negative, and slight traces of calcium have been seen in some samples.

IV. CONCLUSIONS

The initial studies of catalysts and contacting systems has begun at Case Western Reserve University. The high temperature, high pressure, recording thermobalance has made direct kinetic analysis of the carbon weight loss curves straightforward.

The data seems to be well represented by the kinetic model proposed in equation (5). Analysis of the fitting parameters for this model show that for the rate dependence on pressure the order of the reaction is about 1.6.

The temperature dependence of the rate constant determines the initial activation enthalpy. The initial activation enthalpy is about 29.3 kcal/mole. Coupling this with the evaluation of the parameter b from the kinetic model we have found the linear form of the activation enthalpy as a function of conversion for a non-catalyzed char. (See equation (6).)

Some information of the relative volatilities of the two chars is discernable from the y-axis intercept in the plots of the kinetic test for our rate expression. This is the portion of the weight loss curves where the rapid first stage of the reaction is taking place. The application of the kinetic model then precedes from the latter part of these curves, which represent the second, slower part of the reaction. Unfortunately, this semi-empirical model leaves us with the lack of a real mechanism. Possibilities of

ash diffusion and/or chemical effects have not been studied in the detail necessary to shed light upon the subject.

The catalytic systems showed substantial slope increases in the weight loss curves (Figure 21). It was found that $KHCO_3$ and K_2CO_3 exhibited an equivalent catalytic effect which was better than that found for $ZnCl_2$ (see values of b in Table IV). The net result of the catalytic systems on our kinetic model was to change the value of the parameter b, which changed the value of α in the linear expression for the activation enthalpy. For the $KHCO_3$ system the value of α for an average value of $b = -.91$ was $\alpha = -2.21$. The catalyst apparently did not affect the value of ΔH° over the course of the reaction.

Microscopy of the char samples is yielding interesting and qualitative information. Characterization of char structure with the scanning electron microscopy has shown the standard pretreatment skin and the celled particle interior. X-ray analysis of the same particles in the microprobe analyzer and the SEM have shown ash deposits on the surface of the char and good catalyst distributions.

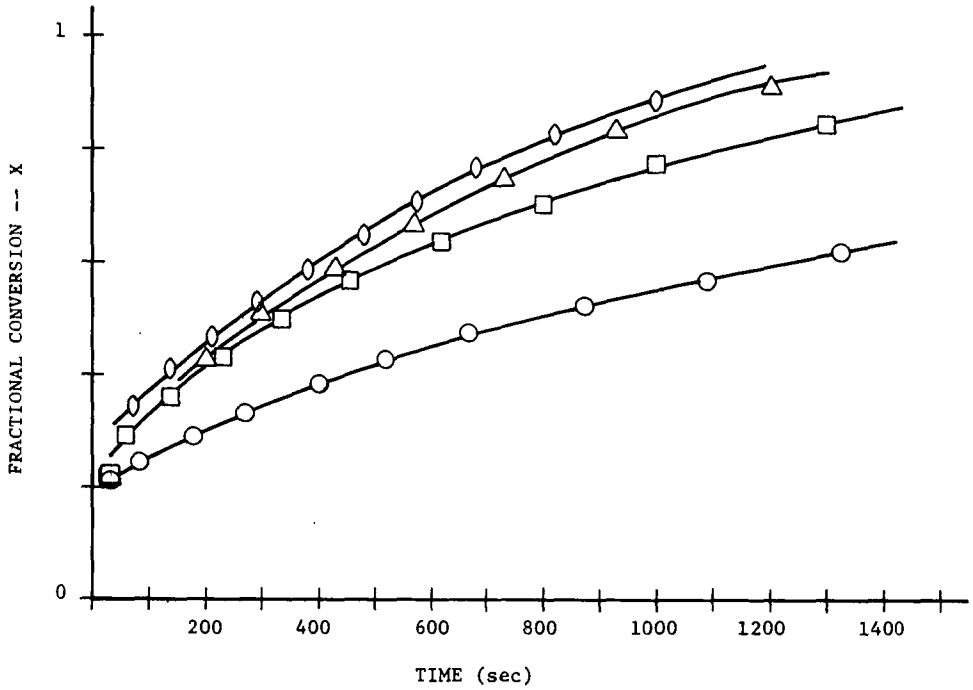

	Run	Char	Catalyst
○ ...	31128	A	none
□ ...	21124	A	$ZnCl_2$
△ ...	11128	A	$KHCO_3$
⬯ ...	31212	B	K_2CO_3

Figure 21. Comparison of Various Char-Catalyst Systems at 950°C and 500 psi.

REFERENCES

(1) Dent, F. J., Blackburn, W. M., and Millett, H. C., Trans. Inst. Gas Engrs., 87, 231 (1937)

(2) Friedman, S., Kaufman, M. L., and Wender, I., J. Org. Chem., 36, 694 (1971)

(3) Weller, S., and Pelipetz, M. G., Ind. & Eng. Chem., 43, 1243 (1951)

(4) Dent, F. J., Blackburn, W. H., and Millett, H. C., Trans. Inst. Gas Engrs., 88, 150 (1938)

(5) Wood, R. E., and Hill, G. R., ACS Division of Fuel Chemistry, Vol. 17, No. 1, Aug. 1972

(6) Feldkirchner, H. L., and Johnson, J. J., Rev. Sci. Instr., 39, No. 8, 1227, Aug. 1968

(7) Blackwood, J. D., and McCarthy, D. J., Aust. J. Chem., 19, 797 (1966)

(8) Moseley, F., and Paterson, D., J. Inst. Fuel, 38, 13 (1965)

(9) Feldkirchner, H. L., and Linden, H. R., Industr. Eng. Chem., 2, 153 (1963)

(10) Johnson, J. J., Seminar on Characterization and Characteristics of U.S. Coals for Practical Use, Pennsylvania State University, 1971

(11) Hiteschue, R. W., Friedman, S., and Madden, R., U.S. Bureau of Mines, Reports of Investigation, Nos. 6027 and 6125, 1962

(12) Gould, R. F., Ed., Fuel Gasification, Advances in Chemistry Series, 69, American Chemical Society, 1967

ACKNOWLEDGEMENTS

We gratefully acknowledge the American Gas Association's support under Contract No. BR-75-1.

The thermobalance was made available by Consolidated Natural Gas Service Company, Inc., without which this work would have been impossible.

Special thanks are given to Raymond R. Cwiklinski and Donald C. Grant for their technical assistance.

Liquefaction Study of Several Coals and a Concept For Underground Liquefaction

Duane R. Skidmore
and
Calvin J. Konya

West Virginia University
School of Mines
213 White Hall
Morgantown, West Virginia

Introduction

In the past, underground coal conversion processes were uneconomical in comparison with cheap energy alternatives or not feasible technically. Some recent changes in technology and economics may have improved the feasibility of underground coal conversion. The selling prices of conventional fossil fuels have been rising because of restricted supply and increasing demand. The price increases should have four effects: (1) the producers of gas and oil are encouraged to find additional sources, (2) the users of these convenient fuels are motivated to restrict their consumption, (3) coal mine operators are inclined toward opening more conventional mines and (4) concepts for alternative energy sources such as underground coal conversion become more attractive for serious engineering evaluation.

The rise of concern for the health and safety of the miners is another factor influencing this renewal of interest in remote coal conversion. Not only have the human costs of conventional mining been large as represented by loss of lives or adverse effects on health but economic costs of industrial accidents have proven considerable. During the summer of 1972 the dreaded pneumoconiosis or "black lung" was the subject of a survivor's benefits bill passed by the U. S. Government in the amount of one billion dollars. The implementation of legislation to protect the health and safety of miners reflects social and economic concern.

The policy alternatives for elimination of energy shortages have been severely restricted by environmental regulations. Surface or strip mining of coal is under severe federal restriction and risks more regulations on the state and federal levels. The spoil banks which result from strip mining, particularly in the eastern United States, have not been reclaimed properly. Siltation of streams has resulted and fish have been killed. Silt has plugged channels and backed up waters to flood areas previously available for recreation and farming. In regions containing high sulfur coal, the streams have become acidic; and additional aquatic life is killed. Public outrage has been predictable.

The need for new technology to extend the coal reserves of the Nation does not and probably should not have a high industrial priority. Domestic coal reserves have been variously estimated but usually are deemed capable of sustaining present total national energy demands for 800 to 4000 years. New technology to utilize coal resources which are presently uneconomical to mine, however, would extend the recoverable energy from a given property and might therefore be worth an intensive research and development effort. The seams of particular interest include those which are low in sulfur and are too deep or too thin for exploitation by presently available methods.

Remote underground coal mines have been developed in northern Europe. As a result, the industry there has become even more increasingly capital intensive. One drawback to this alternative in the United States is that the coal mining industry has had difficulty in borrowing substantial amounts of money for long

time periods at low interest rates. Until the recent shortages of energy became well known and segments of the oil industry entered the coal mining industry, acquisition of equity capital had also been difficult. Some reluctance for stock purchase has been traced to uncertainities over oil import policy and environmental regulations. Futhermore, the European concept requires men underground for equipment maintenance. Finally, some questions have been raised in this country about the acceptability of underground mining for rapid implementation under existing work rules and union contracts.

With the changes in economic and social climate, the United States Bureau of Mines in cooperation with a subsidiary of the Union Pacific Railroad has reopened development work on underground coal gasification.

History

The first reference to underground coal gasification is dated 1868.[1] The most extensive effort occurred in the Soviet Union from the 1930's to about 1960. Premier Stalin had apparently promised the miners some relief from difficult working conditions and had developed underground gasification technology in partial fulfillment of his promise. Some time after Stalin's death, the effort was quietly dropped, probably because extensive oil and natural gas discoveries made underground gasification uneconomical.

The most recent tests in the United States by the Bureau of Mines have defined two main problem areas. The product gas must be confined to the reaction zone and removed under controlled conditions. This implies that an impervious bed of rock must overlay the coal seam. The product gas must be useful for high value energy production. In most circumstances, this would require electrical power generation. Since the gas from underground conversion technology has had low heating value (less than 100 BTU/SCF). The need is obvious for technology to upgrade the product. No previous published work in underground conversion of coal to liquid has been found.

Issues

Underground coal liquefaction concepts include several which are adapted from underground coal gasification. In the blind borehole-backfill system for underground gasification, a simple well is drilled vertically to the coal seam and then horizontally for some distance through the coal. The well is then doubly piped by a smaller diameter pipe within a larger one. Reactants are introduced through the central pipe and products are withdrawn through the outer annulus. The piping system is withdrawn as coal is used up, A void is produced by coal removal and the empty volume is filled with a water or solid waste rock fill material. The blind borehole-backfill system has been recommended for thin coal seams by the USBM report on underground coal gasification.

For somewhat thicker seams, the branched borehole-backfill system has been visualized. The borehole is branched after entering the coal seam so that the reactants can be admitted into the bottom of a seam and products withdrawn from the top. Proper downhole baffling arrangements are required.

Very thick seams lend themselves to the vertical blind borehole-fill system during which the concentric feed and product pipes are withdrawn vertically upward as the coal is produced. Fill from the feed pipe or another piping system readily accumulates in the exhausted volume. Each of the single borehole systems has a multiple borehole counterpart.

Use of a single well for feed reactants and for withdrawal of products obviates the need for connecting separately drilled wells. Boreholes can be connected underground by hydraulic fracturing, explosive fracturing and various modifications of

drilling or electro-linking. Some of these techniques have been successful for gas and petroleum field exploitation and underground coal gasification. Their particular disadvantage for use in underground coal conversion systems lies in the relatively rapid exhaustion of the hydrocarbon reservoir and the need for repeated practice of the linking procedure.

In remote mining schemes, the delivery of hot, hydrogen-donor solvent to the coal is a necessity. The solvent is hydrogenated conventionally and introduced while still hot into the reaction zone underground.

One of the principal problems underground is to maintain the solution temperature in the reaction zone. The total heat to be supplied provides (1) the heat of vaporization for the solvent, (2) the energy to pressurize the solvent vapor in the reaction zone in order to prevent excessive volatilization of the liquid solvent and to activate the solvent for the hydrogen transfer reaction, (3) the activation energy for the coal surface so that the reaction may proceed at an adequate rate, (4) losses to the surrounding rock, and finally (5) losses incurred when the reaction zone has passed and filling or flooding occurs.

The reaction itself is considered to proceed through at least two important thermal stages. First, the coal structure is thermally activated so that pyrolytic cracking or chain breaking of hydrocarbons occurs. Later, hydrogen atoms are released from the donor solvent and added to the coal fragments. Between the first and second phase a gel reaction may occur. During gelation ($\sim$350°C) the coal and solvent form a viscous composite with high resistance to flow. The advantages of maintaining or establishing low slurry viscosities are obvious so that removal of coal is best effected either before or after the gelation step.

Further Set of Issues Involved

The design of an underground liquefaction process requires definition of (1) the types of coal seam most likely to be leached or liquefied by the physical arrangements suggested above and (2) the solvent or slurry material which would be most effective. Work was undertaken at West Virginia University to define the behavior of different types of coal monoliths exposed to several solvents under conditions possible for achievement underground.

Apparatus and Procedure

The test apparatus was a 750 ml carbon steel autoclave fitted with a Bourdon pressure gauge and a thermocouple well. Closure was effected by a gasket and flange arrangement. Gas inlet and exit lines permitted the autoclave to be flushed with nitrogen. No hydrogen was used. Heat was supplied by a large laboratory Bunsen burner. Reproducibility of heating rate is seen in Figure 1. A final temperature of 270 - 280°C was used for one series of experiments.

Procedure consisted of cutting on a mechanical saw a 1" x 1" x 1 1/4" monolith of the coal type to be tested. Coals included an Oklahoma semi-anthracite, an Illinois #6 sub-bituminous, and an Alabama lignite. Typical chemical analyses are shown in Table 1. After being cut, the coal was carefully placed into the autoclave and 250 ml of solvent was added. Solvents included various cuts of anthracene oil (Table 2), and one commercial motor oil (SAE 30). The autoclave was sealed, flushed with nitrogen, and heated by means of the burner. Figure 2 shows the pressure and temperature for a run with Illinois #6 coal in anthracene oil solvent. Figure 3 shows a similar run with SAE 30 motor oil solvent.

Results

The coal reacted, cracked, crumbled, or dissolved to a greater degree if exposed to reaction conditions for a longer time or at a higher temperature. For a series of run at the same time and temperature the coals reacted increasingly from semi-anthracite to lignite to sub-bituminous. When different solvents were used the hydrogen donor anthracene oil was more reactive than motor oil. The motor oil was quite unreactive. Recycled anthracene oil lost reactivity.

The coal was observed to fracture at the planes of least resistance which are typified by the joint and bedding plants. The structure of coal which includes bedding and cleavage planes helps in physical breakdown of the sample. As joints and bedding planes open, the fluid is able to penetrate deep into the sample causing rapid disintegrating of the coal.

Interpretation of Reactions

The effects of different solvents upon the rate of the reaction can be interpreted from the work of Severson et al.[2] Coal solubilization most rapidly proceeds in a solvent which has a high boiling point, the ability to donate hydrogen, a relatively high dipole moment, heterocylic atoms and ring stability. Apparently during one or two cycles, anthracene oil exhausts its available hydrogen and loses the ability to donate until the hydrogen has been replenished. The lack of effect with the motor oil is somewhat more difficult to evaluate unequivocally. The high vapor pressure exhibited at reaction temperature suggests that the solvent will be present in low concentration within the reaction zone. More significantly, the saturated structure of the hydrocarbon makes the motor oil a poor hydrogen releasing solvent.

The gradation in reactivity which was seen with the different coal ranks may be interpreted in the light of suggestions by Wender.[3] Semi-anthracite structures, represented by Wender as analogous to fused carbon ring systems, were visualized as substantially aromatic but with occasional saturated rings. This system was joined by oxygen bridges to adjacent structural units. These were seen as difficult to thermally crack (300 - 375°C) because of extensive opportunities for resonance and as difficult to hydrogenate rapidly for the same reason. The likelihood of easy dissolution was therefore not considered great.

A similar analysis of chemical structures fails to distinguish the solubility of bituminous coal from that of lignite. Earlier work[4,5] has, however, noted that lignite fails to dissolve as extensively or as rapidly as bituminous coal. The lignitic structures in lignite which comprise up to 50 percent by weight of the structure may form a barrier to prevent access by solvent to the internal grain structure.

Hill et al.[6] analyzed the kinetics and mechanism of solution of a high volatile bituminous coal and presented five ways in which the reaction might proceed. These include: (1) dissolving out of included materials, (2) dissolution of the coal structure in the presence of a large volume of solvent, (3) diffusion out of the micropores, (4) hydrogen transfer reactions and (5) solvent imbibition. Applications were discussed for the order of the reaction with respect to the coal and with respect to the solvent. The discussion proceeded on the assumption that little swelling occurred. This assumption was not verified in the present work where gross volume increases of about three times were observed in the case of the Illinois Seam #6 sub-bituminous coal.

The tentative conclusion based on application of the theories of Wender and of Hill to the present research is that the coal imbibes solvent and swells. The

swelling is accompanied by a close association of coal and solvent and a transfer of hydrogen to the cohesive structures between the micelles or microplatlets of coal. The cohesive structure is weakened; the coal forms fragments, and the action of gravity or fluid turbulence removes the coal fragments from the immediate vicinity of the coal face.

Implications for Underground Liquefaction

The implications of this proposed mechanism upon the conceptual design of an underground liquefaction process appear significant. The dissolution of coal need not be completed underground; the reaction may begin underground and be completed at the surface. If the vertical borehole scheme is utilized (Figure 4) the process might be as follows. The borehole is drilled through the thick coal seam and a hot, hydrogen donor solvent is introduced into the bottom of the borehole. The solvent is maintained under pressure to reduce solvent vaporization and to limit the reaction zone as much as possible to the bottom of the coal seam. After some coal has reacted and has fallen from the face of the seam, the recovery step is begun. Solvent, now a slurry medium, under turbulent flow conditions is introduced to suspend coal fragments and carry the fragments to the surface. After significant void volume is produced, the solvent volume would become too great for economy. Water would be introduced to flood the void and to float the solvent upward against the unreacted segment of the coal seam. The loosened coal could be collected periodically in the turbulent stream as before or could be collected continuously with water as the slurry medium. At the surface the coal fragments would be separated by filtration from the water slurry medium or if, in a solvent slurry, would be admitted into the pretreatment step of the complete liquefaction process at the surface.

Host Rock

The host rock would be of special importance in this conceptual design. The host rock would necessarily be impervious to loss of vapor from the solvent or to seepage outward of hydrogen donor solvent and water flood. Moreover, the host rock should be unreactive when exposed to the thermal shocks and high thermal gradients. Some shales may react with hot water or solvent. After swelling and spalling the shale particles would be carried away with the coal and contribute to a high level of waste mineral matter in the subsequent process. Considerable disadvantage is apparent in this case since disposal of mineral waste can be inconvenient and expensive. Possibly, the carbon content of the host rock could be extracted to pay for the disposal of the additional mineral matter. More likely initial tests would be performed on coal seams with unreactive host rock.

Surface Subsidence and Seismic Effects

Surface subsidence and minor seismic shock effects are experienced with most mining techniques. In the present concept their abatement can be planned. The process would be designed to include access wells so placed as to permit coal pillars to remain and to support the roof. Secondary beneficial effects include the reduction of solvent leakage and restriction of the areas into which coal fragments might fall and from which coal particles could be recovered.

Summary

Even in the absence of hydrogen several coal types undergo a swelling and spalling reaction early in their liquefaction reaction with hydrogen donor solvents.

The coals increase their reactivity in the order semi-anthracite, lignite, and sub-bituminous. Increased temperature and reaction time increase the extent of reaction. To utilize these observations a concept is presented which may lead to an underground coal liquefaction process.

TABLE 1

COAL ANALYSES

Oklahoma (Semi-anthracite)

Moisture %	-	S	0.6
Volatile Matter	17.3	H	4.2
Ash	7.6	C	83.8
Fixed Carbon	-	N	1.2
Heating Value (Btu/#)	15,570		92.4

Illinois Number 6 (Sub-bituminous)

Moisture %	14.7	S	4.5
Volatile Matter	37.2	H	4.4
Ash	15.7	C	66.1
Fixed Carbon	47.1	N	1.2
Heating Value (Btu/#)	9980	O	8.1

Alabama (Lignite)

Moisture %	37.8	S	1.1
Volatile Matter	40.8	H	4.3
Ash	11.1	C	64.5
Fixed Carbon	-	N	1.0
Heating Value (Btu/#)	8,010		18.0

TABLE 2

FRACTIONATION OF CRUDE ANTHRACENE OIL IN NITROGEN ATMOSPHERE

	Boiling Range °C	Volume ml	% By Volume
Light Ends	Ambient - 300°C	48	38.7
Middle Fraction	300°C - 400°C	58	46.7
Heavy Ends	400°+C	18	14.6
		124	100.0

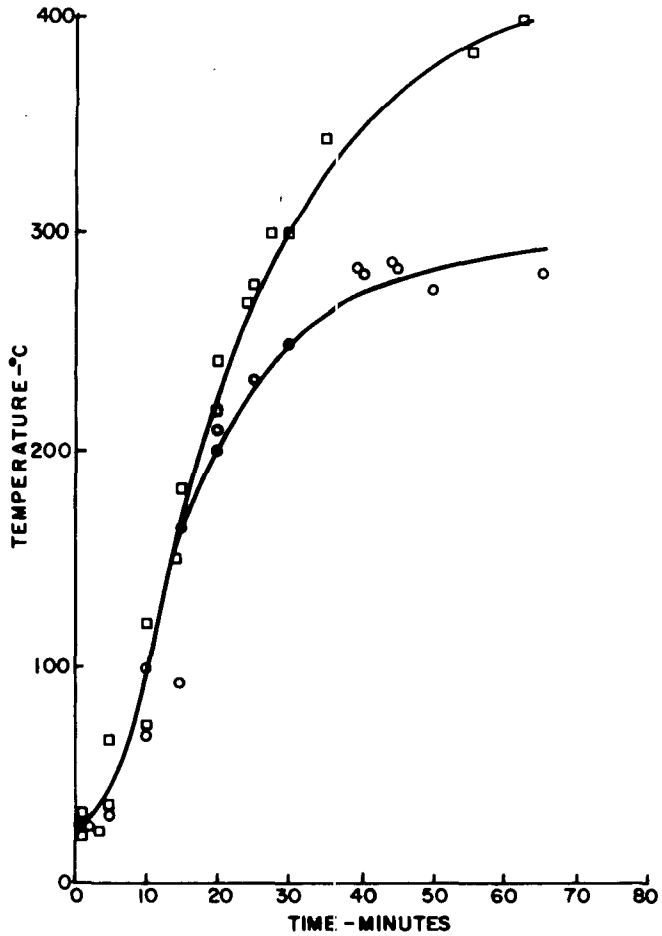

FIG. 1 - THE RELATIONSHIP OF TEMPERATURE AND TIME FOR SIX RUNS.

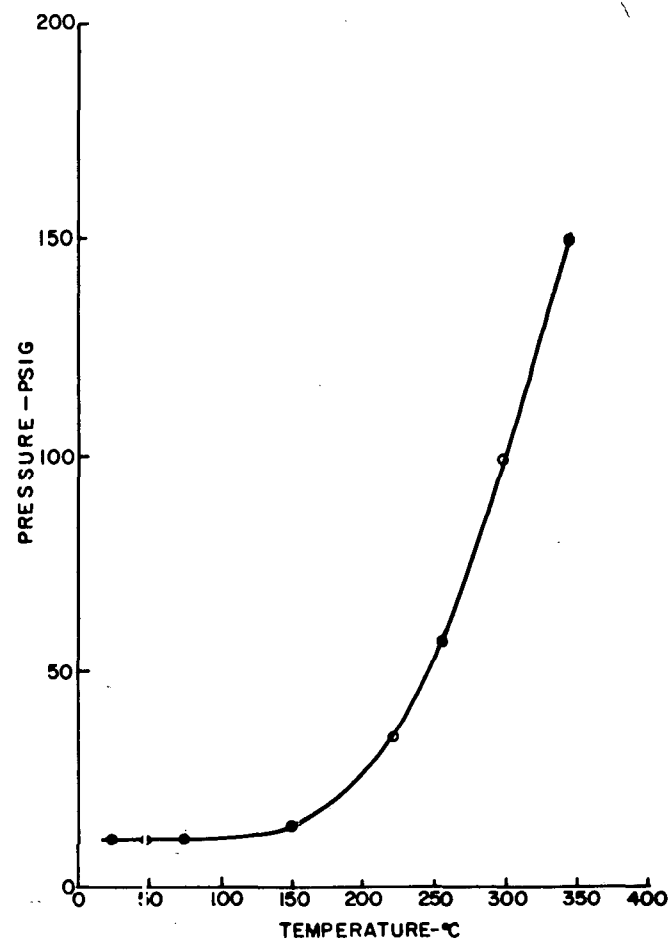

FIG. 2 - THE RELATIONSHIP OF PRESSURE AND TEMPERATURE FOR ANTHRACENE OIL SOLVENT AND ILLINOIS NO. 6 COAL.

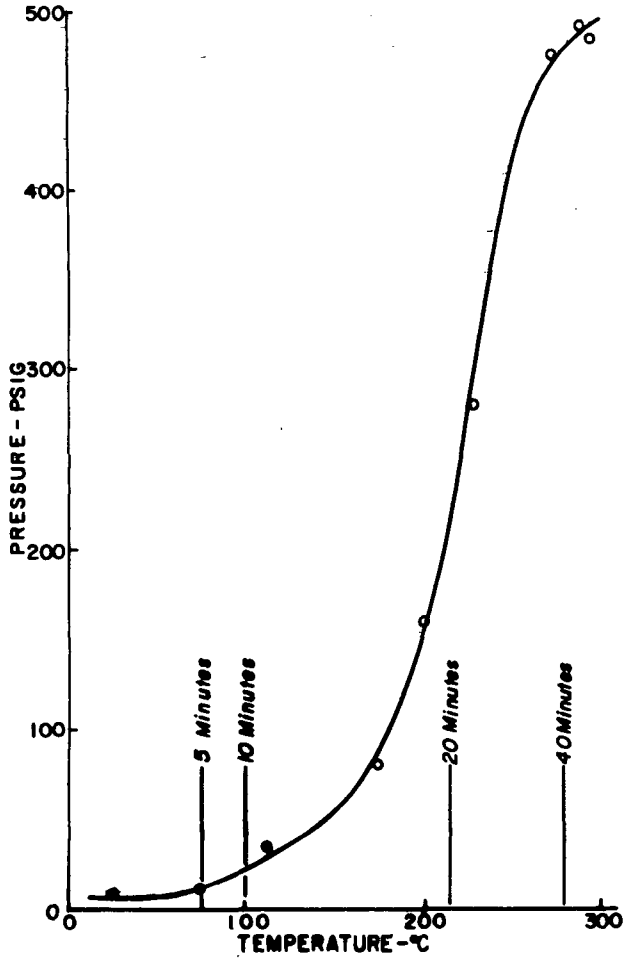

FIG.3 - THE RELATIONSHIP OF PRESSURE AND TEMPERATURE FOR SAE 30 MOTOR OIL SOLVENT AND ILLINOIS NO.6 COAL.

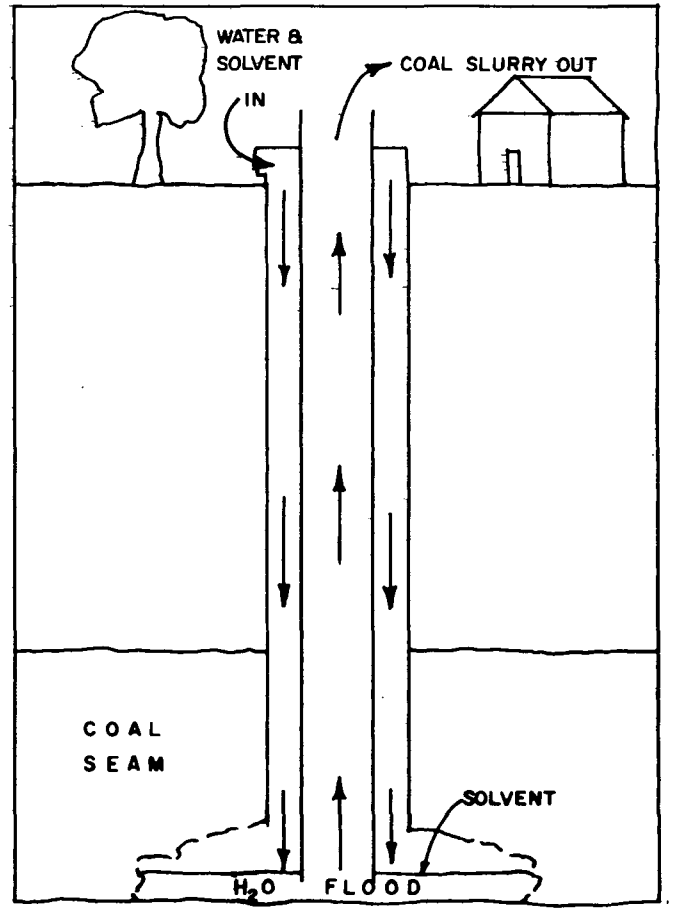

FIG.4 - VERTICAL BLIND BOREHOLE SYSTEM FOR UNDERGROUND COAL MINING AND LIQUEFACTION.

Bibliography

1. A Current Appraisal of Underground Coal Gasification. Report to the United States Bureau of Mines, C-73671, December, 1971.

2. Severson, D. E, Skidmore, D. R., and Gleason, D. S. Solution - Hydrogenation of Lignite in Coal-Derived Solvents. Transactions of the AIME, SME, 247, No. 2, 133-136, 1970.

3. Wender, I., Characteristics of Coal Behavior in Chemical Reactions. Unpublished report.

4. Bull, Willard C., Summary Report of O.C.R. Contract. Pittsburgh and Midway Coal Mining Company, 1965.

5. Appell, H. R., Wender, I. and Miller, R. D. Solubilization of Low Rank Coal With Carbon Monoxide and Water, Chemistry and Industry (London), 1703, 1969.

6. Hill, George R., Hariri, Hassan, Reed, R. I. and Anderson, Larry L., Kinetics and Mechanism of Solution of High Volatile Coal, "Coal Science", ACS Advances in Chemistry Series, No. 55, 1966.

THERMAL SYNTHESIS AND HYDROGASIFICATION OF AROMATIC COMPOUNDS

H. N. Woebcke, L. E. Chambers, P. S. Virk

In order to synthesize low sulfur fuels from coal, the Stone & Webster Coal Solution Gasification Process employs the stepwise addition of hydrogen to coal. Enough hydrogen is added in the first step to convert the coal to liquids, which are then hydrogasified to methane, ethane and aromatic liquid products.

Since both these steps involve reactions of aromatic type molecules, the possible chemical pathways involved for their thermal reactions have been studied, along with the kinetics of some of the limiting cases.

Available data show that aromatics are formed by pyrolyzing any of the simple paraffinic hydrocarbons. Formation appears to proceed through the production of olefinic intermediates.

It was felt that a tool in evaluating the relative rate of decomposition of simple aromatics would be their respective delocalization energies, which can be calculated from simple orbital theory. Available kinetic data showed this to be true.

Of the aromatics studied - benzene, diphenyl, naphthalene, phenanthrene, chrysene, pyrene, and anthracene - the rate of decomposition was found to increase in that order. Anthracene decomposes almost 800 times as rapidly as benzene. Further, it was found that the kinetics for the intermediate compounds are ordered inversely with respect to their delocalization energies.

A further consequence of the relation between delocalization energy and kinetics is that the rate of aromatic decomposition should be independent of the hydrogen partial pressure, or the character of the products. Data showed the rate of decomposition of benzene to be independent of hydrogen partial pressure, from 0.1 to 100 atmospheres.

At high hydrogen partial pressures, benzene decomposes primarily to methane, a probable intermediate being cyclohexadiene.

At low hydrogen partial pressures, coke is the final product. The intermediate in this case is probably diphenyl, with coke formation proceeding through stepwise reactions involving diphenyl rather than the progressive addition of benzene molecules. It appears that the conversion of benzene to diphenyl is rapid, and essentially at equilibrium, with the second step, the production of coke from diphenyl, being rate controlling.

Aromatic Synthesis

When pyrolysis is carried out at low pressure - for example, in steam cracking for olefins production, the yield of methane and benzene increases monatonically as severity is increased, until conversion to coke becomes significant.

Early investigations[1] showed that aromatic liquids could be produced from all simple olefins and paraffins. Maximum aromatic yields of 5 wt % were obtained from methane by pyrolysis at 1,050 C for 10 seconds,

(1)

while propane gave a yield of 12% at 850 C. In general, olefins were found to give higher yields of aromatic liquids than paraffins and at lower temperature. For example, at 10 seconds residence time, propylene yielded 19% aromatics at 800 C, compared to 12% at 850 C already noted for propane.

Most investigators concluded that aromatics formed from paraffins during pyrolysis involved, as a preliminary step, the formation of olefins, all olefins from C_2 to C_4 playing a significant role in the synthesis.

Studies also showed that nitrogen acted as a true diluent, reducing the rate by reducing the partial pressure of the reactants. Oxygen enhanced the formation of aromatics from olefins, while hydrogen inhibited aromatization. Since the formation of aromatics proceeded through olefins, it is reasonable to assume that this was a result of the hydrogenation of the olefinic intermediates.

An interesting observation was that reactions leading to the maximum aromatic yield from different light paraffins and olefins generally produced a liquid having about the same composition, i.e.,

40 wt % Monocyclic Aromatic

20 wt % Dicyclic

10 wt % Tricyclic

As conversion progressed beyond peak aromatic conversion, coke was formed, presumably from aromatic precursors.

Figure 1 shows data of Kunugi and Kinney and Crowley relating methane and aromatics yield with ethylene conversion. The data of both investigators form a smooth curve, the former limited to low conversions.

Figure 2 presents similar information for propylene. For both olefins, aromatics and methane production are linear with conversion up to the point of maximum aromatics production. This is shown more clearly on Figure 3 which is a replot of data from the first two figures.

Cracking data for naphtha obtained from the Stone & Webster bench scale pyrolysis unit show this same characteristic relationship. Here a somewhat unanticipated result is that the relationship between methane and aromatics yield is essentially independent of pressure, over a very wide range of pressure conditions.

Some further insight on the effect of hydrogen partial pressure on the formation of aromatics can be found in the work of Moignard[2] et al. These experimentors found that under conditions selected for the conversion of light paraffinic hydrocarbons to methane and ethane, there was still a significant production of aromatics. In view of the presumption that aromatics are produced from olefins, this suggested that the hydrogenation of the intermediates to paraffins was not rapid enough to inhibit aromatic formation. Using methane formation as a guide to cracking severity, it is interesting to compare Moignard's data for a light paraffinic naphtha, with other noted earlier.

This is shown on Table 1 (Slide 5). As indicated, the presence of hydrogen does significantly reduce the relative yield of benzene to methane.

Aromatic Decomposition

The remainder of this study was limited to noncatalytic reactions involving relatively small aromatic molecules. Some of the compounds studied are shown on Table 2 (Slide 6). The largest, chrysene, has a hydrogen content of 5.3 wt %, compared to benzene with 7.9 wt % H_2.

The detailed chemical pathway(s) for aromatic molecule hydrogenolysis is unknown, but it is convenient to consider it composed of three steps:

1. Aromatic Ring Destabilization
2. Breakdown to Fragments
3. Fragment Reactions

These are described in turn.

Aromatic Ring Destabilization

The above demarcation stems from the well-known chemical premise that aromatic compounds owe their unusual stability to a delocalization of pi-electrons among the ring molecular framework. To get aromatic molecules to react, the "delocalization energy" must be overcome. Since this energy is large, of the order of 40 kcal/mol, initial destabilization of the aromatic ring is invariably the rate determining step. This argument predicts that the reactivity of all aromatic compounds should be ordered inversely to their delocalization energy. These energies can be computed from simple molecular orbital theory.

Some indication of how this agrees with observation is given in Table 3 (Slide 7), which shows the relative rates at which methyl radicals attack some of the compounds of interest. Notice that all the rates are ordered according to the delocalization energy. The same pattern is observed for a wide variety of reactions, such as free radical attack, nitration and sulfonation. Further, note that benzene and anthracene represent the extremes of reactivity.

A second consequence of the initial destabilization step being rate determining is that, since the further course of reaction exerts little influence on the overall rate, a given aromatic molecule should react at a rate essentially independent of the products being formed. This implies, for example, that rates of benzene decomposition during hydrogenolysis and pyrolysis be comparable even though the products - methane and coke - are strikingly different. This second consequence, while qualitatively true, is not quantitatively as well obeyed as the first.

Breakdown to Fragments

Possible pathways for aromatic decomposition are illustrated on Figure 5 (Slide 8).

The destabilized aromatic ring is a short-lived species which will either revert to the original stable aromatic ring or suffer a breakdown to various fragments. In the latter event, some of the fragments will be nonaromatic and hence subject to more conventional reaction pathways. For example, the destabilized benzene nucleus may go to cyclohexadiene,

or it may go to phenyl, pentadienyl or allyl radicals, which will further pyrolyze or be hydrogenated. For aromatics with multiple rings, e.g., anthracene, the initial breakdown products are very likely to contain smaller aromatic rings, e.g., benzene, in addition to nonaromatic fragments.

Fragment Reactions

The nonaromatic fragments formed from aromatic ring breakdown can undergo a great variety of reactions, among which are: (a) Molecular Reactions, such as simple fission (pyrolysis) or hydrogenation-dehydrogenation reaction; (b) Concerted electrocyclic reactions, for example, fission and rearrangements; (c) Free radical chain reactions such as hydrogenation/dehydrogenation, and polymerization.

The complexity of possible fragment pathways can be reduced by certain generalizations.

Molecular fissions have high activation energies about equal to the strength of the bond being broken. As a result, larger hydrocarbons break much faster than the very smallest. Among the paraffins, the order of stability is methane, ethane, propane, butane, and the approximate fission rate constant for ethane is 0.01% that for butane. Likewise, alkyl benzene or other aromatics containing side chains will tend to lose these much faster than the aromatic nucleus is destabilized.

Electrocyclic reactions, which are concerted, are usually much faster than molecular reactions which involve bond breaking or making.

Free radical chains, when operative, can be much faster than molecular pathways. In our case, at the high temperatures required for hydrogenolysis, free radicals will abound.

It is probably reasonable to suppose that the hydrogen-olefin-paraffin chain pathways are so fast that equilibrium prevails among these components.

Rate and equilibrium data indicate that the segments of the pathway from benzene fragmentation to ethane formation are expected to be fast relative to benzene destabilization and ethane pyrolysis. A further point to note is that whereas the ring destabilization step (1) is expected to be essentially unaffected by hydrogen, the subsequent product pathways (steps 2 and 3) - whether hydrogenolysis to gas or pyrolysis to coke - should be quite strongly influenced by hydrogen concentration. Finally, multiple-ring aromatics will break down into both nonaromatic and aromatic fragments, of which the former will decompose further by the reactions of step (3), while the latter will tend to lose side chains and go to benzene, the stablest aromatic, which will then further react via the pathway of Figure 5 (Slide 8).

Data Analysis

The essential theoretical hypothesis that aromatic reaction rates are controlled by the ring destabilization step can be tested by comparing the rates of hydrogenolysis and pyrolysis. If the hypothesis is true, the rates of decomposition of a given aromatic compound should be identical for either process. Further, reaction rates and their associated activation energies should correlate with the delocalization energy of that compound.

Sources of experimental information for the aromatic compounds of interest to us are listed in Table 4, along with associated reaction conditions. In each case, the data were processed by the usual simple methods to yield first order rate constants k_1, sec^{-1} as a function of temperature for the initial decomposition of the aromatic:

$$A \xrightarrow{k_1} \text{Product}; \quad \frac{dC_A}{dt} = -k_1 C_A$$

It should be noted that the assumption of first order kinetics was not generally verifiable from the data and consequently the precision of these inferred rate constants is not especially good; but the rates are probably of the right order of magnitude in all cases.

Results obtained for benzene and anthracene, theoretically expected to be the extreme cases, are presented on Figure 6 (Slide 9).

Benzene Decomposition Rates

It is apparent that, while the data of separate investigators can each be fitted with straight lines of somewhat different slopes, all the data are adequately described by the single heavy line shown. This indicates that the rates of benzene decomposition during hydrogenolysis and pyrolysis are essentially the same over a rather wide range of experimental conditions. In particular, the insensitivity to hydrogen pressure, which varies from 0.1 atm to 100 atm, is noteworthy. The experimentally observed equality among benzene decomposition rates suggests a common rate-determining step which, in turn, lends support to the thought that aromatic ring destabilization, common to both hydrogenolysis and pyrolysis reactions, is rate-determining.

Benzene Decomposition Products

Some further insight into the reaction pathway can be obtained from the reported reaction products. In the presence of substantial hydrogen, the lowest temperature data (Lang, 900 F) show diphenyl as the sole product, whereas the higher temperature data (Schultz, 980-1,200 F, Dent, 1,100-1,500 F) indicate mainly methane and some ethane as products, with the mole ratio C_2/C_1 tending to unity at benzene conversions below 5%, while approaching zero at high benzene conversion. The diphenyl product suggests either a destabilized ring breakdown to a phenyl fragment or a concerted hydrogen elimination from two benzene molecules. It is also interesting because it represents net dehydrogenation of the benzene for purely kinetic reasons even though thermodynamic equilibrium strongly favors gasification.

None of the above authors report coke (carbon) formation, nor do they mention any hydrogenated C_6 liquid products. However, hydrogen balances on Schultz's data reveal that the empirical formula C_6H_n of the C_{6+} components does change from n=6 to n=8 as benzene conversion proceeds from 0 to 50%, indicating at least some direct hydrogenation of the C_6 ring. In the absence of much hydrogen (pyrolysis), the gaseous reaction products are principally hydrogen and methane. The H_2/CH_4 mol ratio is variable, about 2-4 in Dent's experiments (1,100-1,450 F, 50 atm N_2) and 8-30 in Kinney's case (1,450-2,000 F, 1 atm N_2). Dent also reports small amounts of ethane (C_1/C_2=1) at the temperatures of 1,100-1,300 F while Kinney detected traces of acetylene.

Dent makes no mention of coke or condensed products, but Kinney reported diphenyl and carbon (coke) as the major products of benzene pyrolysis and showed further (as shown on Figure 7, Slide 10) that the diphenyl/carbon product ratio decreased in the presence and increased in the absence of coke packing, even though the packing did not appreciably affect the overall benzene decomposition rate. The implications concerning the benzene to diphenyl to coke pathway are, first, that both ring destabilization and breakdown are probably noncatalytic, homogeneous gas phase steps and, second, that the carbon formation reaction is catalyzed by the product, coke, and probably does not involve further benzene participation.

Anthracene Decomposition

The two sources of anthracene decomposition data are Dent and Kinney. For benzene, the coincidence between decomposition rates during pyrolysis and hydrogenolysis also supports the notion that ring destabilization is rate-determining.

Decomposition products from anthracene pyrolysis noted by Kinney were mainly carbon, with the carbon formation catalyzed by coke. Product gases were mainly hydrogen and methane, $H_2/CH_4 = 10$, with traces of acetylene. The hydrogenolysis products noted by Dent were mainly methane and ethane and small aromatic rings, benzene, and naphthalene. No carbon formation was reported. Dent reports only the fraction of anthracene converted to gas. It appears likely that the breakdown of a destabilized anthracene ring, in the presence of

hydrogen, leads to one benzene molecule as a fragment. The gas associated with this initial anthracene breakdown contains methane and ethane in the mol ratios C_1/C_2 = 3.5 at 1,200 F and 5.3 at 1,300 F. This does not yield any clear clues about the nonaromatic fragments except, perhaps, that a 4-carbon specied (which would give C_1/C_2 = 2) may be involved. The change in C_1/C_2 ratio with temperature is too large to be explained by simple ethane pyrolysis with methyl radical hydrogenation.

Other Aromatic Molecules

Decomposition rate data for some of the other aromatic molecules of interest are shown on Figure 8 (Slide 11), Substantially all of the points lie between the anthracene and benzene limits and reasonably straight lines can be drawn to represent the variation of decomposition rate constant vs. temperature for each of the molecules.

Decomposition products observed were as follows:

Diphenyl: During hydrogenolysis at 930 F, 200 atm H_2, benzene was the sole product. The products of pyrolysis, besides coke, are not clear because the diphenyl results are derived from the benzene pyrolysis data of Kinney.

Naphthalene: During hydrogenolysis at 1,160 F and 200 atm H_2, Schultz reports methane, ethane and small amounts of propane in the gas with the molal C_1/C_2 1 at low conversions. Benzene was detected in significant amounts, and traces of toluene and ethylene were also found.

Hydrogen balances indicate some direct hydrogenation of the C_{10} ring as well, but no coke formation was reported. During pyrolysis, Kinney found the gaseous products are mainly hydrogen and methane with traces of acetylene at 1,500-1,800 F in N_2 at 1 atm. The principal product was solid carbon, and traces of condensation products like 2-2' binaphthyl and perilene were also detected. The binaphthyl is, of course, analogous to diphenyl and suggests an analogous pathway to coke.

Chrysene: Orlow found with 70 atm H_2 that the hydrogenolysis reaction products (by weight) were 25% methane, 35% coke, with the remaining 40% containing phenanthrene, naphthalene, benzene, and various hydrides of each. The pyrolysis products were hydrogen and methane with traces of acetylene in the gas, and solid carbon.

Correlation

The experimental decomposition rate constant data can be fitted by the straight lines shown to yield Arrhenius expressions of the form

$$k_1 = A \exp(-E^*/RT)$$

for each molecule. Values of these Arrhenius parameters, the frequency factor A and activation energy E*, are collected in Table 4 (Slide 12), effectively summarizing the available data.

According to Molecular Orbital theory, the activation energy should be proportional to the delocalization energy, i.e., a plot of E* (experimental) vs. delocalization energy (calculated) should have all molecules lying on the line between the origin and the benzene coordinates. Figure 9 (Slide 13), an arithmetic plot of activation energy vs. delocalization

energy, shows a trend in accord with theory. Anthracene and benzene, the two cases with most data, are in especially good agreement.

Effect of Hydrogen

While it appears that the rate-determining aromatic ring destabilization step is essentially unaffected by hydrogen, the products of decomposition most assuredly are. Increasing hydrogen concentration switches the decomposition pathway from pyrolysis, which leads primarily to solid carbon (coke), to hydrogenolysis, where the product is gas, mainly methane. Understanding how hydrogen concentration controls the crossover between pathways is of interest. However, since the detailed pathway is not explicity defined, we will focus only on a few aspects expected to be important. Much of the following discussion refers to benzene decomposition, since this case has the most data.

Thermodynamic Equilibrium

It is of interest to examine the equilibrium concentration of H_2, CH_4, and C_6H_6 dictated by the following reaction:

		K_p at 1,340 F	
		(a)	(b)
(1)	$C_6H_6 + 9\ H_2 \longrightarrow CH_4$	10.5	-4
(2)	$C_6H_6 \longrightarrow 6C + 3H_2$	16.57	+2
(3)	$CH_4 \longrightarrow 2H_2 + C$	1.011	1

where (a) is the exponent to the base 10 and (b) is the power of the pressure term in atmospheres

Calculations for this system show that carbon can always form before benzene has reached gasification equilibrium.

Further, at atmospheric pressure, carbon formation can occur at very low benzene conversions, unless very large excess of hydrogen is used.

At a fixed hydrogen to benzene ratio, increasing the total pressure favors gasification and retards carbon deposition, based on equilibrium considerations.

A study was therefore made of the effect of total pressure, hydrogen to benzene ratio in the feed, and benzene decomposition on the gross heating value of the product gas. The study was limited to conditions at which ratios of hydrogen to methane in the prodcut gas would be in excess of that required to inhibit the presence of carbon at equilibrium. The resultsare presented on Figure 10 (Slide 14).

Note that a 15% decomposition of benzene, the maximum heating value that can be obtained at 1,400 F is about 800 Btu/SCF, while at 1,500 F the GHV would be reduced to about 600 Btu/SCF - under conditions where no carbon could exist at equilibrium. The principal curves, i.e., those relating benzene conversion with GHV of product gas, are those for constant pressure and hydrogen to C_6H_6 ratio in the feed. The H_2/C_6H_6 ratios selected for plotting at any given total pressure were those leading to maximum product GHV for a given benzene conversion.

Carbon Formation

Coke is the terminal product of the aromatic pyrolysis pathway and it is of some interest to explore the formation mechanism. Insight into this process is provided by the benzene pyrolysis data of Kinney (1954) in a flow reactor. The diphenyl concentration vs. time behavior reported by Kinney is characteristic of an intermediate in a sequential reaction A + B C wherein A (benzene) decreases and C (carbon) increases, both monotonic with time, while the intermediate B (diphenyl) increases at small times and decreases at long times. It is also instructive to compare results at the same temperature, 1,800 F, with and without coke packing as shown in Figure 7 (Slide 10). This further suggests that carbon formation proceeds through a sequence of reactions in series

(1) 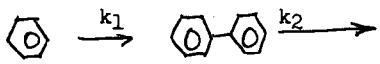

carbon

The first reaction is unaffected by coke, whereas the second is catalyzed by coke. Removal of catalyst would slow down the second reaction, thus increasing the intermediate diphenyl concentration as observed.

In regard to the molecular reactions leading to carbon, the literature contains many references to a benzene-by-benzene addition with hydrogen elimination (2).

Some of the intermediate products, e.g., diphenyl-benzenes and triphenylene have indeed been detected in the tarry residue resulting from benzene pyrolysis. However, if (2) were the main pathway to carbon, it would

essentially involve benzene in every step and so carbon formation should be very high order in benzene. Catalytic effects enhancing carbon formation should strikingly increase the benzene decomposition rate (and vice-versa). This is not the case as noted above. Further, reactions with benzene in every step would face the maximum benzene delocalization energy barrier compared to reactions between more condensed species with less DE than benzene. Thus, although the concentrations of the condensed species would undoubtedly be lower than benzene, the adverse effect of lower concentration on overall reaction rates could easily be offset by the lower activation energies, and hence higher rate constants, of the more condensed molecules. A plausible alternative scheme for the main pathway to carbon formation is therefore of the form

(3) 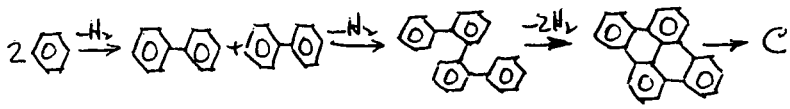

which involves 1,2,4.... benzene nuclei rather than the 1,2,3.... sequence of (2). According to the above scheme, since the bigger molecules are more reactive, the overall rate should be controlled by the first few steps, namely,

(4) 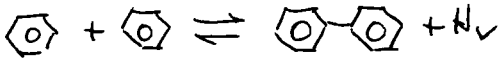

(5) 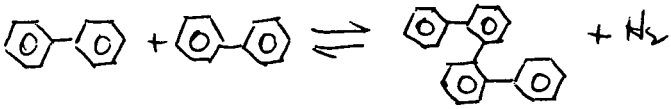

(6) (a & b) 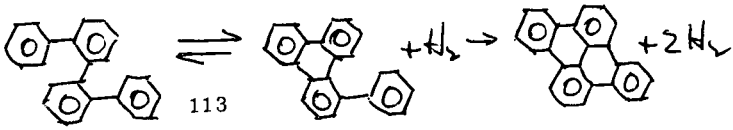

Qualitatively, we can let approximate carbon and since reactions (6) (a) and (b) are intra-molecular hydrogen eliminations which one would expect to be fast compared to the bimolecular hydrogen elimination steps (4) and (5), the reactants of (5) can, in effect, be considered to yield the products of (6b). The essential components of the alternative benzene carbon pathway are thus

(4) 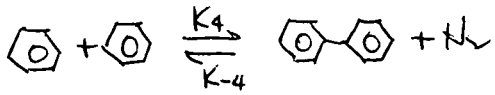

(5) 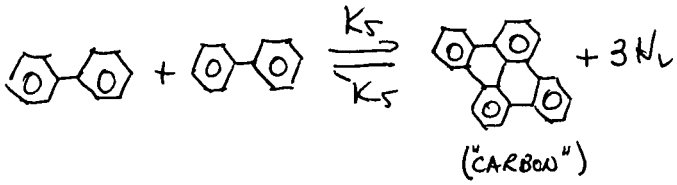

of which (4) is a homogenous gas-phase reaction, unaffected by coke, whereas (5) can be catalyzed by coke product.

Kinney's data for benzene pyrolysis to carbon may be modeled by a scheme of two sequential reactions (4) and (5) simplified such that (a) both reactions are kinetically limited in the forward directions and (b) reaction (4) is at equilibrium while (5) is kinetics controlled. Case (b) is the more plausible for the bulk of the data, but some of the experimental trends at low conversions at the lower temperatures are qualitatively as predicted for case (a). A combination of cases (a)

and (b), in which both forward and backward reaction rates are considered for (4) while (5) is assumed kinetcs controlled in the forward direction, would probably describe all of Kinney's data adequately.

Finally, we consider the effect of hydrogen on carbon formation. The overall equilibrium, discussed earlier, shows that increasing hydrogen/hydrocarbon ratios and increasing total pressure both retard carbon formation and enhance gasification. Kinetically, however, we have to recognize that there exist at least two types of routes to carbon, namely, by surface reaction and by gas-phase reactions. It is not obvious how these combine. The carbon formation model formulated above is primarily a homogeneous gas phase model and its sensitivity to hydrogen must recognize that the gas-phase route is only one of several possible parallel pathways to carbon. The presence of substantial hydrogen will tend to enhance the back reactions for both (4) and (5) and, clearly, the forward kinetics only, scheme (a), will not be adequate. The <u>maximum</u> conceivable carbon formation that can occur is when reaction (4) is at equilibrium (this gives the maximum diphenyl concentration) and reaction (5) is not retarded by products (even though hydrogen is a product). This, of course, is precisely scheme (b) considered above.

KINECTICS OF AROMATIC HYDROGASIFICATION SUMMARY OF EXPERIMENTAL DATA FOR AROMATIC HYDROGENOLYSIS AND PYROLYSIS

	Run Conditions						Reactor	
Compound	Source	Type	Temp, K	Press Atm	HC Mol Fr.	Diluent	Type	Residence, Sec
Benzene	1	H	873-1,123	50	0.10	H_2	F	60
	1	P	873-1,073	50	0.10	N_2	F	60
	2	H	800-973	200	0.15	H_2	B	1,000
	3	P	1,073-1,373	1	0.10	N_2	F	2-40
	4	H	750	250	0.35	H_2	B	10^4
Diphenyl	3	P	1,073-1,373	1	0.05	N_2	F	2-40
	4	H	773	200	0.05	H_2	B	$2x10^4$
Naphthalene	2	H	838-958	200	0.10	H_2	B	1,000
	3	P	1,073-1,273	1	0.02	N_2	F	2-40
Anthracene	1	H	923-1,073	50	0.04	H_2	F	60
	3	P	1,073-1,273	1	0.01	N_2	F	1-40
Chrysene	3	P	1,073-1,273	1	0.005	N_2	F	2-40
	5	H	723	70	0.13	H_2	B	10^5

Sources:
1. Dent, F.J., 43rd report of the Joint Research Committee, British Gas Council, (1939)
2. Schultz, E.B. and M.R. Linden, Ind. Eng. Chem. 49, 2011, (1957)
3. Kinney, C.R. and E. Delbel, Ind. Eng. Chem. 46, 548 (1954)
4. Lang, K. and F. Hoffman, Brenstoff-Chemie 10, 203 (1929)
5. Orlow, N.A. and N.D. Lichatschew, Ber., 62B, 719 (1929)

Abbreviations: H- Hydrogenolysis P- Pyrolysis B- Batch F- Flow

Table 1
(Slide 5)

Investigator	Feedstock	Cracked At Press.	Cracked At H_2	Pounds C_6H_6 Per Pound CH_4
Kunugi, et al	C_2H_4	1	No	1.4
Kunugi, et al	C_3H_6	1	No	1.4
Stone & Webster	(Paraffinic	1	No	0.7
Moignard, et al	(Naphtha	10	Yes	0.14

Table 2
(Slide 6)

MODEL AROMATIC MOLECULES

KINETICS OF AROMATIC HYDROGASIFICATION

RINGS	NAME	STRUCTURE	FORMULA	Tb, F
1	BENZENE		C_6H_6	176
2	NAPTHALENE		$C_{10}H_8$	424
	DIPHENYL	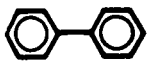	$C_{12}H_{10}$	491
3	ANTHRACENE		$C_{14}H_{10}$	646
	PHENANTHRENE	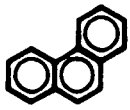	$C_{14}H_{10}$	643
4	PYRENE	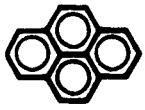	$C_{16}H_{10}$	740
	CHRYSENE	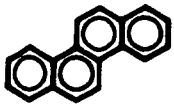	$C_{18}H_{12}$	827

Table 3
(Slide 7)

KINETICS OF AROMATIC HYDROGASIFICATION REACTIVITY TO METHYL RADICAL ATTACK

COMPOUND	DELOCALIZATION ENERGY	EXPERIMENTAL REACTION RATE RELATIVE TO BENZENE[1]
BENZENE	1.155	1
DIPHENYL	1.032	5
NAPHTHALENE	0.904	22
PHENANTHRENE	0.899	27
CHRYSENE	0.833	58
PYRENE	0.755	125
ANTHRACENE	0.632	820

(1) Data from Levy and Swarc, J.A.C.S. 77 1949 (1955)

Table 4
(Slide 12)

KINETICS OF AROMATIC HYDROGASIFICATION

ARRHENIUS PARAMETERS FOR AROMATIC DECOMPOSITION RATES

COMPOUND	A Sec^{-1}	E^* Kcal/Mol	$T_{1/2}$(1,000 °K) Half-life, Sec
BENZENE	4.4×10^8	52.6	499
DIPHENYL	1.6×10^7	43.1	118
NAPHTHALENE	4.5×10^5	36.8	171
CHRYSENE	3.4×10^5	33.5	43
ANTHRACENE	1.8×10^5	30.7	20

Note: $k_1 = A \exp(-E^*/RT)$

$T_{1/2}$ = half-life = $(0.693/k_1)$

Figure I
(Slide I)

PYROLYSIS OF ETHYLENE

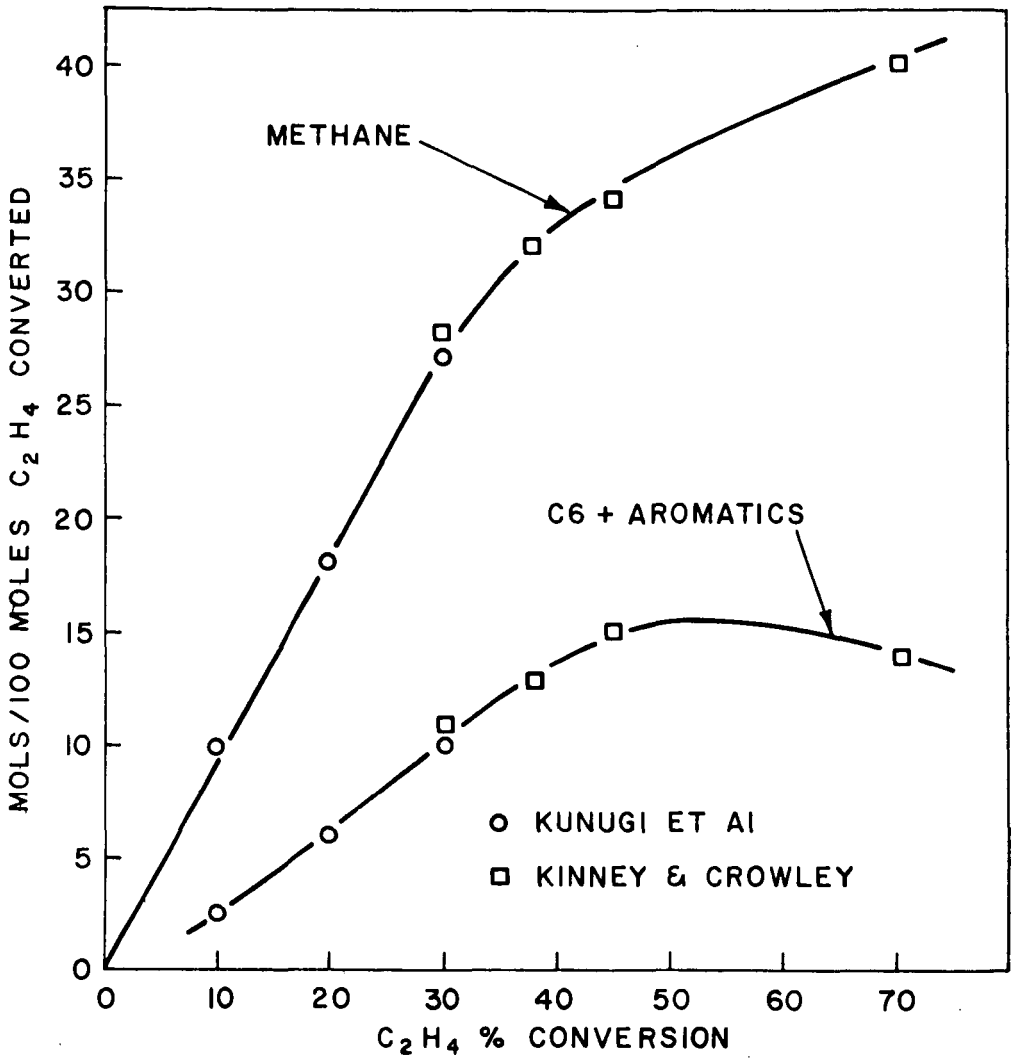

Figure 2
(Slide 2)

PROPYLENE PYROLYSIS

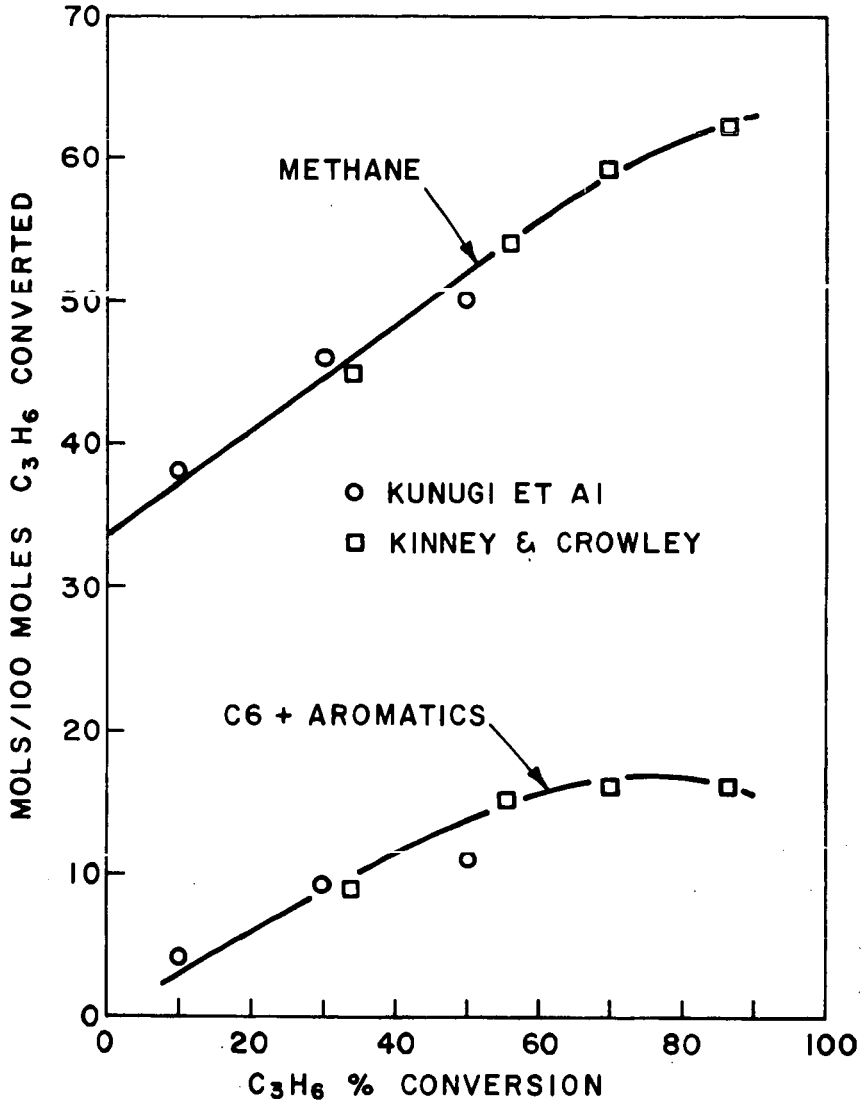

Figure 3
(Slide 3)

ETHYLENE & PROPYLENE PYROLYSIS

(YIELDS AS % FEED CONVERTED)

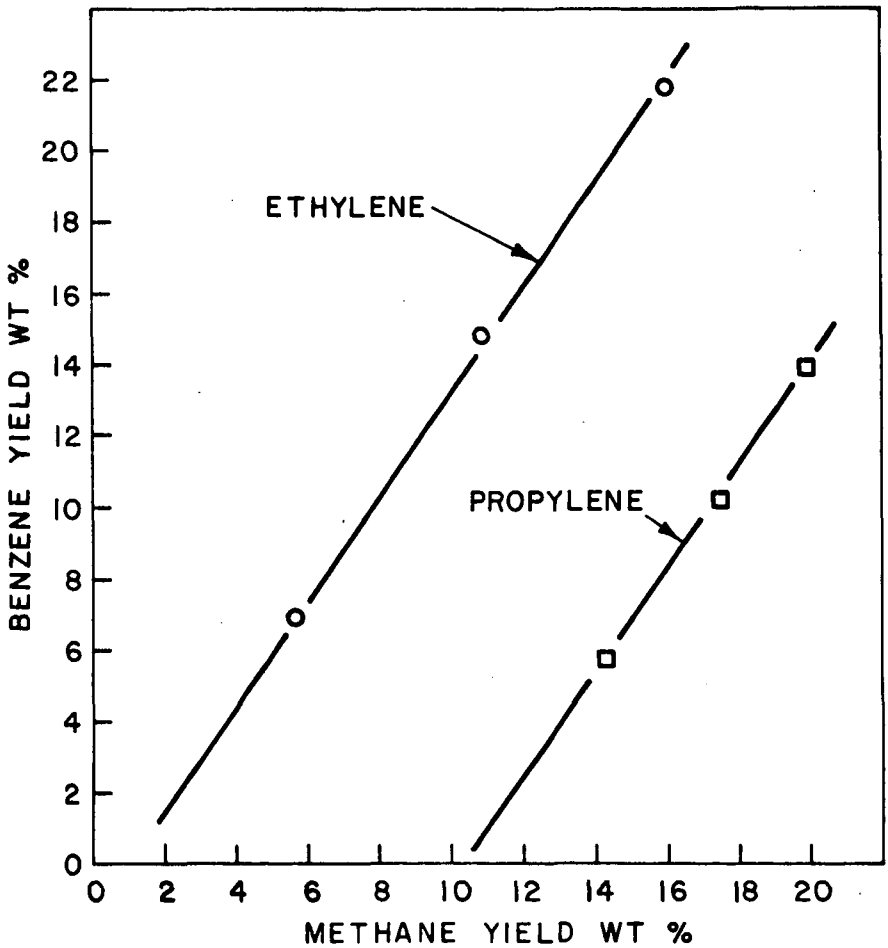

Figure 4
(Slide 4)

NAPHTHA PYROLYSIS

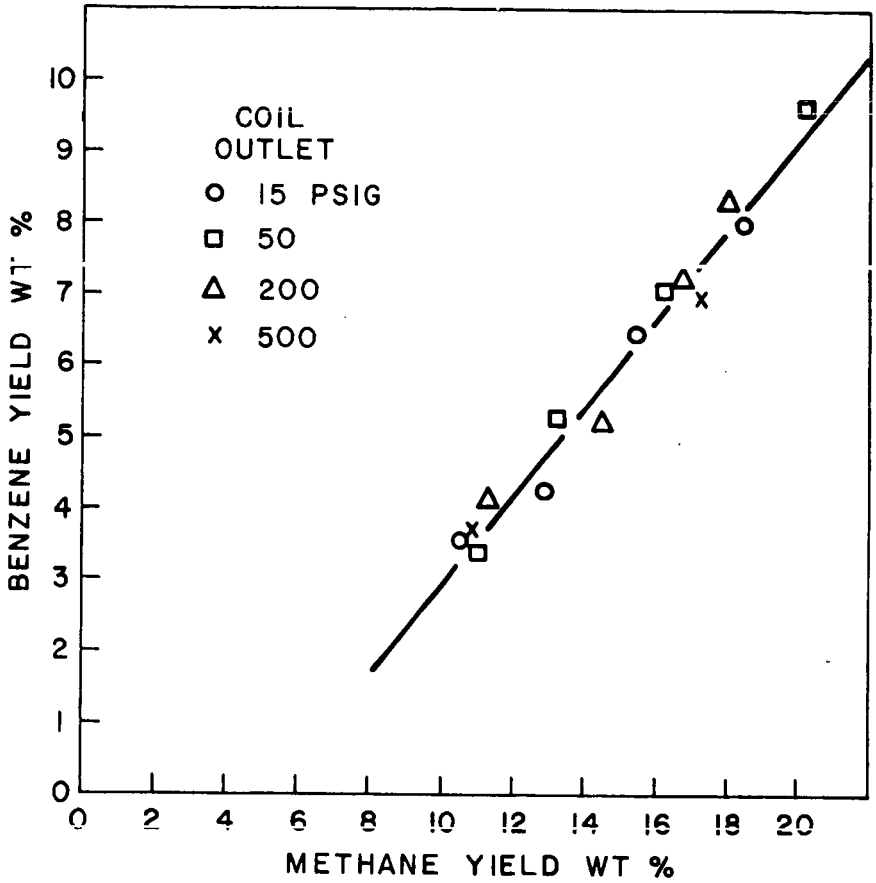

Figure 5
(Slide 8)

BENZENE HYDROGENOLYSIS PATHWAYS

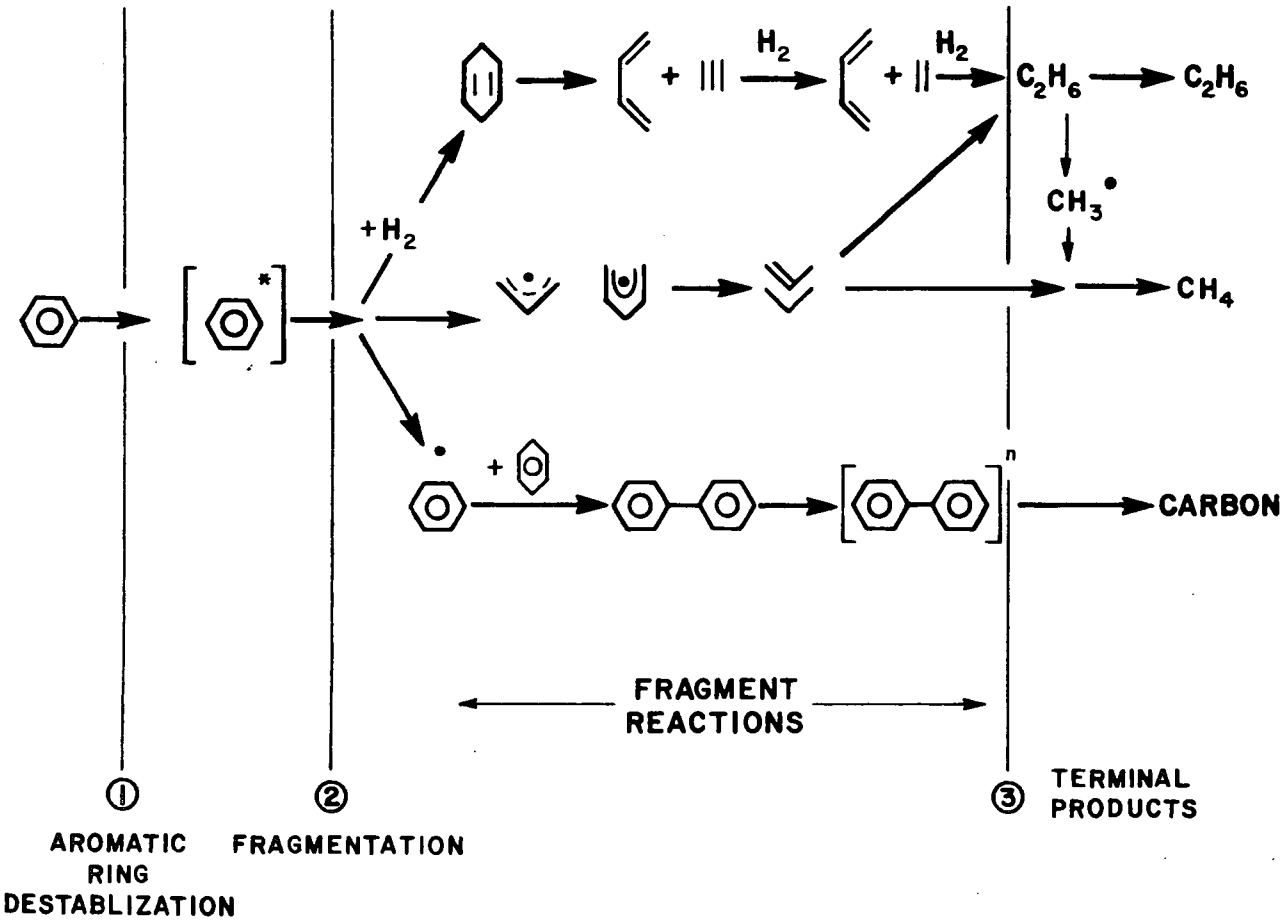

Figure 6
(Slide 9)

RATES OF DECOMPOSITION FOR BENZENE AND ANTHRACENE

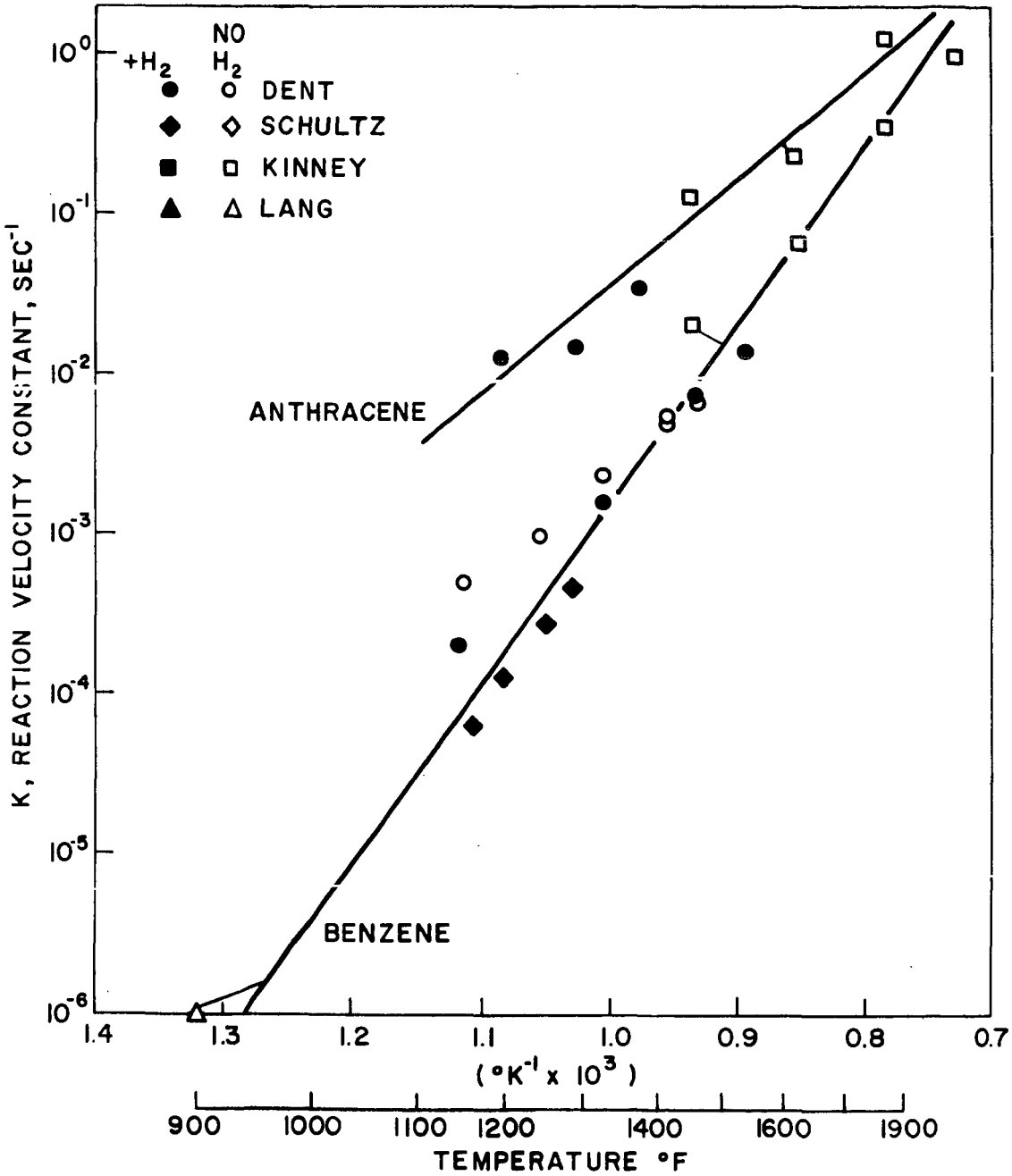

Figure 7
(Slide 10)

EFFECT OF COKE ON PRODUCT DISTRIBUTION FOR BENZENE PYROLYSIS

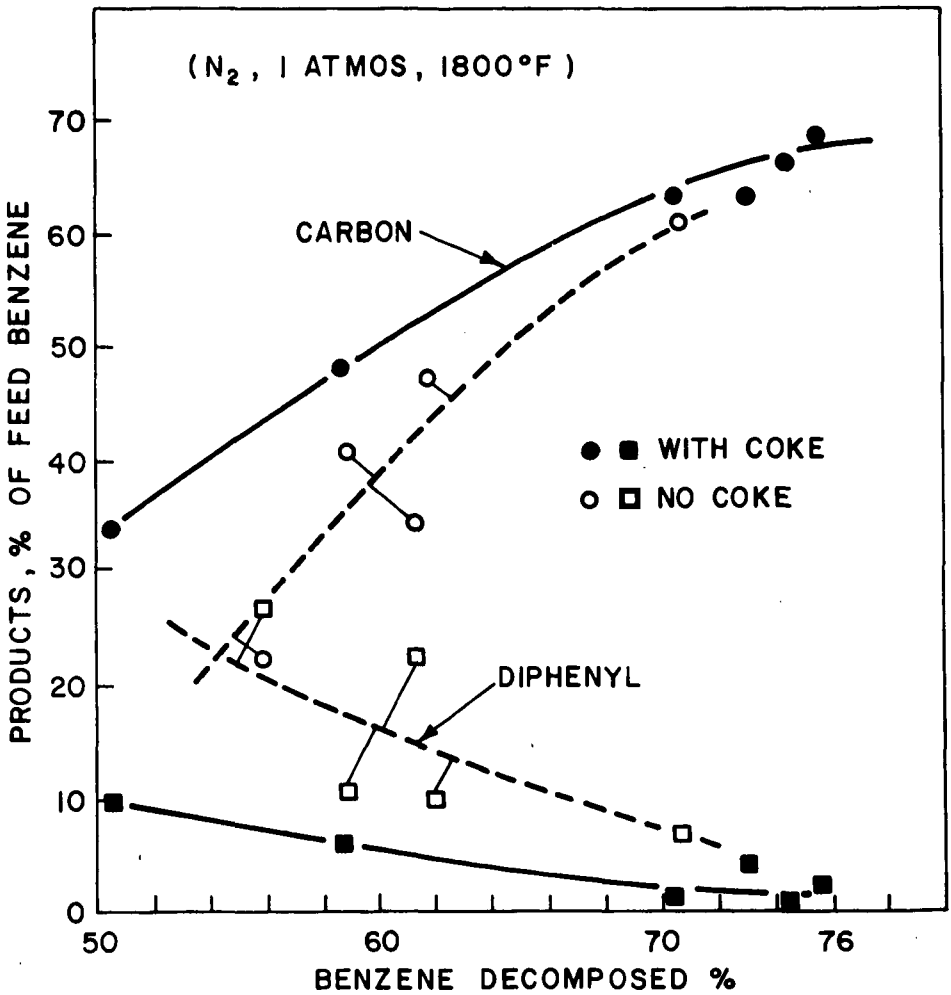

DECOMPOSITION RATES FOR SELECTED AROMATICS

Figure 8
(Slide 11)

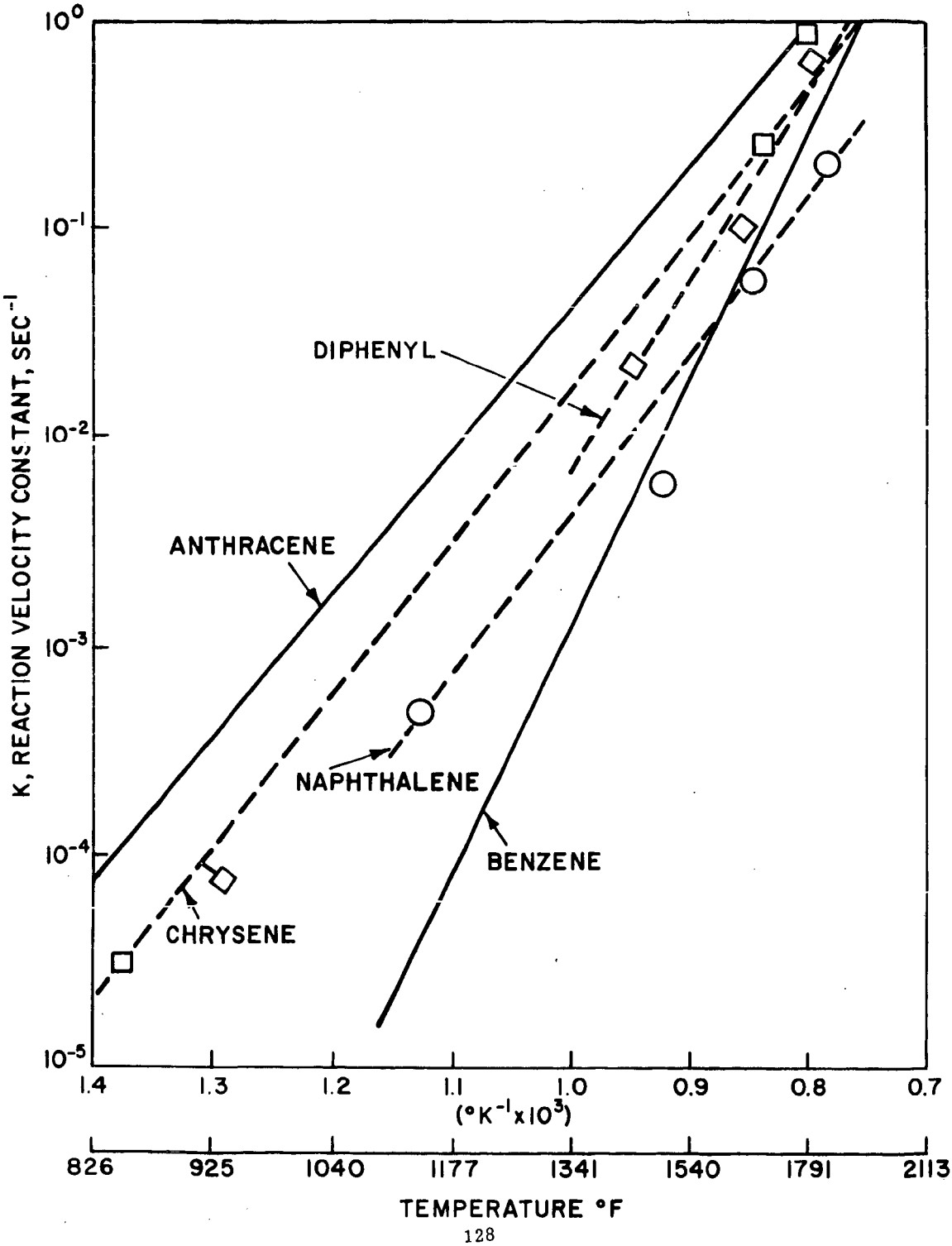

RELATION BETWEEN ACTIVATION AND DELOCALIZATION ENERGIES

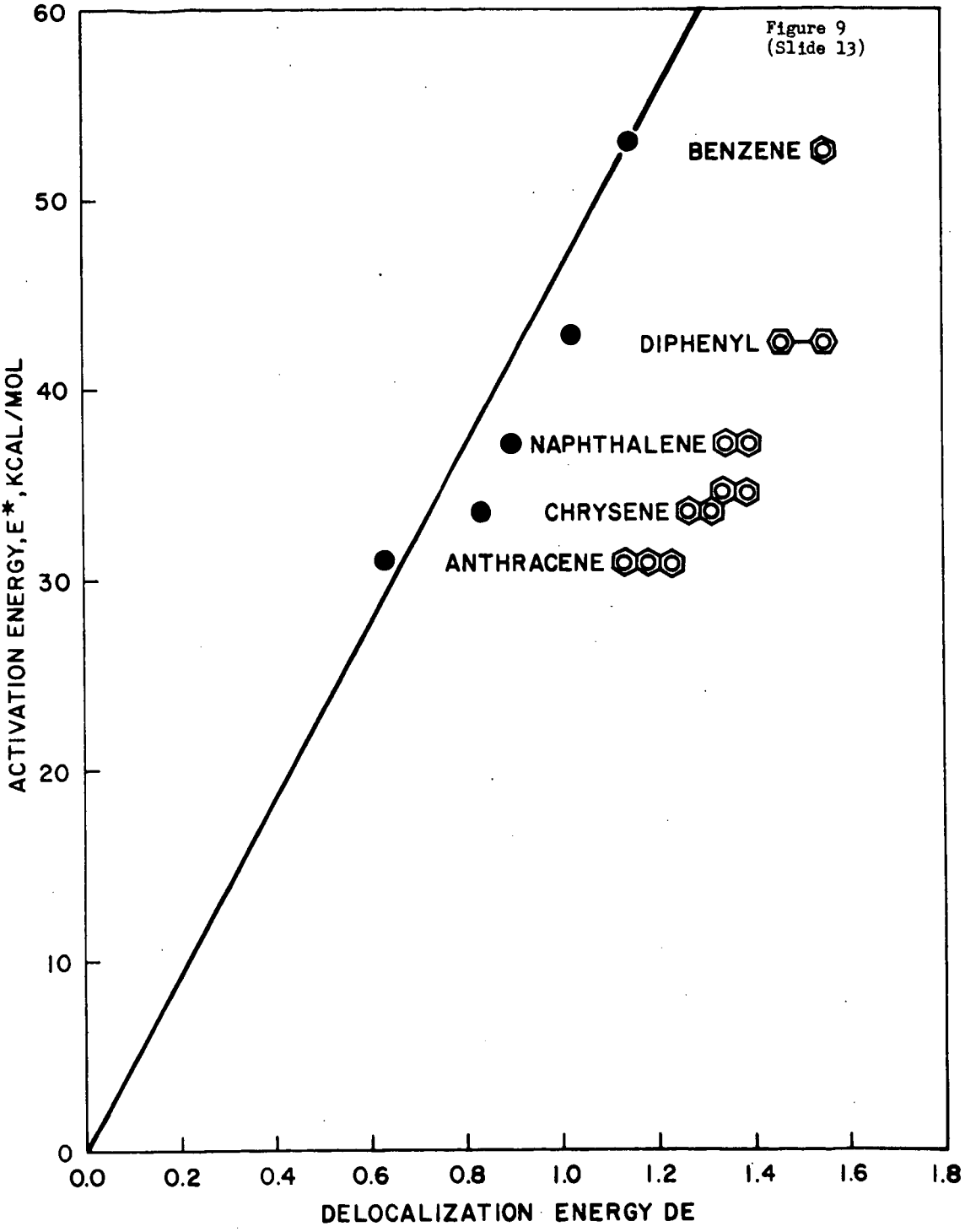

EFFECT OF OPERATING VARIABLES ON GASIFICATION OF AROMATICS
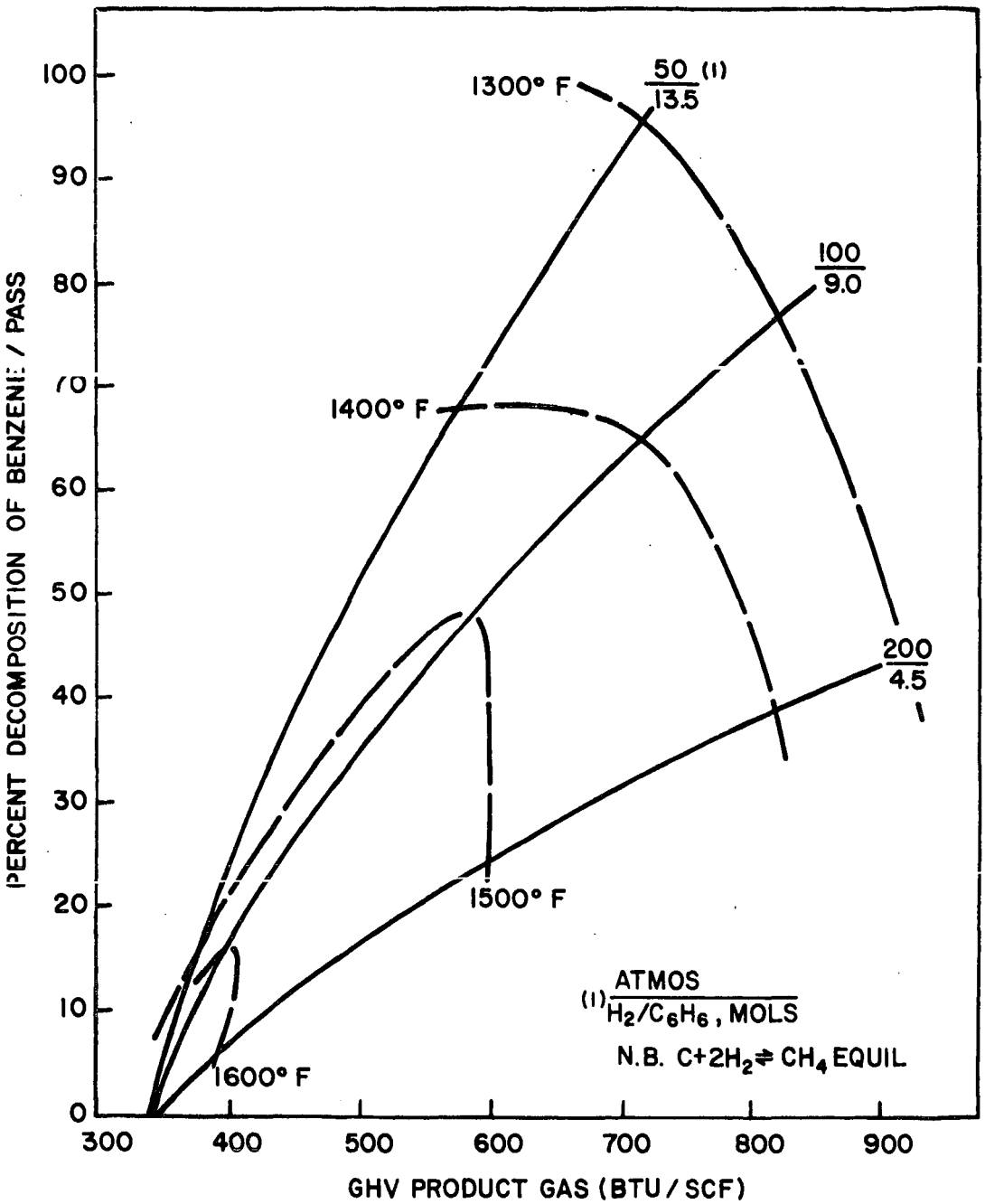
Figure 10
(Slide 14)